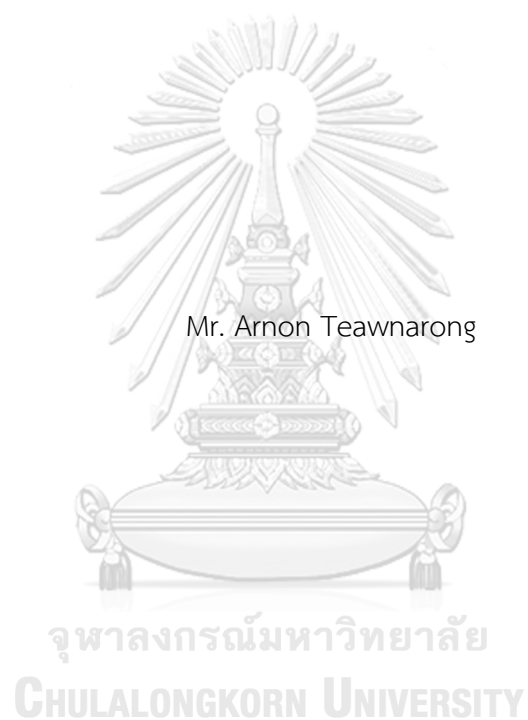


APPLICATION OF BATTERY ENERGY STORAGE SYSTEM FOR FREQUENCY REGULATION  
OF MAE HONG SON MICROGRID



A Thesis Submitted in Partial Fulfillment of the Requirements  
for the Degree of Master of Engineering in Electrical Engineering

Department of Electrical Engineering

FACULTY OF ENGINEERING

Chulalongkorn University

Academic Year 2019

Copyright of Chulalongkorn University

การประยุกต์ใช้ระบบกักเก็บพลังงานแบตเตอรี่เพื่อการควบคุมความถี่ของไมโครกริดแม่ฮ่องสอน



วิทยานิพนธ์นี้เป็นส่วนหนึ่งของการศึกษาตามหลักสูตรปริญญาวิศวกรรมศาสตรมหาบัณฑิต  
สาขาวิชาวิศวกรรมไฟฟ้า ภาควิชาวิศวกรรมไฟฟ้า  
คณะวิศวกรรมศาสตร์ จุฬาลงกรณ์มหาวิทยาลัย  
ปีการศึกษา 2562  
ลิขสิทธิ์ของจุฬาลงกรณ์มหาวิทยาลัย



อานนท์ เตียวณรงค์ : การประยุกต์ใช้ระบบกักเก็บพลังงานแบตเตอรี่เพื่อการควบคุม  
 ความถี่ของไมโครกริดแม่ฮ่องสอน. ( APPLICATION OF BATTERY ENERGY  
 STORAGE SYSTEM FOR FREQUENCY REGULATION OF MAE HONG SON  
 MICROGRID) อ.ที่ปรึกษาหลัก : ดร.พิสิษฐ์พล จีรพจนานุกรักษ์

ไมโครกริดแม่ฮ่องสอนในสภาวะแยกโดดมีความเฉื่อยต่ำ ดังนั้นเมื่อเกิดการรบกวนขึ้น  
 ความถี่ของระบบจะเบี่ยงเบนไปมาก ซึ่งอาจจะทำให้เกิดไฟฟ้าดับได้ การติดตั้งระบบกักเก็บ  
 พลังงานแบตเตอรี่จะช่วยเพิ่มสมรรถนะการตอบสนองเชิงความถี่ของระบบไมโครกริด ทั้งในขณะ  
 แยกโดดและในขณะที่เชื่อมต่อกับระบบไฟฟ้าหลัก วิทยานิพนธ์นี้มีวัตถุประสงค์เพื่อศึกษาและ  
 เปรียบเทียบวิธีการควบคุมระบบกักเก็บพลังงานแบตเตอรี่เพื่อตอบสนองต่อความถี่ในระดับปฐม  
 ภูมิและทุติยภูมิ ผลการศึกษาพบว่า การควบคุมระบบกักเก็บพลังงานแบตเตอรี่เพื่อตอบสนองต่อ  
 ความถี่ในระดับปฐมภูมิด้วยวิธีรูปเสมือนและวิธีความเฉื่อยเสมือน สามารถลดการเบี่ยงเบนของ  
 ความถี่ในไมโครกริดได้ นอกจากนี้การควบคุมระบบกักเก็บพลังงานแบตเตอรี่เพื่อตอบสนองต่อ  
 ความถี่ในระดับทุติยภูมิ สามารถทำให้ความถี่ของระบบกลับมาสู่ค่ามาตรฐานได้

จุฬาลงกรณ์มหาวิทยาลัย  
 CHULALONGKORN UNIVERSITY

สาขาวิชา วิศวกรรมไฟฟ้า  
 ปีการศึกษา 2562

ลายมือชื่อนิสิต .....  
 ลายมือชื่อ อ.ที่ปรึกษาหลัก .....



# # 6170336121 : MAJOR ELECTRICAL ENGINEERING

KEYWORD: Microgrid, low inertia, frequency regulation, power system stability,  
battery energy storage system

Arnon Teawnarong : APPLICATION OF BATTERY ENERGY STORAGE SYSTEM  
FOR FREQUENCY REGULATION OF MAE HONG SON MICROGRID. Advisor:  
PISITPOL CHIRAPONGSANANURAK, Ph.D.

Mae Hong Son microgrid in an isolated mode has low inertia. Therefore, when a disturbance occurs, the system frequency is subjected to a large deviation, which may lead to a blackout. The installation of a battery energy storage system (BESS) will improve the frequency response performance of the microgrid system in both islanding and grid-connected modes. The objective of this thesis is to investigate and compare BESS control methods for providing primary and secondary frequency response. The results show that the control of BESS for providing primary frequency response using virtual droop and virtual inertia approaches can reduce the frequency deviation in the microgrid. Moreover, the control of BESS for providing secondary frequency response can bring the system frequency to standard values.



จุฬาลงกรณ์มหาวิทยาลัย  
CHULALONGKORN UNIVERSITY

Field of Study: Electrical Engineering

Student's Signature .....

Academic Year: 2019

Advisor's Signature .....

## ACKNOWLEDGEMENTS

First and foremost, I would like to express my sincere gratitude to my advisor Dr Pisitpol Chirapongsananurak for the continuous support of my Master of Engineering (M.Eng.) study and research, for continually and convincingly conveyed a spirit of adventure regarding research and scholarship and excitement about teaching. His guidance helped me in all the time of research and writing of the thesis. Without his advice and persistent help, this thesis would not have been possible.

Besides my advisor, I would like to express my sincere thanks to the rest of my thesis committee: Assoc. Prof. Naebboon Hoonchareon and Assoc. Prof. Wijarn Wangdee for sharing their assistance and suggestion throughout my thesis, including for their encouragement and insightful comments.

Moreover, I would like to express the most profound appreciation to the Department of Electrical Engineering, Faculty of Engineering, Chulalongkorn University, for providing the EECU Master Honours Program Scholarship for my M.Eng study and research.

Last, I would like to thank my family and friends for their constant source of inspiration.



จุฬาลงกรณ์มหาวิทยาลัย  
CHULALONGKORN UNIVERSITY

Arnon Teawnarong

## TABLE OF CONTENTS

	Page
ABSTRACT (THAI).....	iii
ABSTRACT (ENGLISH).....	iv
ACKNOWLEDGEMENTS.....	v
TABLE OF CONTENTS.....	vi
Chapter 1 Introduction.....	16
1.1 Background and Motivation.....	16
1.2 Objective.....	17
1.3 Scope of Works.....	17
1.4 Methodology.....	17
1.5 Expected Contribution.....	18
1.6 Literature Review.....	18
Chapter 2 Fundamental for Frequency Control in a Power System.....	21
2.1 Swing Equation.....	21
2.2 Model of an Electric System for Studying Frequency in Transient State.....	23
2.2.1 Model of Generator and Load.....	23
2.2.2 Model of a Speed Controller and Engine Prime Mover of Generator.....	25
2.2.3 Model of Equilibrium of an Electric Power and Frequency of a Power System.....	28
2.3 Frequency Response of a Power System.....	28
2.3.1 Primary Control.....	28
2.3.1.1 Primary Control in Grid-Tied Mode.....	29

2.3.1.2 Primary Control in Islanded Mode .....	30
2.3.2 Secondary Control.....	30
2.3 Tertiary Control.....	33
2.4 Interconnection of Microgrids with Tie-Line. ....	33
Chapter 3 Frequency Control of a Power System using Battery Energy Storage Systems (BESSs).....	36
3.1 Basic Idea .....	36
3.2 Literature Review Frequency Control of a Power System by Using BESS.....	37
3.2.1 Virtual inertia technique of BESS .....	37
3.2.2 Frequency control with two frequency control methods .....	38
3.2.3 Droop control for dynamic of SOC in Response to Frequency Change....	39
3.2.4 Transfer Functions of Energy Storage System using Time Delay .....	40
3.3 Virtual Droop Frequency Control.....	40
3.4 Virtual Inertia Frequency Control.....	41
Chapter 4 Power System of Mae Hong Son District .....	43
4.1 The Fundamental Data of Mae Hong Son Province .....	43
4.2 The Power Generation in Mueang Mae Hong Son District.....	44
4.3 The Power Distribution of Mueang Mae Hong Son District.....	45
Chapter 5 Investigation the Possibility of BESSs Design for Increasing the Stability of Frequency Response when the Large Disturbance Happens.....	48
5.1 Primary Response.....	48
5.1.1 Test System.....	48
5.1.2 Simulation Results .....	50
5.1.2.1 Effect of Various Virtual Droop Constant.....	50

5.1.2.1.1	Frequency Response .....	51
5.1.2.1.2	Rate of Change of Frequency.....	52
5.1.2.1.3	Power and Energy Discharged from the Battery.....	52
5.1.2.1.4	Power Generated from the Synchronous Generator.....	53
5.1.2.2	Effect of Various Virtual Inertia Constant.....	55
5.1.2.2.1	Frequency Response .....	56
5.1.2.2.2	Rate of Change of Frequency.....	56
5.1.2.2.3	Power and Energy Discharged from the Battery.....	56
5.1.2.2.4	Power Generated from the Synchronous Generator.....	57
5.1.2.3	Investigation Compares Help from BESS with Varying Control Methods .....	59
5.1.2.3.1	Frequency Response .....	59
5.1.2.3.2	Rate of Change of Frequency.....	60
5.1.2.3.3	Power and Energy Discharged from Battery .....	60
5.1.2.3.4	Power Generation from the Synchronous Generator.....	60
5.2	Primary and Secondary Response.....	63
5.2.1	Test System for the Microgrid on the Isolated Mode .....	63
5.2.2	Simulation Results for the Microgrid on the Isolated Mode.....	64
5.2.2.1	Effect of Various Virtual Droop Constant.....	65
5.2.2.1.1	Frequency Response .....	66
5.2.2.1.2	Rate of Change of Frequency.....	66
5.2.2.1.3	Power and Energy Discharged from the Battery.....	66
5.2.2.1.4	Power Generated from the Synchronous Generator.....	67
5.2.2.2	Effect of Various Virtual Inertia Constant.....	69

5.2.2.2.1	Frequency Response .....	70
5.2.2.2.2	Rate of Change of Frequency.....	70
5.2.2.2.3	Power and Energy Discharged from the Battery.....	70
5.2.2.2.4	Power Generated from the Synchronous Generator.....	71
5.2.2.3	Effect of varying the integral gain on the secondary response .....	73
5.2.2.3.1	Frequency Response .....	74
5.2.2.3.2	Rate of Change of Frequency.....	74
5.2.2.3.3	Power and Energy Discharged from the Battery.....	74
5.2.2.3.4	Power Generated from the Synchronous Generator.....	75
5.2.3	Test System for the Microgrid on the Connected Mode.....	77
5.2.4	Simulation Results for the Microgrid on the Connected Mode .....	80
5.2.4.1	Effect of an Instantaneous Load Increases on the Microgrid .....	80
5.2.4.1.1	Frequency Response .....	80
5.2.4.1.2	Rate of Change of Frequency.....	81
5.2.4.1.3	Power and Energy Discharged from Battery .....	82
5.2.4.1.4	Power Generation from the Synchronous Generator.....	82
5.2.4.1.5	Power at Tie-Line .....	83
5.2.4.2	Effect of Power at Tie-Line Instantaneous Disconnects .....	86
5.2.4.2.1	Frequency Response .....	86
5.2.4.2.2	Rate of Change of Frequency.....	86
5.2.4.2.3	Power and Energy Discharged from Battery .....	87
5.2.4.2.4	Power Generation from the Synchronous Generator.....	87
5.2.4.2.5	Power at Tie-Line .....	88

Chapter 6 Investigation the Possibility of BESSs Design for Increasing the Stability of Frequency Response when Using the Power from the Solar Cell .....	91
6.1 Islanding mode .....	91
6.1.1 The Highest Variation of Power Output from the Solar Cells During the Day.....	92
6.1.1.1 Test System .....	92
6.1.1.2 Simulation results.....	92
6.1.1.2.1 Frequency Response.....	92
6.1.1.2.2 Rate of Change of Frequency.....	93
6.1.1.2.3 Power and Energy Discharged from Battery .....	93
6.1.1.2.4 Power Generation from the Synchronous Generator.....	93
6.2 Grid Connected.....	96
6.2.1 The Highest Variation of Power Output from the Solar Cells During the Day.....	96
6.2.1.1 Test System .....	96
6.2.1.2 Simulation Results.....	97
6.2.1.2.1 Frequency Response.....	97
6.2.1.2.2 Rate of Change of Frequency.....	98
6.2.1.2.3 Power and Energy Discharged from Battery .....	98
6.2.1.2.4 Power Generation from the Synchronous Generator.....	99
6.2.1.2.5 Power at Tie-Line .....	100
Chapter 7 Conclusion and Future Work .....	103
7.1 Conclusion .....	103
7.2 Future Work.....	105
REFERENCES .....	106

VITA..... 112



จุฬาลงกรณ์มหาวิทยาลัย  
**CHULALONGKORN UNIVERSITY**



## LIST OF FIGURES

Figure 1.1 Example for setting the suitable frequency response of the synchronous generator operation .....	20
Figure 2.1 Model of frequency control at the synchronous generator.....	23
Figure 2.2 Dynamic model of generator .....	24
Figure 2.3 Dynamic model of load .....	24
Figure 2.4 Dynamic model of feedback control of generator and load .....	25
Figure 2.5 Simplified dynamic model of feedback control of generator and load .....	25
Figure 2.6 Droop characteristic of the generator.....	26
Figure 2.7 Dynamic model of a speed controller and engine prime mover.....	27
Figure 2.8 Dynamic model of the frequency control system of the synchronous generator .....	27
Figure 2.9 Dynamic model of a generator with primary control and secondary control .....	31
Figure 2.10 Droop characteristic of a generator when is adjusted a power generation .....	31
Figure 2.11 Interconnection model of two areas with tie-line connection.....	34
Figure 2.12 Block diagram of two interconnected microgrid systems .....	35
Figure 3.1 Model of the battery and the frequency control using virtual inertia techniques.....	38
Figure 3.2 Frequency Control Algorithm of Energy Storage System .....	39
Figure 3.3 Dynamic model of a battery controlled by droop characteristic.....	41

Figure 3.4 Dynamic model of a power system for studying the behaviour of frequency response which is a battery controlled by droop characteristic .....	41
Figure 3.5 Dynamic model of a battery controlled by virtual inertia .....	42
Figure 3.6 Dynamic model of a power system for studying the behaviour of frequency response which is a battery controlled by virtual inertia .....	42
Figure 4.1 Areas of the power distribution in Mae Hong Son province.....	44
Figure 4.2 Generation resource in Mueang Mae Hong Son province .....	45
Figure 4.3 Single line diagram of Mueang Mae Hong Son district.....	47
Figure 5.1 Simplified single line diagram of a system on the isolated mode .....	49
Figure 5.2 Block diagram of the test system.....	50
Figure 5.3 Block diagram of the test system with a virtual droop control.....	51
Figure 5.4 Effect of various virtual droop constant on only the primary response.....	54
Figure 5.5 Block diagram of the test system with a virtual inertia control.....	55
Figure 5.6 Effect of various virtual inertia constant on only the primary response .....	58
Figure 5.7 Effect of the microgrid with $RBESS = 2\%$ , $HBESS = 10 s$ , and combined $RBESS$ and $HBESS$ of the battery on only the primary response .....	62
Figure 5.8 Block diagram of the test system.....	64
Figure 5.9 Block diagram of the test system with a virtual droop control.....	65
Figure 5.10 Effect of Various Virtual Droop Constant on Both the Primary and Secondary Response.....	68
Figure 5.11 Block diagram of the test system with a virtual inertia control .....	69
Figure 5.12 Effect of Various Virtual Inertia Constant on Both the Primary and Secondary Response.....	72

Figure 5.13 Block diagram of the test system with combined the two control methods .....	73
Figure 5.14 Effect of Various Integral Gain of the Microgrid and Using the BESS with Combined the Virtual Droop and Virtual Inertia .....	76
Figure 5.15 Simplified single line diagram of a system on the connected mode.....	78
Figure 5.16 Block diagram for two areas with the combined model between a virtual droop and a virtual inertia.....	80
Figure 5.17 Effect of the Microgrid with or without Applying the BESS when the Large Disturbance Happens on the Microgrid.....	85
Figure 5.18 Effect of Disconnecting Switch at Tie-Line with or without Applying the BESS on the Microgrid.....	90
Figure 6.1 The Highest Variation of Power Output from the Solar Cells During the Day on an Isolated Microgrid.....	95
Figure 6.2 The Highest Variation of Power Output from the Solar Cells During the Day on a Connected Mode Microgrid.....	102

## LIST OF TABLES

Table 5.1 Value of each parameter in a block diagram of the test system .....	50
Table 5.2 Value of each parameter in a block diagram of the test system with a virtual droop control and only primary response .....	51
Table 5.3 Value of each parameter in a block diagram of the test system with a virtual inertia control and only primary response .....	55
Table 5.4 Value of each parameter in a block diagram of the test system with primary and secondary response .....	64
Table 5.5 Value of each parameter in a block diagram of the test system with a virtual droop control and secondary response.....	65
Table 5.6 Value of each parameter in a block diagram of the test system with a virtual inertia control and secondary response .....	70
Table 5.7 Value of each parameter in a block diagram of the test system with combined the two control methods.....	74
Table 5.8 Value of each parameter in a block diagram of the test system for two areas with the combined model between a virtual droop and a virtual inertia .....	79

## Chapter 1

### Introduction

#### 1.1 Background and Motivation

Nowadays, many microgrids can isolate entirely from the main grid. In a microgrid, local generators have a potential to generate the electric power to feed the local load by themselves. For example, a small local distributed generator system supplies the electric power directly to the committed load or an isolated island is supplied by distributed generators. However, when a large disturbance happens, the microgrids should balance the local generation and load by themselves and keep distributing power to a local load. However, to control power in an isolated microgrid is complicated.

However, in large power systems, synchronous generators provide frequency regulation. The isolated microgrids have low inertia because there are few synchronous generators. Many generations in the microgrids are renewable energy generations, such as photovoltaic power generation and wind power generation. These two generations are connected through the inverter and do not provide inertia. Therefore, when a disturbance occurs, a large frequency deviation happens on a system, and a blackout may occur. Isolated microgrids use the battery energy storage systems (BESSs) to handle the issue due to the fast response.

The BESSs are connected to the microgrid system through inverters due to the high flexibility of controlling real power and reactive power. Furthermore, to design the strategy to control electricity through inverter has many issues such as the impact of low inertia on microgrid stability [1], effect of high penetration of renewable energy sources in low inertia microgrids [2], voltage sags and swells subsequent to the islanding transition of microgrids [3], and generation and load balance in microgrids during islanded operation [4].

According to [5], BESS is installed in the microgrid to help the synchronous generator for increasing the stability of the microgrid frequency. The structures of the BESS control system [6], such as a virtual droop [7] and virtual inertia [8] - [9], provide different frequency responses. There are limitations to charge and discharge the

amount of power and energy to BESS, which depending on the size of the BESS. The frequency response results can be the guideline for choosing the size of BESS installed in the microgrid.

This thesis focuses on using BESS to maintain the appropriate range of microgrid frequency during a disturbance in isolated mode and grid-connected mode. The primary and secondary frequency response of BESS are investigated.

### **1.2 Objective**

The objective of this thesis is to study and compare the performance of control strategies of BESS for providing primary and secondary frequency support of the microgrid in grid-connected and isolated modes.

### **1.3 Scope of Works**

1. Consider a microgrid in grid-connected and isolated modes.
2. Consider a microgrid that consists of a synchronous generator, photovoltaic power plant, BESS, and load.
3. Consider a large disturbance such as a rapid increase of load a continuous variation of solar generation.
4. Consider both primary and secondary responses of a microgrid to a frequency deviation.
5. Not consider the voltage stability of a microgrid.

### **1.4 Methodology**

1. Review literature on both primary and secondary responses of the microgrid in grid-connected and isolated modes.
2. Review literature on the effects of an isolated low moment of inertia and methodology to increase the frequency stability of the microgrid.
3. Review literature on using BESS to provide frequency support in the microgrid.
4. Formulate problem and design thesis structure and methodology.
5. Study a model of a microgrid system and build a model to investigate the stability of frequency response when a large disturbance happens.

6. Perform case studies to evaluate the performance of BESS in providing both primary and secondary responses to the microgrid in grid-connected and isolated modes.
7. Discussion of the results and conclude the work.

### 1.5 Expected Contribution

The microgrid in both grid-connected and islanding mode can operate with high stability of frequency with the help from BESS when a large disturbance happens.

### 1.6 Literature Review

There is an increase of a ratio between a generator without a moment of inertia and a synchronous generator over the last few years. In a power system, this phenomenon is called a low inertia system. From the research [2], by analysing the problem and effect of the event in the past, the moment of inertia in an extensive system was constant. However, an inverter has played an essential role in a power system over the last few years. A moment of inertia of a system changes over time based on load and the weather, e.g., sunlight and wind. From the reason above, a frequency regulation device should be able to regulate deviated frequency instantaneously. Moreover, from the research [10], the loss of stability of frequency so that a load is cut off from a system and a blackout occurs and spreads out to a large area. The leading cause does not come from a fault in the system but comes from the disconnecting of an inverter that connects between a renewable energy generation and the primary grid. The inverter can control in an instantaneous time to maintain the stability of a system. The research [5] proposes an idea of frequency response, which can categorise into two parts: primary control and secondary control by the speed of frequency response devices: a synchronous diesel generator and a battery connected through an inverter. The research above shows that the speed of frequency response significantly depends on the types of devices. The study [7] proposes an equation for calculating a critical time of a system, which is how long before a system losing its frequency stability. With considering a critical time to set a delay time on a device, therefore frequency stability of a system is increased.

The researches [6-9] propose an idea of increasing the stability of a power system by controlling the dynamic behaviour of an inverter to be the same as in the synchronous generator. This idea called the synchronous virtual machine, which can generate a moment of inertia for a power system. An input power resource of an inverter is a device that is a DC power such as a solid oxide fuel cell: SOFC [6], Supercapacitor [9], and battery [5,8]. A controllable inverter creates a dynamic behaviour to be the same as in synchronous generator when a large disturbance happens.

The research [11] shows that when a massive renewable energy generation connects to a grid, the frequency stability is subject to decrease. Hence, the vast renewable energy generation is required to have a spinning reserve to online-generate a power to generate power to a grid when a disturbance happens. The research [12] proposes a control system of the vast renewable energy generation to use a controller that can control by nonlinear control. The objective of a nonlinear control is to increase stability to a system due to it is a wide range for frequency activity.

From the researches above, a power system is subject to maintain the stability of the frequency of a system when a disturbance happens, and the synchronous generator still operates on a frequency deviated from a standard value[13]. Three frequency response indices are used to evaluate the status of a system

1. frequency nadir–the maximum frequency deviation,
2. rate of change of the frequency (*ROCOF*), and
3. standard deviation (*S*) of the frequency response follows:

$$S = \sqrt{\frac{1}{N-1} \sum_{i=1}^N (x_i - \bar{x})^2} \quad (1.1)$$

where  $\bar{x}$  is the sample mean of the group of frequency data,  
 $N$  is the number of sample frequency data.

In practice, a generator has a protection device (Underfrequency Relay: 81U) to prevent a heavy damage form the large frequency deviation. However, the period in some disturbances is a little bit short. If the generator is cut out from the system on that period, it may contribute the large damage to the system and a blackout certainly happens. Hence, the time setting delay of protection device [13] is the



significant factor for this situation to consider shedding load. Figure 1.1 shows how to set the protection device by considering the frequency nadir and the *ROCOF*. The generator will not be allowed to trip out from the system. The generator can help the system to regulate the frequency and increase the stability of the system. The time delay is set into the generator when has a low frequency by considering from the turbine prohibited area [13].

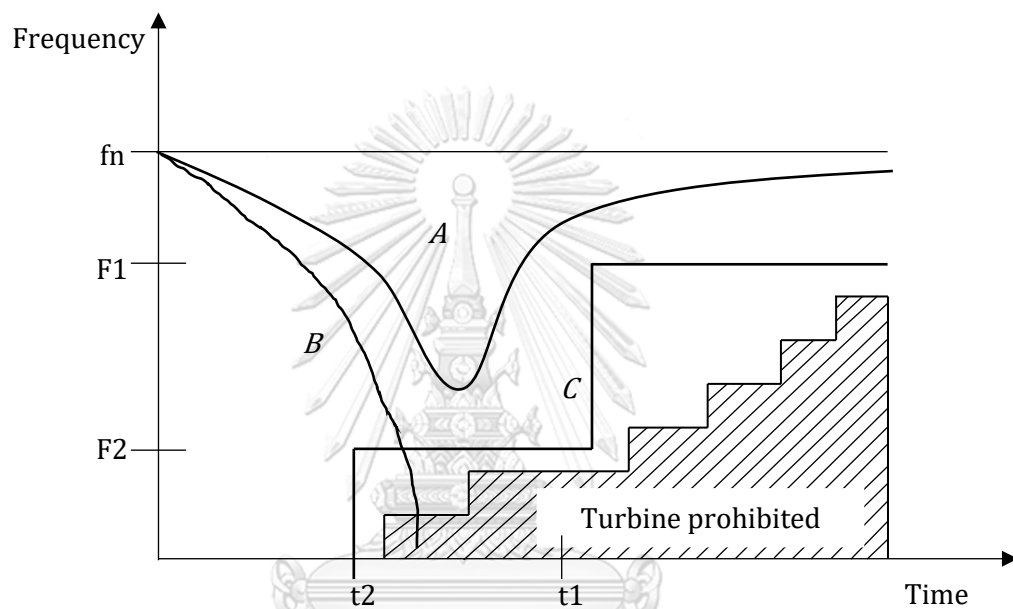


Figure 1.1 Example for setting the suitable frequency response of the synchronous generator operation

- where
- A* System frequency response with minimum load shed for recovery,
  - B* System frequency response with under shedding of load,
  - C* Optimum underfrequency protection characteristic.

## Chapter 2

### Fundamental for Frequency Control in a Power System

The concept for controlling frequency in a power system is to maintain the appropriate range of frequency. In other words, power generation and power usage should be equal. A generator is a device that maintains the power generation to produce approaches to power usage. The first section describes the swing equation, which explains the behaviour of the synchronous generator. The second section describes a model of power system for studying frequency in a transient state, the frequency response when the frequency deviates from the standard level. The third section describes the interconnection of microgrids with a tie-line.

#### 2.1 Swing Equation

The swing equation describes the behaviour of a rotor at the synchronous generator. By considering Newton's law, the moment of the rotor follows:

$$T_m - T_e = J \frac{d\omega_m}{dt} \quad (2.1)$$

where  $T_m$  is a mechanical torque supplied by the prime engine mover (newton - meter),  
 $T_e$  is an electrical torque output of the alternator (newton - meter),  
 $J$  is the total moment of inertia of the rotor at synchronous generator and turbine prime mover (kilogram - square meter),  
 $\omega_m$  is synchronous angular speed (radian per second).

A mechanical torque of a generator is equal to the opposite direction of an electrical torque in a steady-state. Therefore, a generator always rotates with a constant speed of synchronous speed.

By multiplying by  $\omega_m$ . The result follows:

$$T_m \omega_m - T_e \omega_m = J \omega_m \frac{d\omega_m}{dt} \quad (2.2)$$

$$P_m - P_e = J \omega_m \frac{d\omega_m}{dt} \quad (2.3)$$

where  $P_m$  is a mechanical power supplied by the prime engine mover (watt),

$P_e$  is an electrical power output of the alternator (watt).

Since,

$$\omega_m = \frac{d\theta_m}{dt} \quad (2.4)$$

$$\frac{d\omega_m}{dt} = \frac{d^2\theta_m}{dt^2} \quad (2.5)$$

and

$$\theta_m = \omega_{sm}t + \delta_m \quad (2.6)$$

$$\frac{d\theta_m}{dt} = \omega_{sm} + \frac{d\delta_m}{dt} \quad (2.7)$$

$$\frac{d^2\theta_m}{dt^2} = \frac{d^2\delta_m}{dt^2} \quad (2.8)$$

where  $\theta_m$  is an angular position of the rotor respect to a stationary axis (radian),

$\omega_{sm}$  is synchronous angular speed (radian per second),

$\delta_m$  is an angular position of the rotor respect to a mechanical rotor axis (radian).

By substituting (2.8) in (2.3). The result follows:

$$P_m - P_e = J\omega_m \frac{d^2\delta_m}{dt^2} \quad (2.9)$$

Usually, the power loss of a generator does not consider. Moreover, the kinetic energy from a rotating of the rotor depends on the angular speed of the rotor. In practical, an angular speed of a generator is always approximately equal to an angular synchronous speed either in a steady-state or disturbance happens. From the reason above, the kinetic energy can consider in terms of a constant value. The aggregated system inertia ( $H$ ) defines the constant kinetic energy. The aggregated system inertia is a ratio between the kinetic energy and the rated power of a generator. The equation follows:

$$H = \frac{\frac{1}{2}J\omega_{sm}^2}{S_{base}} \quad (2.10)$$

where  $H$  is the aggregated system inertia of synchronous generator and a prime mover (second),

$S_{base}$  is the rated power of the synchronous generator (volt-ampere).

By dividing (2.9) by  $S_{base}$  and then substituting (2.7). The result follows:

$$\bar{P}_m - \bar{P}_e = \frac{2H}{\omega_m} \frac{d^2\delta_m}{dt^2} \quad (2.11)$$

where  $\bar{P}_m$  is a mechanical power supplied by the prime engine mover (per unit),

$\bar{P}_e$  is an electrical power output of the alternator (per unit).

## 2.2 Model of an Electric System for Studying Frequency in Transient State

The model of the electric system is to study frequency in a transient state. The objective of the study is to maintain the frequency of the power system when the generator is rapidly changed power generation or when the load usage is instantaneous increased/decreased. The model consists of the structure in a dynamic state of an electrical power device. The frequency control system adjusts the deviated frequency by sending an input signal to a generator to increase or decrease a generation power. Figure 2.1 presents a model of frequency control at the synchronous generator.

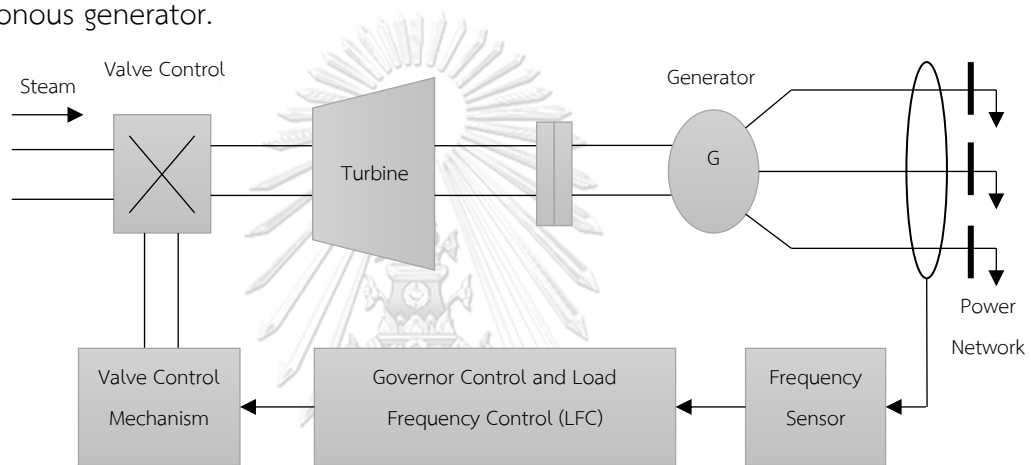


Figure 2.1 Model of frequency control at the synchronous generator

### 2.2.1 Model of Generator and Load

A mathematical model of a generator is starting from linearise (2.11). Then the equation follows:

$$\frac{\omega_m}{2H} (\Delta \bar{P}_m - \Delta \bar{P}_e) = \frac{d^2 \Delta \delta_m}{dt^2} \quad (2.12)$$

where  $\Delta \delta_m$  is the change of an angular position of the rotor respect to a mechanical rotor axis (radian),

$\Delta \bar{P}_m$  is the change of mechanical power supplied by the prime engine mover (per unit),

$\Delta \bar{P}_e$  is the change of an electrical power output of the alternator (per unit).

By substituting (2.4) in (2.12) and dividing by  $\omega_m$ . Then the equation follows:

$$\frac{1}{2H} (\Delta \bar{P}_m - \Delta \bar{P}_e) = \frac{d \Delta \bar{\omega}_m}{dt} \quad (2.13)$$

where  $\Delta \bar{\omega}_m$  is the change of synchronous angular speed (per unit).

By taking Laplace transform to (2.13). The result follows:

$$\frac{1}{2Hs} [\Delta\bar{P}_m(s) - \Delta\bar{P}_e(s)] = \Delta\bar{\omega}(s) \quad (2.14)$$

The generator model comes from transforming (2.14) to a block diagram.

Figure 2.2 presents a dynamic model of a generator.

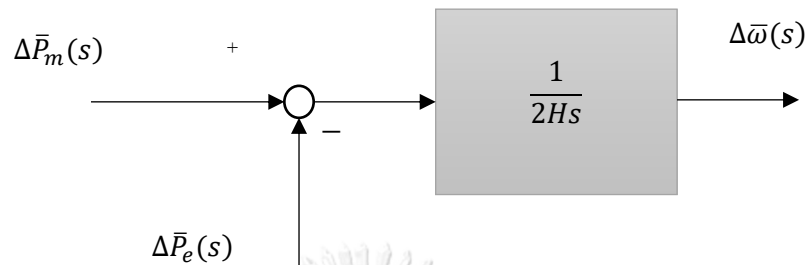


Figure 2.2 Dynamic model of generator

Load in a power system can categorise into two groups: independent load and dependent load. An independent load does not depend on the frequency of a system, such as an incandescent light bulb and heater. On the opposite, a dependent load is excited by the sinusoidal source, such as capacitors and inductors. The (2.15) presents the total load in a system.

$$\Delta\bar{P}_e = \Delta\bar{P}_L + D\Delta\bar{\omega} \quad (2.15)$$

where  $\Delta\bar{P}_L$  is the change of independent load power (per unit),  
 $D$  is a ratio between the change of power at load and the change of frequency.

The first term and the second term of (2.15) show the change of independent load power and independent load power, respectively. By taking Laplace transform to (2.15). Then the equation follows:

$$\Delta\bar{P}_e(s) = \Delta\bar{P}_L(s) + D\Delta\bar{\omega}(s) \quad (2.16)$$

Figure 2.3 presents a dynamic model of the total load in a system after taking the Laplace transform.

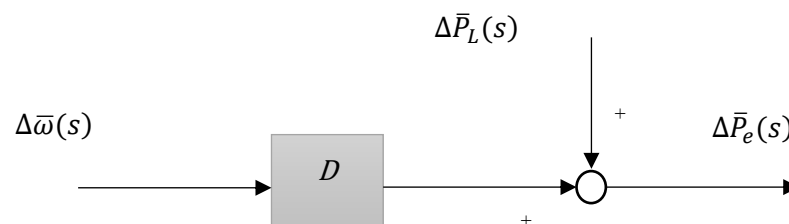


Figure 2.3 Dynamic model of load

The (2.17) presents a feedback control of the generator and load by combining (2.14) and (2.16). The equation follows:

$$\frac{1}{2Hs} [\Delta\bar{P}_m(s) - \Delta\bar{P}_L(s) - D\Delta\bar{\omega}(s)] = \Delta\bar{\omega}(s) \quad (2.17)$$

Figure 2.4 presents a dynamic model of feedback control of generator and load.

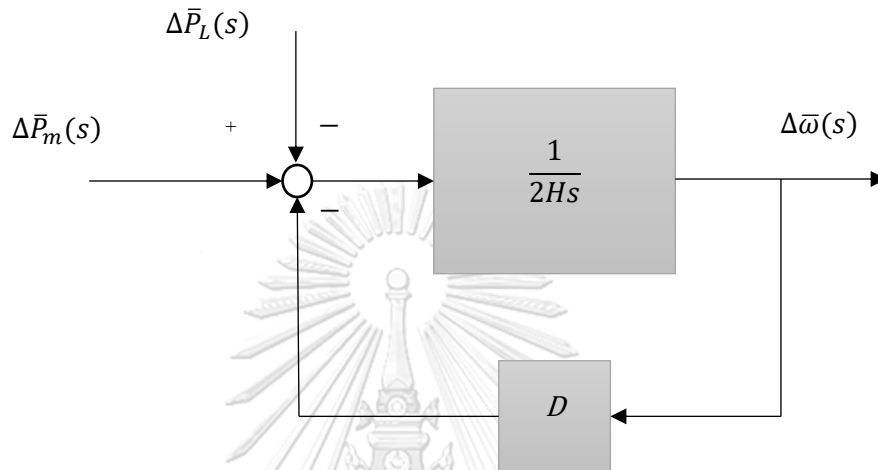


Figure 2.4 Dynamic model of feedback control of generator and load

Figure 2.5 is the simplified dynamic model of feedback control of the generator and load from figure 2.4.

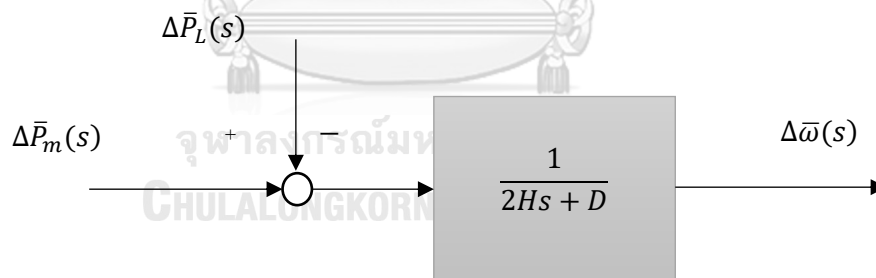


Figure 2.5 Simplified dynamic model of feedback control of generator and load

### 2.2.2 Model of a Speed Controller and Engine Prime Mover of Generator

A mechanical power generated from a generator is converted to electrical power by coming from various prime engine movers such as steam turbines and gas turbines. There are two components in power conversion, which are a governor and a prime engine mover. First, a governor is a speed controller of a generator that adjusts the speed of a turbine approach to the synchronous speed. The controller receives a frequency deviation signal. After that, the controller evaluates to increase

or decrease the generation of the generator by adjusting at the valve control mechanism. The valve controls the direction of steam if it is a steam turbine or adjusts an angle of the door which controls the amount of water if it is a water turbine.  $\tau_G$  is time constant for speed control of a speed controller device of the generator. Second, a prime engine mover. When a speed controller is already turned on, the mechanical output power from the prime mover converts to the electrical power on a delayed time constant  $\tau_T$ . The delayed time constant depends on the types and complexity of the turbine.

An input signal is the change of a reference signal ( $\Delta\bar{P}_{ref}$ ) which control the speed of an engine prime mover ( $\Delta\bar{P}_G$ ). The speed control of prime engine mover is operated by following droop characteristic. Figure 2.6 shows the droop characteristic graph. A slope of the graph is a droop constant. An equation of droop characteristic follows:

$$\Delta\bar{P}_G = -\frac{1}{R}\Delta\bar{\omega} + \Delta\bar{P}_{ref} \quad (2.18)$$

where  $\Delta\bar{P}_{ref}$  is the change of a reference signal of the generator (per unit),  
 $R$  is droop characteristic of the frequency of a system.

By taking Laplace transform to (2.14). Then the equation follows:

$$\Delta\bar{P}_G(s) = -\frac{1}{R}\Delta\bar{\omega}(s) + \Delta\bar{P}_{ref}(s) \quad (2.19)$$

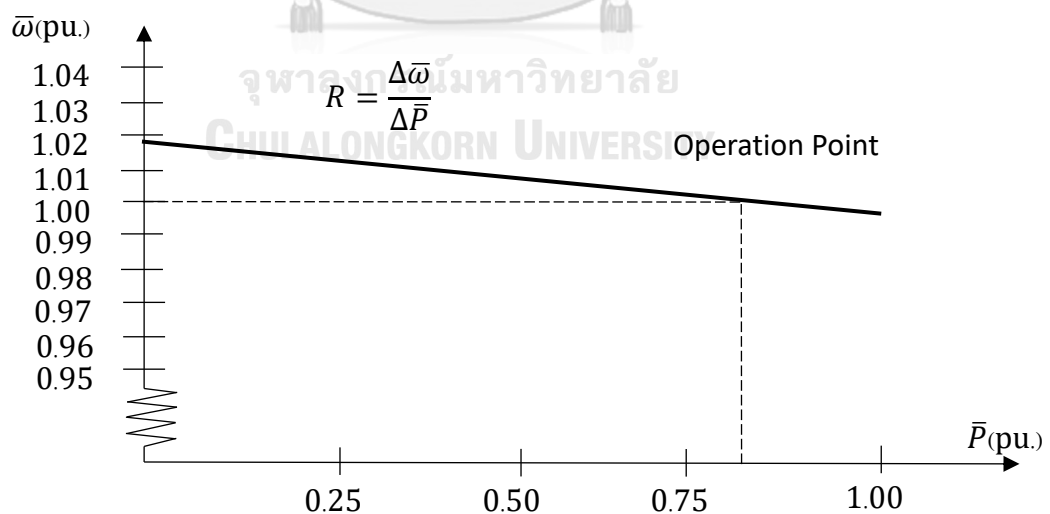


Figure 2.6 Droop characteristic of the generator

Figure 2.7 presents a dynamic model of a speed controller device and prime engine mover of a generator. The governor receives  $\Delta\bar{P}_G$  from droop control to adjust

the power at valve control ( $\Delta\bar{P}_V$ ). The relationship between  $\Delta\bar{P}_G$  and ( $\Delta\bar{P}_V$ ) is followed by:

$$\Delta\bar{P}_V(s) = \frac{1}{1+\tau_G s} \Delta\bar{P}_G(s) \quad (2.20)$$

where  $\Delta\bar{P}_V(s)$  is the change of the power at valve control (per unit),  
 $\Delta\bar{P}_G(s)$  is the change of the power at governor (per unit),  
 $\tau_G$  is time constant for speed control of a speed controller device of the generator,

and the relationship between  $\Delta\bar{P}_V$  and ( $\Delta\bar{P}_m$ ) is followed by:

$$\Delta\bar{P}_m(s) = \frac{1}{1+\tau_T s} \Delta\bar{P}_V(s) \quad (2.21)$$

where  $\tau_T$  is time constant for speed control of a speed controller device of turbine.

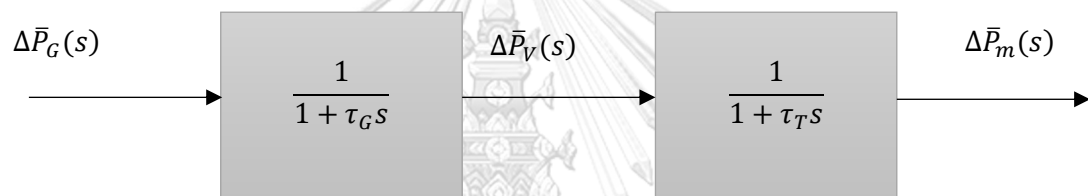


Figure 2.7 Dynamic model of a speed controller and engine prime mover

Figure 2.8 presents a dynamic model of power system when merges a model of a speed controller and prime engine mover of the generator with a dynamic model of feedback control of generator and load.

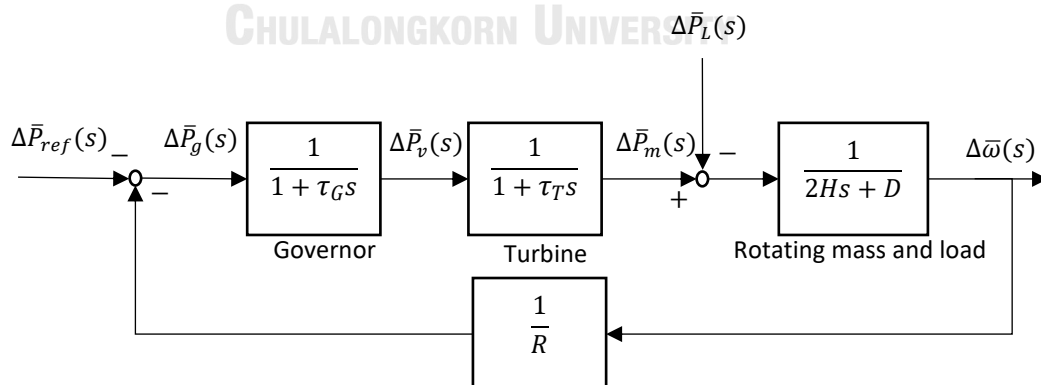


Figure 2.8 Dynamic model of the frequency control system of the synchronous generator



### 2.2.3 Model of Equilibrium of an Electric Power and Frequency of a Power System

A model of the frequency of the power system comes from a model of the frequency of the synchronous generator. The model can apply by setting the frequency of the synchronous generator to be equal to the frequency of a system and adjust all parameters of the model to be a parameter of a system. The (2.22) shows a moment of inertia of the system and (2.23) shows a ratio of change of power at load and change of frequency of a system.

$$H_{sys} = \frac{\sum_i^{n_g} H_i S_i}{S_{sys}} \quad (2.22)$$

$$D_{sys} = \frac{\sum_i^{n_g} D_i S_i}{S_{sys}} \quad (2.23)$$

where  $H_{sys}$  is a moment of inertia of a system,  
 $D_{sys}$  is a deceleration of a system,  
 $H_i$  is a moment of inertia of each generator,  
 $D_i$  is a deceleration of each generator,  
 $S_i$  is a rated power of each generator,  
 $S_{sys}$  is the total rated power of generators in a system (real-time),  
 $n_g$  is the number of online-generators in a system (real-time).

### 2.3 Frequency Response of a Power System

The objective of frequency control of a generator is to maintain the frequency of a power system approaches to an appropriate range of frequency during a disturbance. For example, a large generator suddenly turns off or instantaneous load increases/decreases. The size of a disturbance may be large or small, but it positively affects the frequency of a system. Frequency response in a power system can categorise into two types by considering a control system on a generator: primary control and secondary control.

#### 2.3.1 Primary Control

Primary control automatically occurs on the synchronous generator. The primary control can provide the combined actions of the speed governor control at the generating units and the frequency sensitive damping effects at the load to stop

the frequency deviation. The frequency control mechanism of the primary control can categorise into two mechanisms.

### **Moment of Inertia of Generator and Prime Engine Mover**

When a disturbance happens, mechanical power is not equal to the electrical power. A generator will produce/consume the stored kinetic energy at a rotor to compensate inequality of power between the mechanical power and to the electrical power. This compensation effects the speed of the rotor in a generator and frequency of a system. A large generator has a high moment of inertia; therefore, the speed of a generator will a little bit change compared to a small generator, which has a low moment of inertia.

### **Droop Characteristic of a Generator**

Figure 2.7 is a relationship between the speed of a generator and an electrical power produced from a generator. A slope of the graph (Droop constant) usually is 3 – 5 per cent. Figure 2.8 explains the behaviour of the frequency response. When the frequency of a system decreases, a generator will increase the generation of an electrical power to stop decreasing the frequency of a system. Moreover, the droop characteristic of a generator will control each generator to operate following a ratio of deviated frequency and a nominal value.

Moreover, the literature reviews [14], [15], [16], [17], [18], [19], and [20] can conclude the primary response to two modes: grid-tied mode and islanded mode.

#### *2.3.1.1 Primary Control in Grid-Tied Mode*

The current source inverter works in grid-connected mode to collect voltage and frequency setpoints from the main grid. The host grid sets up the voltage and frequency of the microgrid system. The local controller in a microgrid is trying to extract maximised power by exploiting the maximum power point tracking (MPPT) algorithm [21], [22] from renewable energy sources. The current source inverter uses two regulating loops: the first loop for regulating current injected to the grid, and the second loop is to set the current reference to deliver proper power to the grid. The different current regulating techniques can categorise into two types: linear and non-linear controllers [22], [23].

### 2.3.1.2 Primary Control in Islanded Mode

In the primary control in islanded mode is divided into two modes: control without communication and control with communication.

#### **Control without Communication**

Droop method is commonly used in this level of control because there is no need for any communication link in the droop method. From literature review [14], [17], [24], [25], and [26] can separate the droop control into three droop controlling stages: internal voltage/current regulation loop, intermediate virtual impedance loop to minimise line impedance effect on droop based control, and external power-sharing loop for proper sharing of real power and reactive power with the parallel-connected inverters. The reasons that there are three loops are preventing circulating current without communication and regulating the voltage and current references to be supplied in the internal regulating loop. Although the advantage of the droop method is no need for any communication, there are many drawbacks effects discussed in [14], [17], [27], and [28], which limit its applications.

#### **Control with Communication**

There is a high bandwidth communication link such as LAN/Ethernet, Optical fibre transmission, between communication-based control modules to achieve good proper power-sharing and good voltage regulation. However, with the distributed system in islanded mode; therefore, it uses long-distance communication lines, which are expensive. Moreover, there are problems with limits system reliability due to the system can easily get affected, and the problem with plug-n-play capability. However, there is some example of communication-based methods such as concentrated control [16], distributed control method, including, distributed networked control [28], master/slave control method including auto master/slave control strategy [29], and control with or without central controller [30].

### 2.3.2 Secondary Control

The secondary control refers to a supplementary control effort to return the frequency to the nominal value, e.g., 50 or 60 *Hz*, through an integral control action. The other name of secondary control is automatic generation control: AGC. A system receives a deviated frequency signal from a controller and then sending a new

reference signal to each generator. The generators adjust a generation rate following the new reference signal to bring a frequency back to a nominal value. Figure 2.9 describes a mechanism of an increase or a decrease of a power generation of a generator followed by adjusting a reference power signal ( $\Delta\bar{P}_{ref}$ ). Figure 2.10 shows that when synchronising a generator to the main grid, a generator speed is at a constant synchronous speed in nominal value. From an ideal droop characteristic graph suggests that by shifting the graph to the left, the power generation of a generator will decrease, but the speed of the generator still not change.

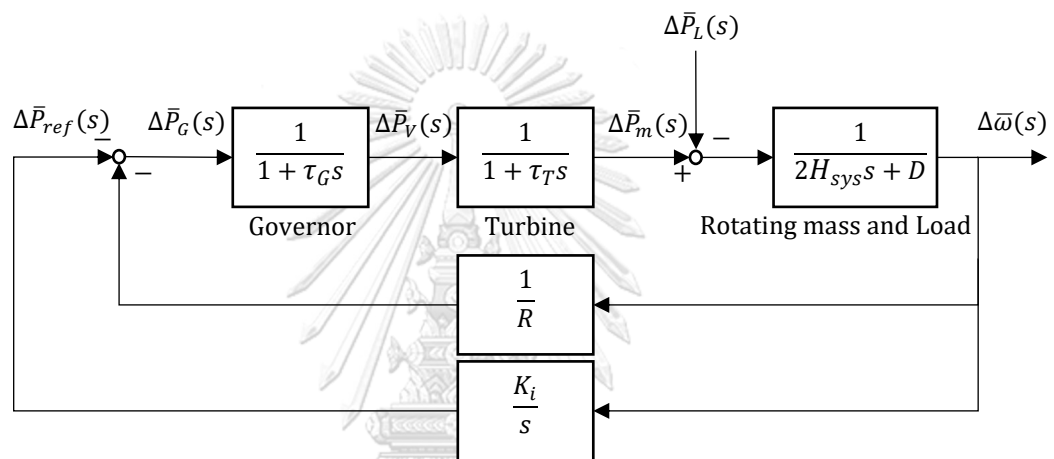


Figure 2.9 Dynamic model of a generator with primary control and secondary control

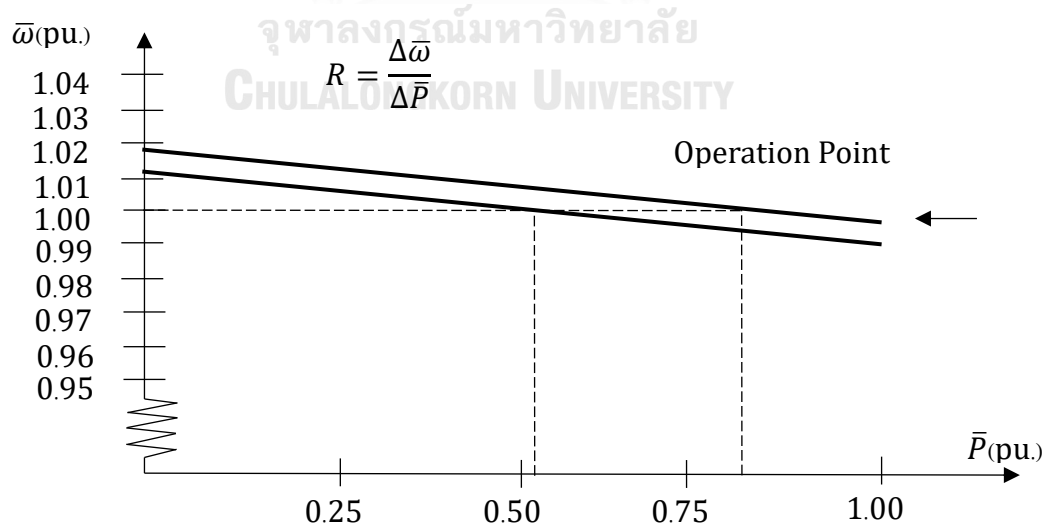


Figure 2.10 Droop characteristic of a generator when is adjusted a power generation

Moreover, from the literature reviews [14], [28], [31], and [32] can conclude the secondary response to three controlling concepts: centralized control, distributed control, and decentralized control concept.

### **Centralised Secondary Control**

The centralised technique uses a high-speed communication link between control modules. The centralised control can control by the utilisation of a microgrid central controller. The fundamental control levels consist of three levels: distributed management system, local micro-source and controller, and microgrid central controller. The local controller is the device that incorporates the primary control level. The microgrid central controller can activate an online optimisation framework by using a limited bandwidth interaction link to generate relevant information at a singular point instantaneously [14], interfaces between the distribution management system and microgrid. The central secondary response can examine power produced by renewable energy generators in the microgrid and can regulate load demand to serve or shed controllable loads for balancing demand and supply from the central controller [31].

However, there are some drawbacks with centralised secondary control such as it suitable for small microgrid where the system arrangement is almost stable and issue about single point breakdown in the microgrid control centre or any communication system.

### **Distributed Secondary Control**

The literature review [28] presents a distributed networked control scheme. The distributed technique uses wireless communication such as Zigbee and WiFi, to communicate between control modules. Due to this scheme does not require to use a communication link, the distributed control can happen for an extensive and flexible microgrid system. Any decision making is successful based on local information without help from the microgrid control centre or any high bandwidth communication facilities [32]. The monitoring interaction in each unit of distributed control can allocate controlling duty among the units to control duty to various units depending on operation in various time frames [28]. The example of the distributed control techniques are multi-agent system based techniques including combination

of multi-agent system with cooperative control [33], distributed cooperative control [34], hierarchical multi-agent system based energy management system [35], agent base control of islanded microgrid [36], distributed model predictive control [37], averaging PI control [38], and non-linear distributed control [39].

### **Decentralised Secondary Control**

Without having any communication facility among the subsystem in decentralised controlling, the decentralised technique does not require to have any communication framework among distributed generator units [32]. This control scheme presents poor system-wide performance [28]. The only controller used in this control scheme is the droop control controller that is similar in the primary control without communication.

### **2.3 Tertiary Control**

The literature reviews [14], [17], [22], and [28] present that the tertiary control level or global control level is the final controlling stage of the microgrid. The tertiary control is mainly operated on grid-tied mode and remain inactive in islanded mode. The objective of tertiary control of the microgrid is to facilitate energy generation and market policy by utilising a market operator which acts on market and distribution network operator which connects with different microgrids. The microgrid should regulate high-quality power flow between the main grid and microgrid.

Furthermore, the tertiary control of microgrid must utilise transmission system operator and microgrid operating manager to produce set points of frequency and voltage for the secondary control level. Also, the tertiary control of microgrid should integrate a main grid and microgrid or additional microgrid sub-systems, including predicting instantaneous load changes and storages capabilities.

Moreover, non-planned islanding detection, overall supervision of reactive power, and offering the best economic performance by utilising gossiping based method and game theory are also including in an objective of the tertiary control.

### **2.4 Interconnection of Microgrids with Tie-Line.**

Considering the reliability of power supply to the connected load can achieve by the help of interconnection neighbouring isolated microgrids through tie-line. For more than one area of a power system, the microgrid can assume as the control

area. The control characteristic of each area to determine participation to respond to system frequency variation can control through the tie-line. When the disturbance happens, the tie line can use to exchange energy between control areas to inter-area support.

Figure 2.11 presents an interconnection microgrid with two areas. The deviate frequency of each area occurs when a mismatch between the power generation and load usage [40].

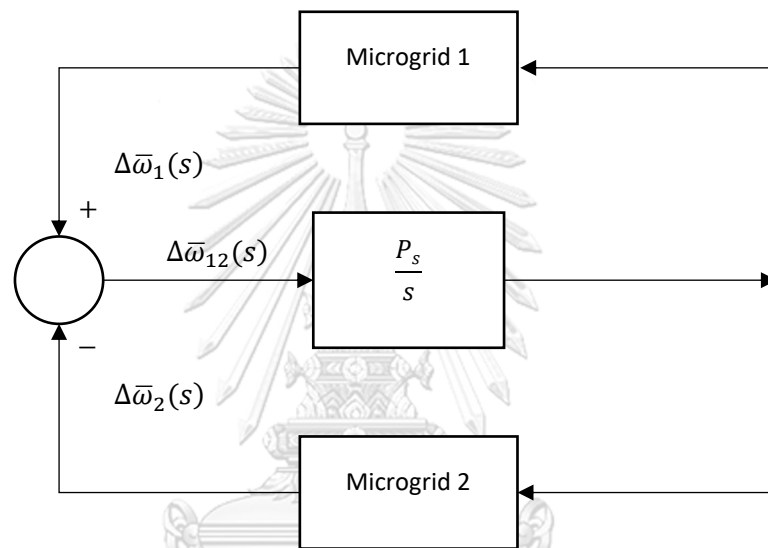


Figure 2.11 Interconnection model of two areas with tie-line connection

To explain to the relationship between two areas with the tie-line connection. The tie-line power deviation can describe as:

$$\Delta \bar{P}_{tie} = P_s (\int \Delta \bar{\omega}_1 dt - \int \Delta \bar{\omega}_2 dt) \quad (2.24)$$

where  $\Delta \bar{P}_{tie}$  is tie-line power deviation (per unit),  
 $P_s$  is synchronising power coefficient,  
 $\Delta \bar{\omega}_1$  is the change of synchronous angular speed in area 1 (per unit),  
 $\Delta \bar{\omega}_2$  is the change of synchronous angular speed in area 2 (per unit).

By taking Laplace transform to (2.24). The result follows:

$$\Delta \bar{P}_{tie}(s) = P_s \cdot \frac{1}{s} \Delta \bar{\omega}(s) \quad (2.25)$$

$$\frac{\Delta \bar{P}_{tie}(s)}{\Delta \bar{\omega}(s)} = \frac{P_s}{s} \quad (2.26)$$

The area control error (ACE) of the  $i^{th}$  microgrid can describe as (2.27) and figure 2.12 presents the block diagram of two interconnected microgrid systems that shows the microgrid can control by frequency deviation ( $\Delta\bar{\omega}$ ) or ACE.

$$ACE_i = \sum_{j=1}^n \Delta\bar{P}_{ij} + B_i \Delta\bar{\omega}_i \quad (2.27)$$

where  $ACE_i$  is the area control error of  $i^{th}$  microgrid,  
 $\bar{P}_{ij}$  is the power transferred from  $i^{th}$  microgrid to  $j^{th}$  microgrid,  
 $B_i$  is the frequency bias factor for  $i^{th}$  microgrid,  
 $\Delta\bar{\omega}_i$  is the change of synchronous angular speed in the area  $i^{th}$  (per unit).

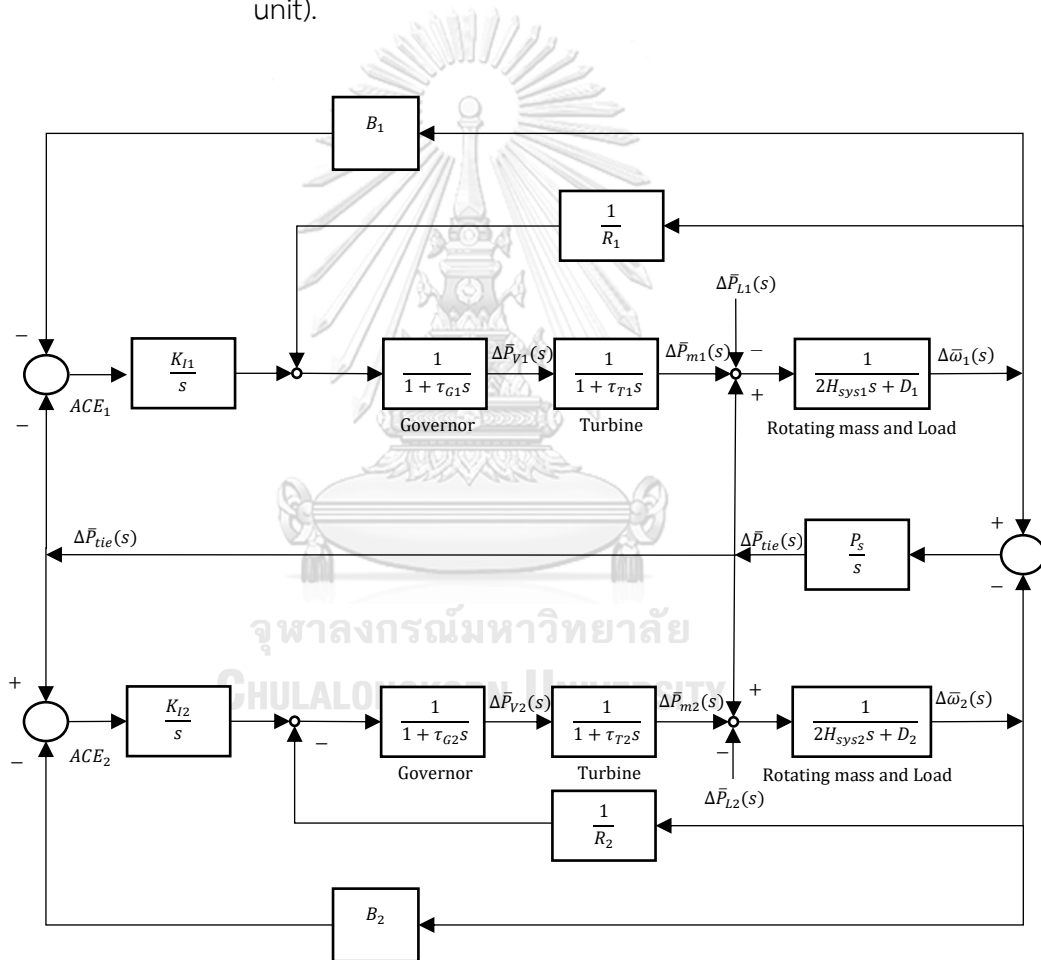


Figure 2.12 Block diagram of two interconnected microgrid systems



## Chapter 3

### Frequency Control of a Power System using Battery Energy Storage Systems (BESSs)

This chapter describes a basic idea of controlling battery energy storage systems (BESSs) to have a dynamic behaviour equivalent to the synchronous generator. The main idea for controlling the BESSs is to increase the stability of a power system when the frequency has deviated from a nominal value. The concept of controlling the BESSs can be categorised into two methods: virtual droop control and virtual inertia control.

#### 3.1 Basic Idea

Frequency on a power system has deviated from a nominal value when a generation power is not equal to load, and the sizes of a disturbance are various. The basic idea of frequency control of a power system is to adjust a generation power to be equal to load. A cause of disturbance comes from many events such as a short circuit at a transmission line, a generator is cut off by maloperation of a protection device, instantaneous load increases/decreases, and a distributed transmission line is cut off. The reason above leads a generation power to be not equal to load.

When a disturbance happens, frequency responses, both primary and secondary control, are automatically operated to stop the deviated frequency and bring the frequency back to the nominal value. On the other hand, the mechanism of frequency control is adjusting a power generation to be equal to power at load before a protection device detecting over/under frequency. Because of cutting a generator off while a system is subject to a large frequency deviation, a blackout may occur and sending effect to a large area. A moment of inertia of an isolated system is low because a high ratio between a renewable energy generation and the synchronous generator and size of synchronous generator small, then it also provides a small moment of inertia. For these reasons, an isolated power system cannot handle deviated frequency when a large disturbance happens.

The thesis brings a basic idea using BESSs to handle the stability of frequency. The battery can connect to the microgrid through an inverter that converts DC power

to AC power. If it can control an inverter to have a dynamic behaviour as a synchronous generator, the inverter will provide frequency response when a disturbance happens and increase the stability of the frequency response in an isolated system.

A method of frequency control in an isolated system can categorise into two methods: virtual droop control and virtual inertia control. A control signal forms the two methods send a signal to an inverter to instantaneous adjust an electric power output from an inverter.

In a practical, the control strategy of the real power and the imaginary power method from an inverter is independent. From instantaneous electric power theory, real power can control through the d-axis, and imaginary power can control through the q-axis. The objective of the thesis is to control an inverter to produce/consume the real power, which can adjust by controlling an electric current on d-axis. Hence, the imaginary power on the q-axis will not consider.

### **3.2 Literature Review Frequency Control of a Power System by Using BESS**

Literature reviews about a frequency control of a power system by using a device connected through an inverter can increase the stability of frequency in a system, especially which has a low moment of inertia. The strategy of dynamic frequency control of an inverter comes from many ideas and equations. At last, they can conclude in 4 methods.

#### **3.2.1 Virtual inertia technique of BESS**

The literature review [41] presents that the virtual synchronous generator control strategy can implement in the BESS control. Figure 3.1 shows the model of the battery and the frequency control. The virtual inertia technique of BESS uses both the outer and the inner control of the BESS inverter. The inner frequency control loop controls the output powers, which are the active and reactive power from the inverter. The outer loop can use to generate the active power reference for the inner loop by using frequency-active power the characteristics. The inverter with the virtual inertia technique of BESS provides power damping and frequency support to the grid.

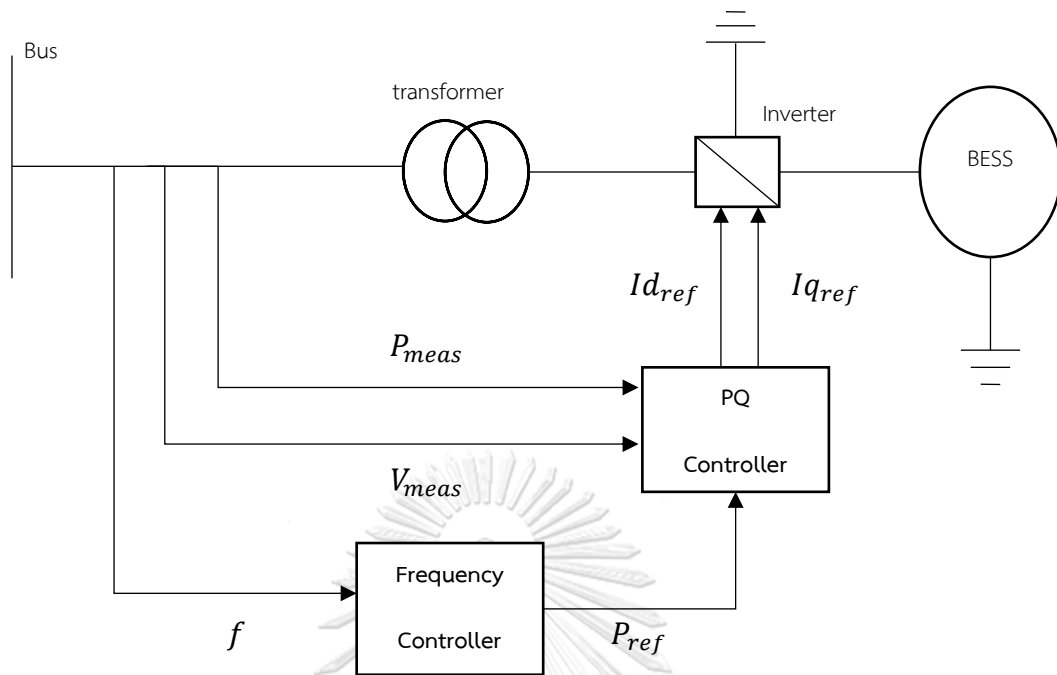


Figure 3.1 Model of the battery and the frequency control using virtual inertia techniques

The frequency controller model aims to provide an enhancement of system stability. The reference power output of the frequency controller which respects to the derivative of the frequency deviation can describe as

$$P_{ref} = K_d \cdot \Delta f + K_i \cdot \frac{d\Delta f}{dt} \quad (3.1)$$

where  $K_d$  is droop constant,

$K_i$  is the derivative gain of inertia.

### 3.2.2 Frequency control with two frequency control methods

The literature review [42] presents that the frequency control consists of two methods for automatic frequency control: frequency response and frequency regulation. The frequency response can operate when a large disturbance has occurred. By using droop control, the frequency response controls the output power of the resource to suppress frequency fluctuation. The frequency regulation controls the output power by receiving the automatic generation control signal from the utility. This control strategy is suitable for severing small frequency fluctuation or restoration of frequency after a large disturbance. Figure 3.2 shows the frequency algorithm of an energy storage system that has two frequency control methods. An

automatic generation control signal from the utility adjusts the base power. The output power of frequency response is controlled by following the frequency deviation from the standard frequency.

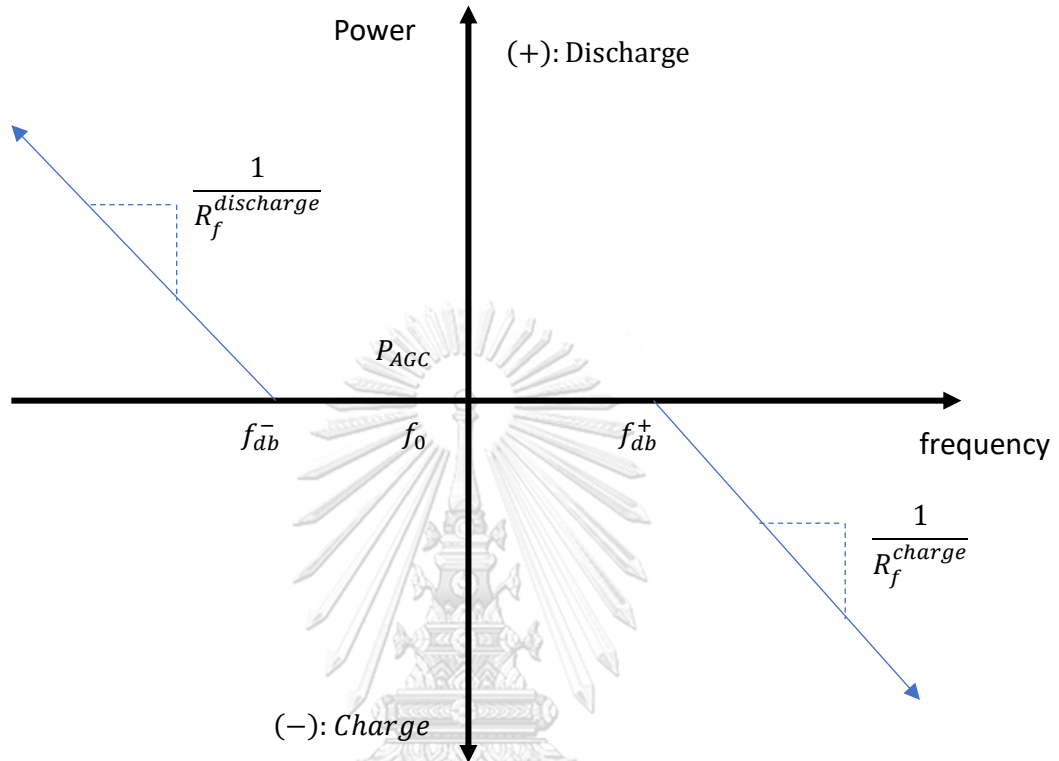


Figure 3.2 Frequency Control Algorithm of Energy Storage System

### 3.2.3 Droop control for dynamic of SOC in Response to Frequency Change

The literature review [43] presents that droop control can use to share the burden between the synchronous generator and energy storage systems for frequency regulation. The control by droop control can describe as (3.2). The droop constant  $R_{ESS}$  will provide the different degrees of power in response to the frequency deviation. The (3.3) describes the relation between power and the state of charge (SOC), which can express as the relation between SOC and frequency variation.

$$\Delta P_{ESS}(t) = \frac{1}{R_{ESS}} \cdot \Delta f(t) \quad (3.2)$$

$$\frac{\Delta SOC(s)}{\Delta f(s)} = \frac{1}{R_{ESS}} \cdot \frac{1}{E \cdot h} \cdot \frac{1}{s} = \frac{1}{R_{ESS} K_E s} \quad (3.3)$$

where  $R_{ESS}$  is droop constant,  
 $SOC$  is the state of charge of the battery,  
 $K_E$  is the energy of ESS (Joule).

### 3.2.4 Transfer Functions of Energy Storage System using Time Delay

The literature review [44] presents that the hybrid power system with an energy storage system is very fast to maintain system stability. The energy storage system with rapid power electronics technology can control both active and reactive power output well above the  $kHz$  range. With advanced power electronics technology, it can provide additional damping to power system swings to improve both dynamic and transient stability [4]. The transfer function with a time delay can express as

$$G_{ESS}(s) = \frac{\Delta P_{ESS}}{\Delta \omega} = \frac{K_{ESS}}{1+sT_{ESS}} \quad (3.4)$$

where  $G_{ESS}(s)$  is a transfer function of the energy storage system,

$K_{ESS}$  is gain constant of the energy storage system,

$T_{ESS}$  is a time delay constant of the energy storage system.

### 3.3 Virtual Droop Frequency Control

Virtual droop control is coming from (2.18). By using the same concept of droop characteristics and rearranging (2.18). The virtual droop equation describes follows:

$$\Delta P_{BESS} = -\frac{1}{R_{inv}} \Delta \omega \quad (3.5)$$

where  $\Delta P_{BESS}$  is the change of the discharging power of the BESS,

$R_{inv}$  is a virtual droop constant,

$\Delta \omega$  is the change of the frequency.

The virtual droop of BESS acts the same as the droop characteristic of the synchronous generators in the transient state. By taking Laplace transform to (3.5). Then the equation follows:

$$\Delta P_{BESS}(s) = -\frac{1}{R_{inv}} \Delta \omega(s) \quad (3.6)$$

Figure 3.3 shows a dynamic model of a battery controlled by droop characteristics to increase the stability of a power system when a disturbance happens.

Figure 3.4 shows a dynamic model of a power system for studying the behaviour of frequency response, which is a battery controlled by droop characteristics.

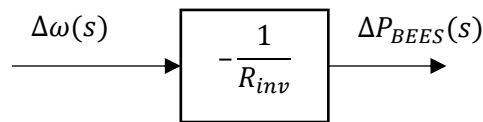


Figure 3.3 Dynamic model of a battery controlled by droop characteristic

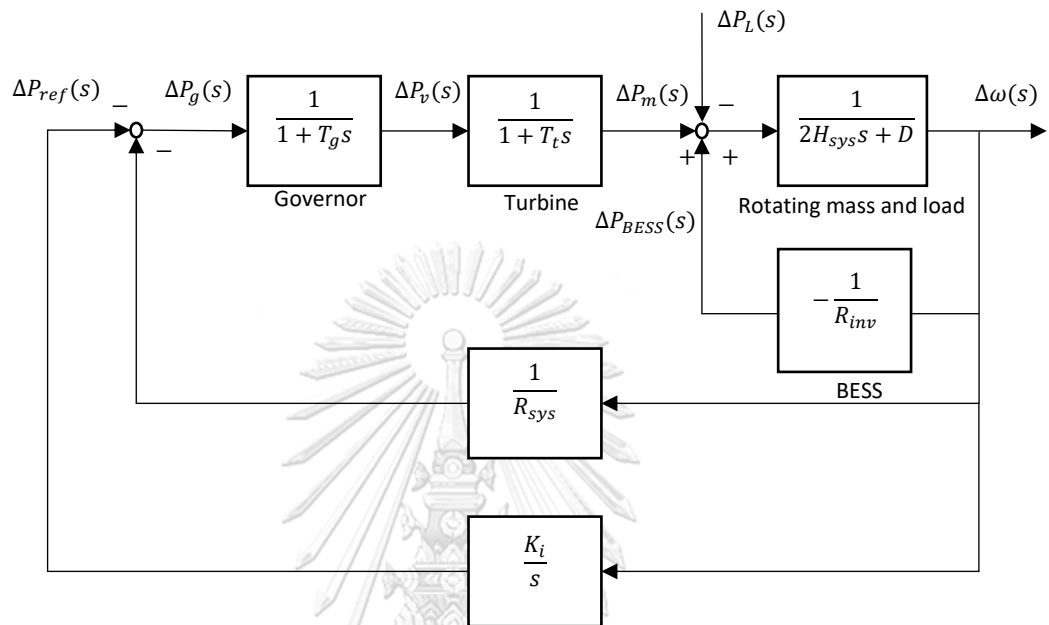


Figure 3.4 Dynamic model of a power system for studying the behaviour of frequency response which is a battery controlled by droop characteristic

### 3.4 Virtual Inertia Frequency Control

A virtual inertia control is coming from (2.13), which explains the behaviour of rotation of a generator. By rearranging the equation, an inverter is controlled behaviour to the same as the synchronous generator. Then the equation follows:

$$\Delta P_{BESS} = -2H_{inv} \frac{d\Delta\omega}{dt} \quad (3.7)$$

where  $\Delta P_{BESS}$  is the change of the discharging power of the BESS,

$H_{inv}$  is virtual inertia constant,

$\Delta\omega$  is the change of the frequency.

The virtual inertia of the BESS acts the same as the inertia of the synchronous generators in the transient state. By taking Laplace transform to (3.7). Then the equation follows:

$$\Delta P_{BESS}(s) = -2H_{inv}s\Delta\omega(s) \quad (3.8)$$

Figure 3.5 shows a dynamic model of a battery controlled by virtual inertia to increase the stability of a power system when a disturbance happens.

Figure 3.6 shows a dynamic model of a power system for studying the behaviour of frequency response, which is a battery controlled by virtual inertia.

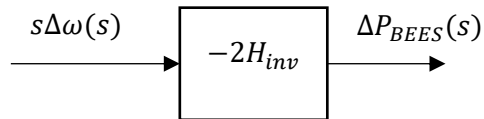


Figure 3.5 Dynamic model of a battery controlled by virtual inertia

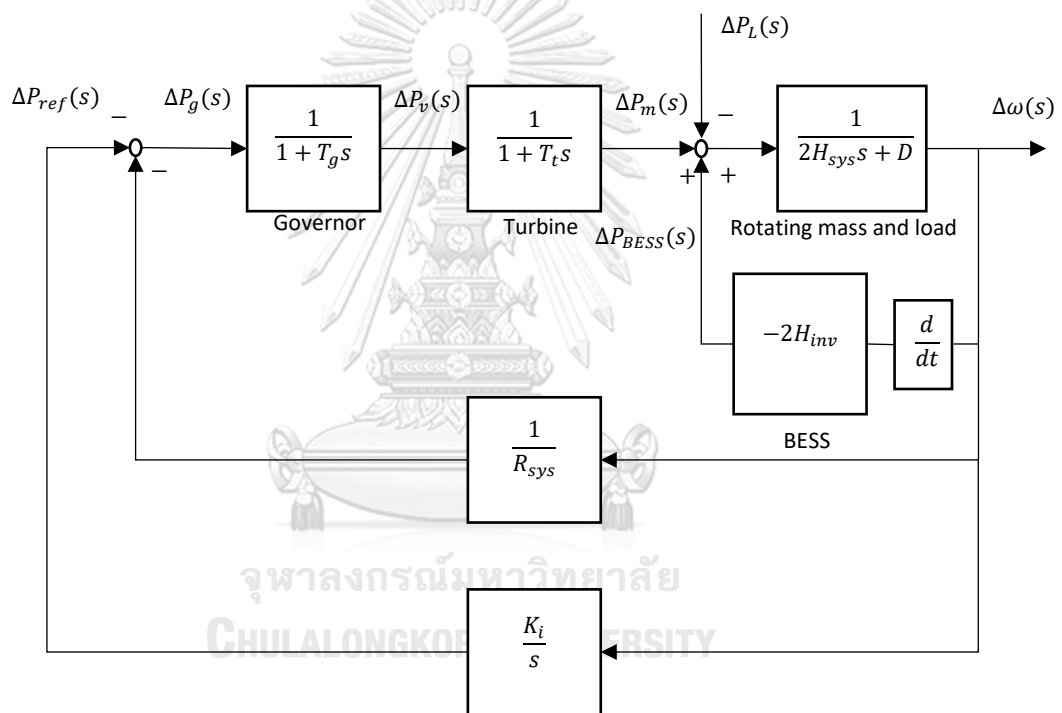


Figure 3.6 Dynamic model of a power system for studying the behaviour of frequency response which is a battery controlled by virtual inertia

## Chapter 4

### Power System of Mae Hong Son District

This chapter presents the fundamental data of Mae Hong Son province, the power generation in Mueang Mae Hong Son district and the power distribution of Mueang Mae Hong Son district.

#### 4.1 The Fundamental Data of Mae Hong Son Province

The Mae Hong Son province is the first area of Thailand that is an example area of the microgrid. The geography of the district is surrounded by mountain and sanctuary area. Moreover, the forest area covers more than 87.75 per cent of the region. From the geographic reason above, the settling of the transmission line to transmit the electric power must use a long distance of the line. On the other word, the transmission power to the district is similar to be sending the power to an isolated island. With a long-distance of the transmission line, there are problems with the frequency control on the district and challenge with a lot of loss that happens on the long transmission line. From the reason above, the Mae Hong Son province is suitable to be a model of the microgrid. Figure 4.1 presents areas of the power distribution in Mae Hong Son province. The province can divide the power distribution into three areas; area1-eastern area, area2-Mueang Mae Hong Son province, and area3-southern area.

First, area1-eastern area covers Pai district and Pang Mapha district. The power in this area receives from the Mae Tang substation that is operated by EGAT. The power is transmitted through 115kV and 22kV of transmission line that belongs to MEA. Second, area2- Mueang Mae Hong Son district covers Mueang Mae Hong Son district and some part of the area of Khun Yuam district. The area receives the power from Pai substation with 115 kV of the transmission line. This area also has power generations that are Mae Sa Nga small hydropower plant, Pa Bong small hydropower plant, and Pa Bong solar power plant.

Moreover, the area connects to the southern area bypassing the power to the Jom Thong substation on 22 kV transmission line and to Mae Sariang substation that locates on Khun Yuam district and Mae Sariang district, respectively. Last, area3-southern area covers Mae Sariang district, Sop Moei district, Mae La Noi district, and



some part of the area of Khum Yuam district. The area receives power from the Jom Thong substation on 22 kV transmission line. The ranking of an electricity consumption in Mae Hong Son province can descending order by area2-Mueang Mae Hong Son district, area3-southern area, and area1-eastern area, respectively.



*Figure 4.1 Areas of the power distribution in Mae Hong Son province*

#### **4.2 The Power Generation in Mueang Mae Hong Son District**

The power generation resource in Mae Hong Son province locates in Mueang Mae Hong Son district. The power generation resource can categorise to two types, renewable energy generation and diesel generator. Figure 4.2 can describe the power generation resource and installed capacity (kW) in Mueang Mae Hong son district. The renewable generation, there are four generators install on Mae Sa Nga small hydropower plant, two-2520kW generators and two-2650kW generators. An 850kW hydro generator and a 500kW solar generator installs on Pa Bong small hydropower plant and solar power plant, respectively. On the diesel generation, there are five generators install on Mae Hong Son diesel power plant, two-1000kW generators and three-800kW generators.

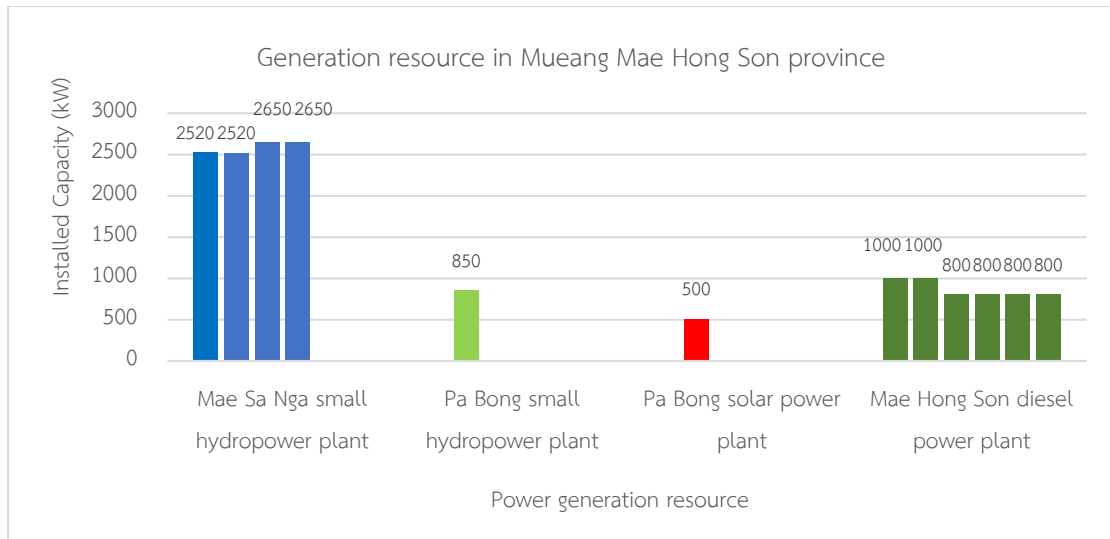


Figure 4.2 Generation resource in Mueang Mae Hong Son province

#### 4.3 The Power Distribution of Mueang Mae Hong Son District

The electricity consumption of Mueang Mae Hong Son district is 11 MW which is the most electricity consumption in Mae Hong Son province. Figure 4.3 presents a single line diagram of Mueang Mae Hong Son district. The area receives the power from Pai substation at 115kV of a transmission line. The substation of Mueang Mae Hong Son district installs two 25-MVA transformers to step the voltage down from 115kV to 22kV. There are two incoming circuits, which are INC01 and INC02, to sending the power to two main distribution boards which are skidding 1 and skidding 2, respectively.

The skidding 1 consists of feeder number 1-5. This circuit contributes the power to an outer area of Mueang Mae Hong Son district. The skidding 2 consists of feeder number 6-10. This circuit contributes the power to an inner area of Mueang Mae Hong Son district, where has a high density of load usage. Moreover, skidding 2 also connects to the power generation resources in Mueang Mae Hong Son district. The detail of each feeder can describe the following:

- Feeder 1 transmits the power from the skidding 1 to Khum Yuam district and sometimes receives the power from Jom Thong substation. The peak load of the area is less than 5 MW.
- Feeder 2 transmits the power to the small load nearby the feeder 2. The peak load of the area is less than 1 MW.

- Feeder 3 transmits the power to the northern area of Mueang Mae Hong Son district. The feeder can receive the power from 22kV-temporary Pai substation. The peak load of the area is less than 3.5 MW.
- Feeder 4 transmits the power to the eastern area of Mueang Mae Hong Son district. The peak load of the area is less than 1 MW.
- Feeder 6 transmits the power to the loads which are along the way to Pa Bong sub-district. The feeder 6 also connects to the power generation resources; 3.85 MW-Pa Bong small hydropower plant, 3.5 MW- Pa Bong small solar power plant. 4MW/1 MWh-battery system, and 3.85MW-Mae Hong Son diesel generation.
- Feeder 7 transmits the power to the eastern area of Mueang Mae Hong Son district. The peak load of the area is less than 1 MW.
- Feeder 8 transmits the power to the significant loads in Mueang Mae Hong Son district that are Mueang Mae Hong Son municipality office, Mae Hong Son airport, and Mae Hong Son provincial hospital. The peak load of the area is less than 1.5 MW.
- Feeder 9 only connects to 10MW-Mae Sa Nga small power plant. However, the maximum transmission power from the Mae Sa Nga small power plant to skidding 2 is less than 6.7 MW, due to the limitation of the protection device of the feeder.
- Feeder 5 and 10 are the switch circuit which connects between skidding 1 circuit and skidding 2 circuits for transferring the power between two areas.

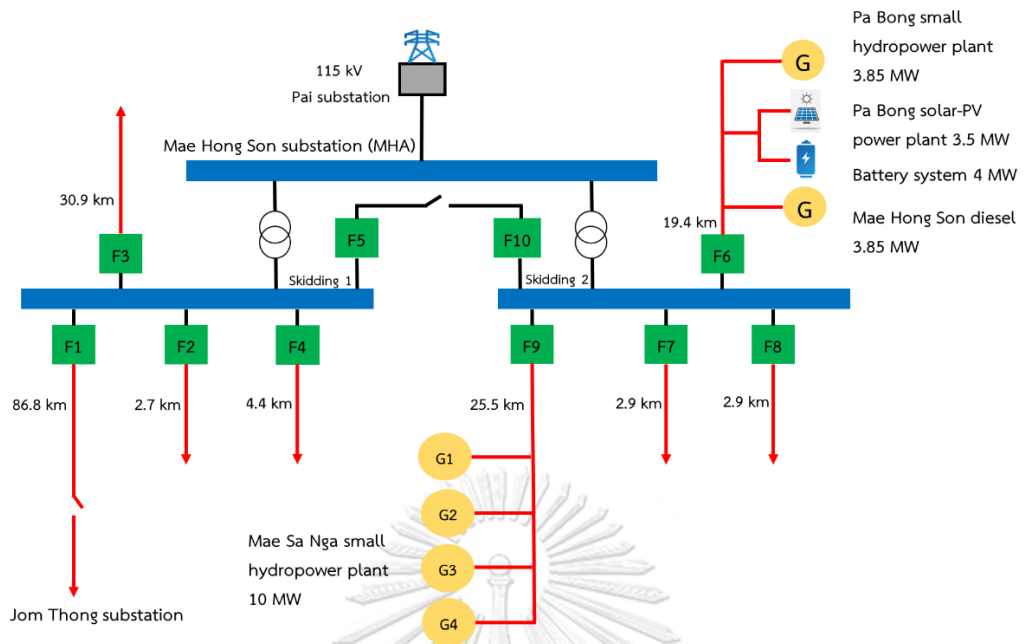


Figure 4.3 Single line diagram of Mueang Mae Hong Son district

## Chapter 5

### Investigation the Possibility of BESSs Design for Increasing the Stability of Frequency Response when the Large Disturbance Happens

This chapter shows an investigation of the possibility of a BESSs design for increasing the stability of frequency response. The BESS is installed in the microgrid to help the synchronous generator for increasing the stability of the microgrid frequency. The structures of the BESS control system, such as a virtual droop and virtual inertia, provide different frequency responses. The objective of the chapter is to investigate the performance of BESS on the stability of the microgrid in the isolated mode and connected mode. The simulation can divide the investigation into two situations which are considering only the primary response and considering both the primary and the secondary response.

#### 5.1 Primary Response

The simulation is the microgrid with considering only the primary response. The BESS is installed in the microgrid to enhance the stability of the frequency response. The investigation compares the impacts of the virtual droop constant and the virtual inertia constant on the frequency deviation in the microgrid. Moreover, the investigation also compares among the combined the virtual droop control and the virtual inertia control, only the virtual droop control, and only the virtual inertia control.

##### 5.1.1 Test System

Figure 5.1 represents the simplified single line diagram of the test system. The test system consists of a 3-MW synchronous generator on Mae Sa Nga small hydropower plant, a 3.5-MW solar cell generator installs on Pa Bong solar cell power plant, a 4-MW BESS system on Pa Bong hydropower plant, and a 3-MW load on Mueang Mae Hong Son district. The system operates at a steady-state frequency of 50 Hz. The test system is simplified a block diagram. The block diagram of the test system represents in Figure 5.2. Table 5.1 shows each parameter value in a block diagram. The system inertia ( $H_{sys}$ ) is 5 s which can calculate from (2.9). The time constants  $T_g$  and  $T_t$  are 0.2 s and 0.5 s, respectively. The system droop constant

( $R_{sys}$ ) is 0.05 and the integral gain ( $K_i$ ) is 7. This thesis assumes that there is no frequency-dependent load, i.e.,  $D$  is zero.

The simulation can perform in MATLAB/Simulink. In the simulation, the BESS can control to provide the primary response by using two control methods: the virtual droop control and the virtual inertia control. For each simulation scenario, a 2- $MW$  load increase occurs at  $t = 5$  s.

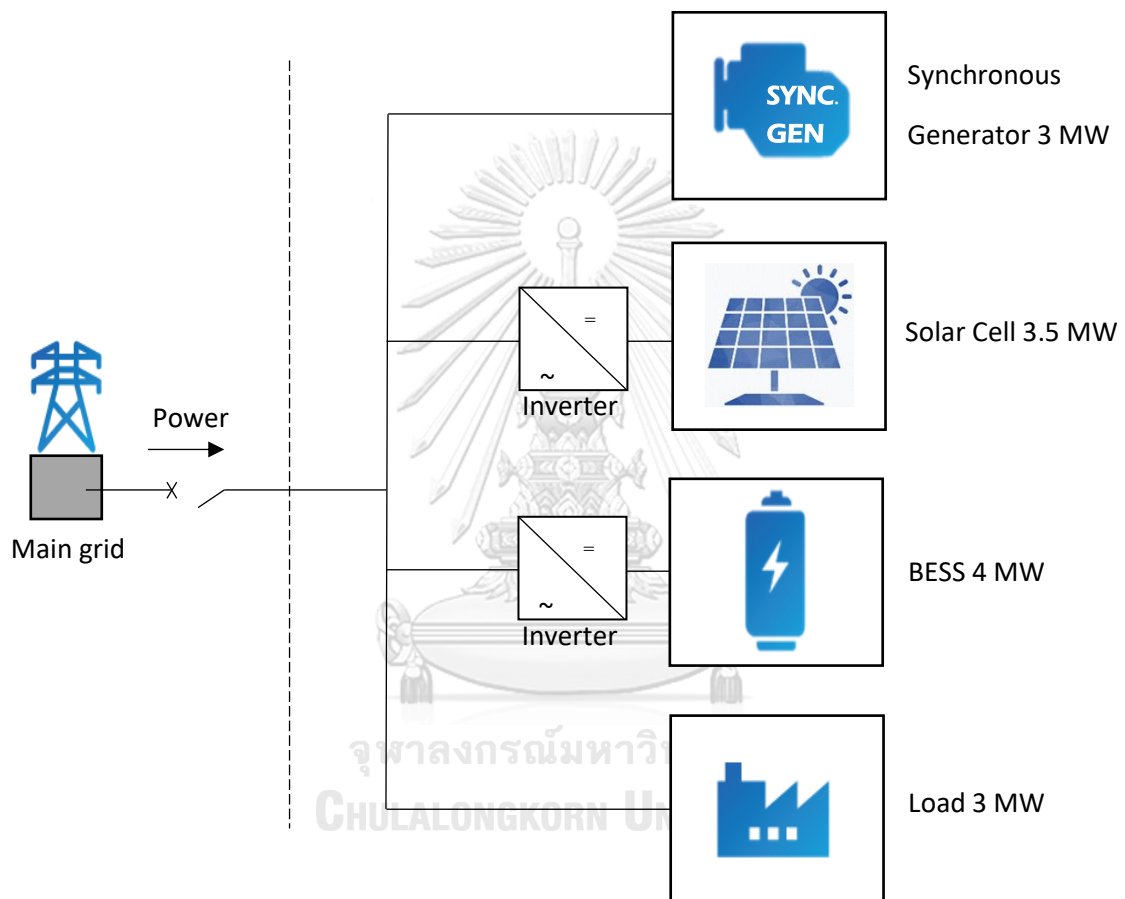


Figure 5.1 Simplified single line diagram of a system on the isolated mode

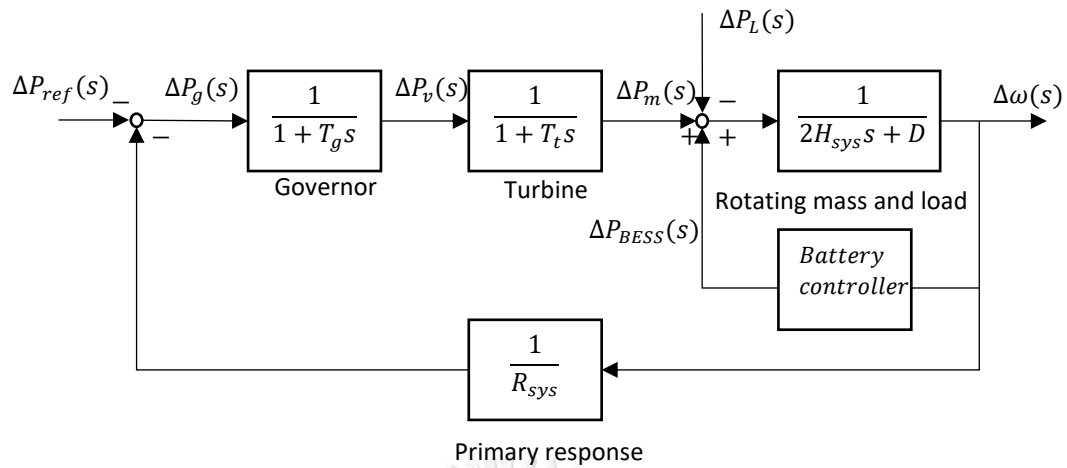


Figure 5.2 Block diagram of the test system

Parameter	Value
System inertia ( $H_{sys}$ )	5 s
Governor time constant ( $T_g$ )	0.2 s
Turbine time constant ( $T_t$ )	0.5 s
System droop constant ( $R_{sys}$ )	0.05
Frequency-dependent load ( $D$ )	0
Reference power ( $\Delta P_{ref}$ )	0

Table 5.1 Value of each parameter in a block diagram of the test system

### 5.1.2 Simulation Results

Two case studies investigate the effects of virtual droop control and virtual inertia control approaches on the microgrid frequency response on only the primary response. The simulation is performed in MATLAB/Simulink to analyse the performance of both control methods when the microgrid test system is operating in an islanding mode. Moreover, the investigation also compares help from BESS with varying control methods.

#### 5.1.2.1 Effect of Various Virtual Droop Constant

Figure 5.3 shows a block diagram with a virtual droop control by considering only the primary response. A virtual droop control can control by using (3.1). The dynamic model presents in figure 3.1 is added to the block diagram of the test system. Table 5.2 shows each parameter value in a block diagram.

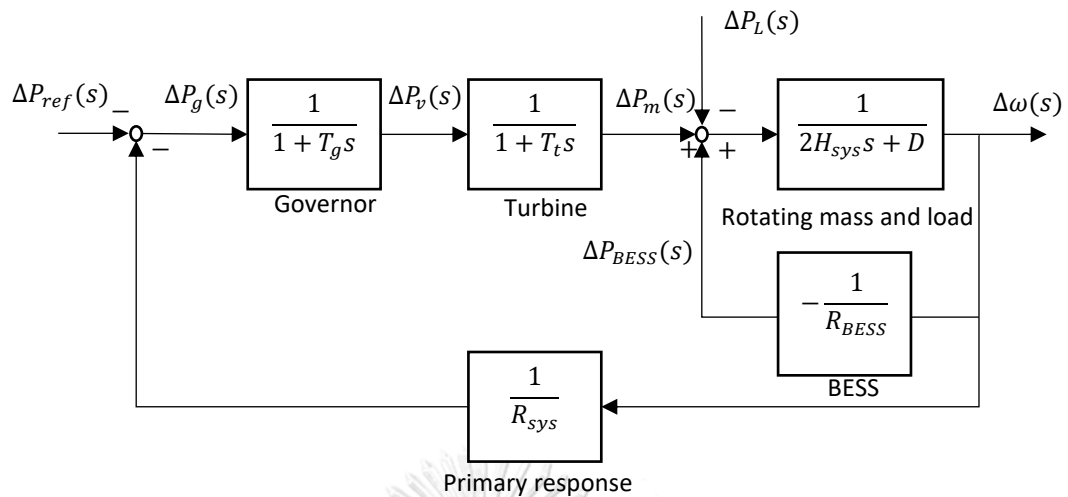


Figure 5.3 Block diagram of the test system with a virtual droop control

Parameter	Value
System inertia ( $H_{sys}$ )	5 s
Governor time constant ( $T_g$ )	0.2 s
Turbine time constant ( $T_t$ )	0.5 s
System droop constant ( $R_{sys}$ )	0.05
Frequency-dependent load ( $D$ )	0
Reference power ( $\Delta P_{ref}$ )	0
Virtual droop constant ( $R_{BESS}$ )	2% to 8%.

Table 5.2 Value of each parameter in a block diagram of the test system with a virtual droop control and only primary response

This case study varies the virtual droop constant from 2% to 8%. In this case, the energy storage uses for providing the primary response to stop the frequency deviation. Figure 5.4a shows that a 2-MW load increase that occurs at  $t = 5$  s.

#### 5.1.2.1.1 Frequency Response

Figure 5.4b presents the frequency response in a microgrid. When without applying the BESS, the frequency nadir is 49.26 Hz, and the frequency goes to 49.52 Hz in the end because there is no AGC from the synchronous generator. The period of the frequency response under 49.5 Hz is 1.664 s. When applying the virtual droop control, the frequency nadir is equal to 49.58 Hz at  $R_{BESS} = 8\%$  and the frequency



goes to 49.7 *Hz* in the end. When the virtual droop constant decreases, the frequency nadir is reduced to 49.828 *Hz* at  $R_{BESS} = 2\%$  and the frequency goes to 49.86 *Hz* in the end. In other words, the results can suggest that the less the values of the virtual droop constant, the less the frequency deviation. However, the frequency is not going back to the nominal value at the end because the investigation applies only the primary response.

#### 5.1.2.1.2 Rate of Change of Frequency

Figure 5.4c presents the rate of change of the frequency (*ROCOF*). The graph indicates that the *ROCOF* for all ranges of the virtual droop constant, including the base case, is commonly equal to -1 *Hz/s* at  $t = 5$  s. After  $t = 5$  s, when the virtual droop constant has a small value, the *ROCOF* is lower than when the virtual droop constant has a large value. The highest *ROCOF* after  $t = 5$  s is -0.175 *Hz/s* at  $R_{BESS} = 8\%$  and the lowest *ROCOF* is 0.062 *Hz/s* at  $R_{BESS} = 2\%$ . For the base case, the highest *ROCOF* is equal to 0.320 *Hz/s*.

#### 5.1.2.1.3 Power and Energy Discharged from the Battery

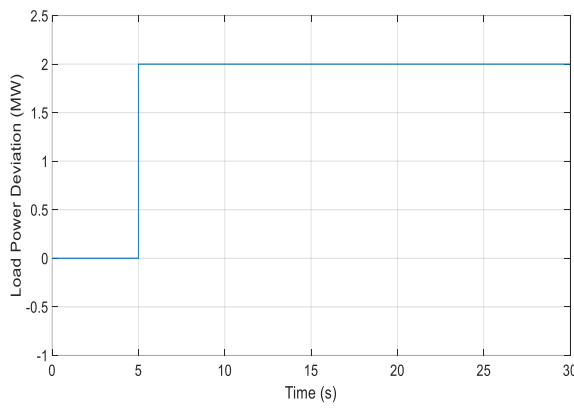
Figure 5.4d and Figure 5.4e show the power and energy discharged from the battery, respectively. The graph power discharged indicates that the power discharges from the BESS at  $t = 5$  s. The maximum power discharged is a large value when the  $R_{BESS}$  is small value. The highest powers discharged are 1.73 *MW*, 1.43 *MW*, 1.21 *MW*, and 1.05 *MW* for  $R_{BESS}$  is equal to 2%, 4%, 6%, and 8%, respectively. However, the battery decreases the level of power discharged after reach to the peak of the power discharged and then continue discharging at the constant value which depends on the  $R_{BESS}$  value. The battery powers constantly discharge at 1.41 *MW*, 1.15 *MW*, 0.90 *MW*, and 0.75 *MW* for  $R_{BESS}$  is equal to 2%, 4%, 6%, and 8%, respectively.

On the same direction, the battery energy graph shows that the BESS discharges high energy when the  $R_{BESS}$  is small value. The highest batteries energy discharged are 9.829 *kWh*, 7.606 *kWh*, 6.203 *kWh*, and 5.237 *kWh* for  $R_{BESS}$  is equal to 2%, 4%, 6%, and 8%, respectively and continue going up in the end.

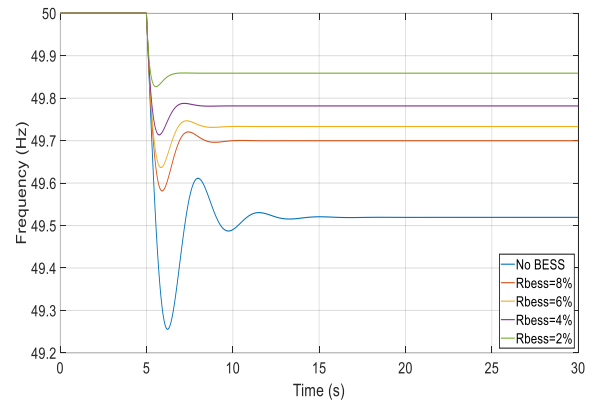
#### 5.1.2.1.4 Power Generated from the Synchronous Generator

Figure 5.4f shows the power generated from the synchronous generator. The initial power generation from the synchronous generator in the microgrid is 3 *MW*. The result shows that when the  $R_{BESS}$  has a small value, the power generation is lower than when the  $R_{BESS}$  has a large value. The power generation of the synchronous generator when the  $R_{BESS} = 2\%$  is 3.5 *MW* and continue generating at constant 3.5 *MW* until to the end. The synchronous generator provides a small overshoot of power when the BESS has a higher  $R_{BESS}$ . The maximum overshoot is on  $R_{BESS} = 8\%$  which is 1.45 *MW* from the initial generation power of the synchronous generator.

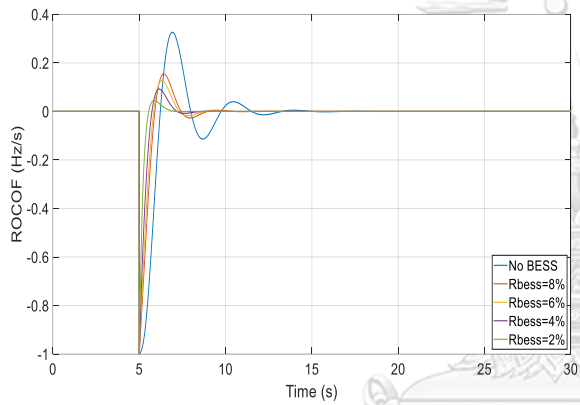
Moreover, the graph suggests that the power generation of the synchronous generator when without applying the BESS is noticeable higher power generation than when applying the BESS in the microgrid. The maximum overshoot of the power generation is 5.6 *MW* or 2.6 *MW* from the initial generation power of the synchronous generator. After that, the power generation drops down and generates the power at 4.9 *MW* until to the end.



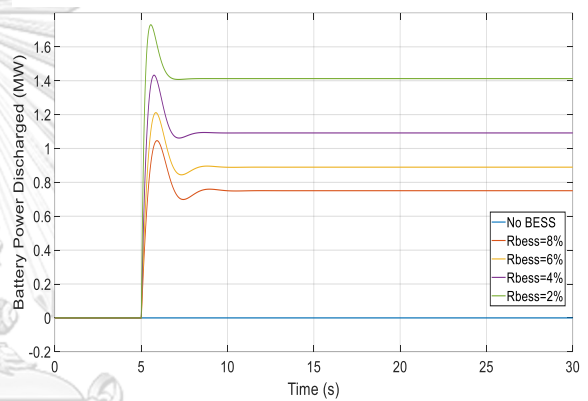
a) Instantaneous 2-MW load increase occurs at  $t = 5$  s in the Mueang Mae Hong Son province



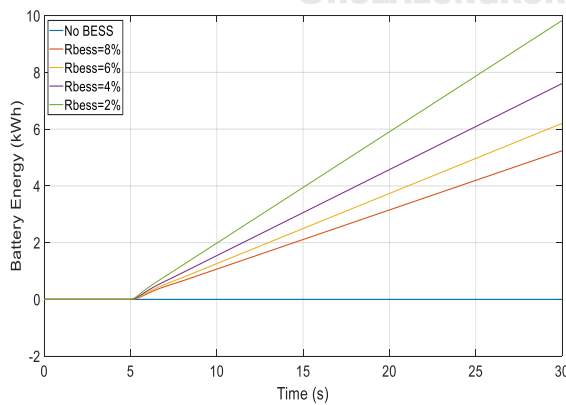
b) Frequency response with various virtual droop constant of the battery on only the primary response



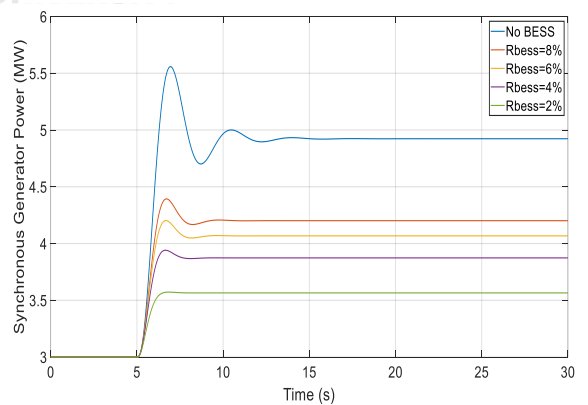
c) *ROCOF* with various virtual droop constant of the battery on only the primary response



d) Power discharged from the battery with various virtual droop constant of the battery on only the primary response



e) Energy discharged of the battery with various virtual droop constant of the battery on only the primary response



f) Power generation from the synchronous generator with various virtual droop constant of the battery on only the primary response

Figure 5.4 Effect of various virtual droop constant on only the primary response

### 5.1.2.2 Effect of Various Virtual Inertia Constant

Figure 5.5 shows a block diagram with a virtual inertia control. The virtual inertia can control by using an equation 3.3. The dynamic model presents in figure 3.4 is added to the block diagram of the test system. Table 5.3 shows each parameter value in a block diagram.

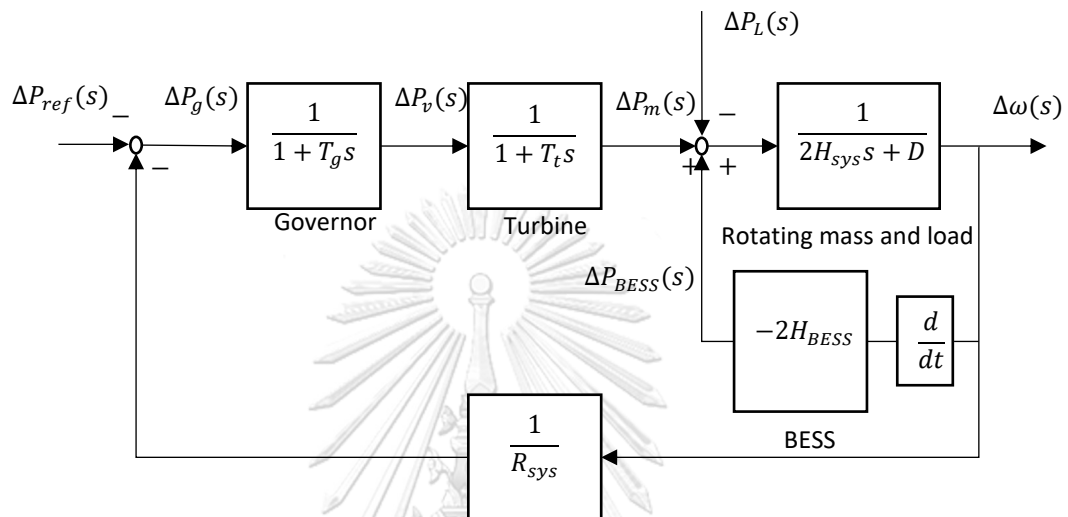


Figure 5.5 Block diagram of the test system with a virtual inertia control

Parameter	Value
System inertia ( $H_{sys}$ )	5 s
Governor time constant ( $T_g$ )	0.2 s
Turbine time constant ( $T_t$ )	0.5 s
System droop constant ( $R_{sys}$ )	0.05
Frequency-dependent load ( $D$ )	0
Reference power ( $\Delta P_{ref}$ )	0
Virtual inertia constant ( $H_{BESS}$ )	2 s to 10 s

Table 5.3 Value of each parameter in a block diagram of the test system with a virtual inertia control and only primary response

This case study investigates the effect of varying virtual inertia constant that is provided by the BESS between 2 s and 10 s. Figure 5.6a shows that a 2-MW load increase that occurs at  $t = 5$  s.

#### 5.1.2.2.1 Frequency Response

Figure 5.6b presents the microgrid frequency response. The graph shows that the frequency response deviates from the nominal value of 50 Hz when the load is instantaneously increased by 2 MW at  $t = 5$  s. When without applying BESS, the frequency nadir is 49.26 Hz. The period of the frequency response under 49.5 Hz is 1.664 s. The frequency response has a large deviation when the virtual inertia constant has a small value. The frequency nadir is 49.32 Hz at  $H_{BESS} = 2$  s and the frequency nadir is 49.45 Hz at  $H_{BESS} = 10$  s. The periods of the frequency response under 49.5 Hz are 1.808 s and 2.067 s, respectively. However, the end of the behaviour of the frequency response is not the same as when applying the BESS by various virtual droop constant, and the frequency response goes to 49.52 Hz in the end either with or without the BESS.

#### 5.1.2.2.2 Rate of Change of Frequency

Figure 5.6c shows the effects of the virtual inertia control on the *ROCOF*. For the base case, the highest *ROCOF* is equal to -1 Hz/s. The results suggest that when the  $H_{BESS}$  has a large value, the *ROCOF* is lower than when the  $H_{BESS}$  has a small value. The maximum *ROCOF* is -0.8296 Hz/s at  $H_{BESS} = 2$  s and the minimum *ROCOF* is -0.4992 Hz/s at  $H_{BESS} = 10$  s.

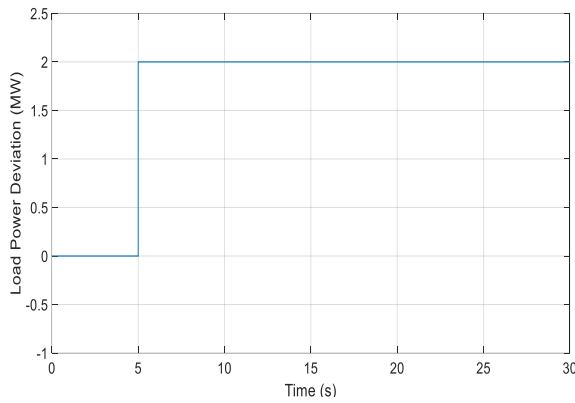
#### 5.1.2.2.3 Power and Energy Discharged from the Battery

Figure 5.6d and Figure 5.6e represent the power and energy discharged from the battery, respectively. The result shows that the battery power instantaneous discharges the power after increasing load of 2 MW at  $t = 5$  s. The maximum power and energy discharged from the battery have a large value when the  $H_{BESS}$  has a large value. After that, the battery charges the power back until the frequency goes to 49.52 Hz. In the end, the power discharged from the battery goes to zero. The maximum of the power and energy discharged from the battery happens when applying the BESS with  $H_{BESS} = 10$  s. The maximum power discharged is 1 MW and the maximum energy discharged is 0.315 kWh. The battery energy decreases the energy discharged from 0.315 kWh to 0.27 kWh in the end because the power from the microgrid is charged back to the battery. The minimum power discharged is 0.3

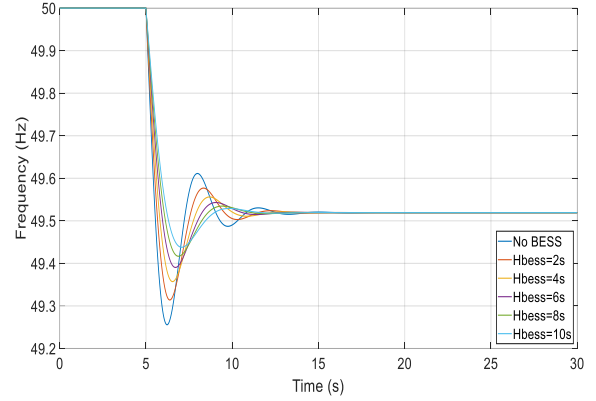
$MW$  and the maximum energy discharged is  $0.075 kWh$ . The battery energy decreases the energy discharged from  $0.075 kWh$  to  $0.052 kWh$  in the end.

#### 5.1.2.2.4 Power Generated from the Synchronous Generator

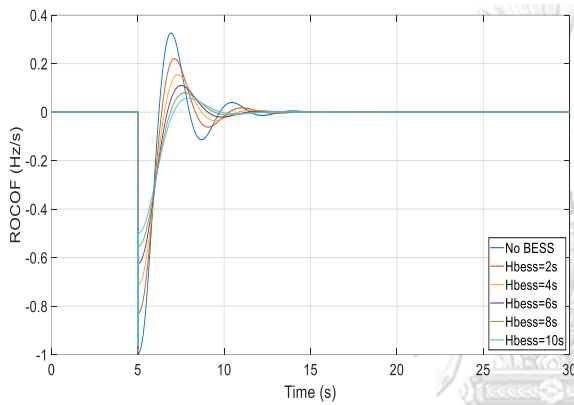
Figure 5.6f presents the power that can generate from the synchronous generator. The initial power generation from the synchronous generator in the microgrid is  $3 MW$ . The result acts in the opposite direction of the power discharged from the battery. In other words, the less the value of the  $H_{BESS}$ , the more power generation from the synchronous generator. The synchronous generator provides the maximum overshoot of power at  $5.6 MW$  when without applying the BESS. The graph also indicates that the maximum power generation decreases when applying the BESS in the microgrid. The maximum of the power generated from the synchronous generator is on  $5.4 MW$  at  $H_{BESS} = 2 s$  and the minimum of the power generated from the synchronous generator is on  $5.15 MW$  at  $H_{BESS} = 10 s$ . In addition, the power generated from the synchronous generator drops down to  $4.9 MW$  in the end on either with or without applying the BESS because there has not the AGC from the synchronous generator.



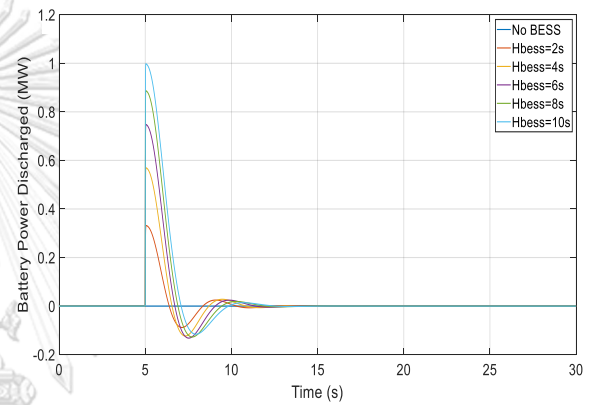
a) Instantaneous 2-MW load increase occurs at  $t = 5$  s in the Mueang Mae Hong Son province



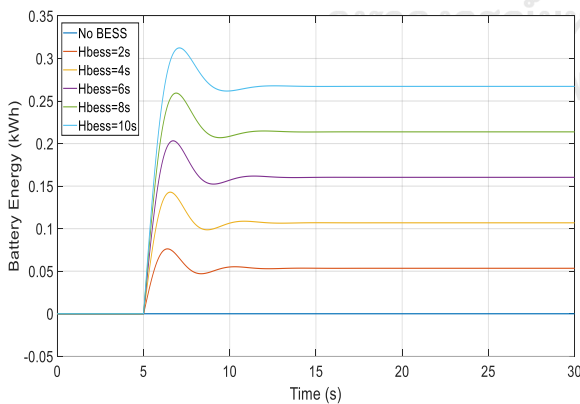
b) Frequency response with various virtual inertia constant of the battery on only the primary response



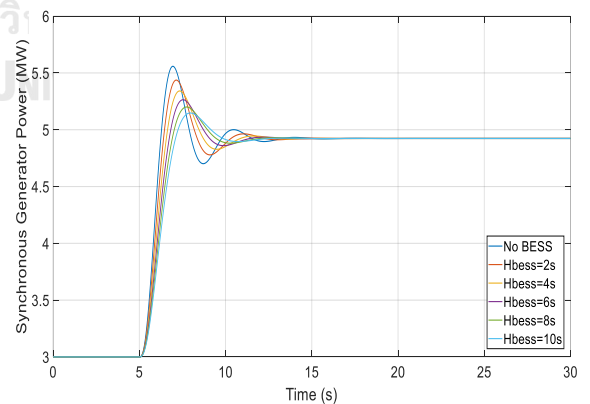
c) *ROCOF* with various virtual inertia constant of the battery on only the primary response



d) Power discharged from the battery with various virtual inertia constant of the battery on only the primary response



e) Energy discharged of the battery with various virtual inertia constant of the battery on only the primary response



f) Power generation from the synchronous generator with various virtual inertia constant of the battery on only the primary response

Figure 5.6 Effect of various virtual inertia constant on only the primary response

### 5.1.2.3 Investigation Compares Help from BESS with Varying Control

#### Methods

the investigation compares among the frequency response when without applying the BESS, applying the BESS with only the virtual droop control at  $R_{BESS} = 2\%$ , applying the BESS with only the virtual inertia control at  $H_{BESS} = 10 \text{ s}$ , and combined the virtual droop and the virtual inertia control at  $R_{BESS} = 2\%$  and  $H_{BESS} = 10 \text{ s}$ , respectively. The investigation considers only the primary response. Figure 5.7a shows that a 2-MW load increase that occurs at  $t = 5 \text{ s}$ .

#### 5.1.2.3.1 Frequency Response

Figure 5.7b presents among the frequency response when without applying the BESS, with various BESS control methods that are only a virtual droop control, only a virtual inertia control, and combined a virtual droop and a virtual inertia control. The graph shows that the frequency response can divide into two groups by considering from the end of the behaviour of the graphs. The end of the behaviour of the graphs are going to 49.52 Hz, on without applying the BESS and only applying the BESS with a virtual inertia control, and going to 49.86 Hz, on only applying the BESS with a virtual droop control and combined a virtual droop and a virtual inertia control, respectively.

The frequency nadir when without applying the BESS and only applying the BESS with a virtual inertia control are 49.26 Hz and 49.45 Hz, respectively. After that, the frequency response reaches to constantly 49.52 Hz in the end. The highest frequency response when only applying the BESS with a virtual droop control and combined a virtual droop and a virtual inertia control are 49.82 Hz and 49.84 Hz, respectively. After that, the frequency response reaches to constantly 49.86 Hz in the end.

In addition, The graph can conclude that the frequency deviation when only applying the BESS with only a virtual droop control and combined a virtual droop and a virtual inertia control is noticeable smaller than when without applying the BESS or only applying the BESS with a virtual inertia control.



#### 5.1.2.3.2 Rate of Change of Frequency

Figure 5.7c presents the rate of change of frequency (*ROCOF*). The graph shows that the highest *ROCOF* is going to  $-1 \text{ Hz/s}$  for all with or without applying the BESS. However, the *ROCOF* when without applying the BESS has the overshoot that is higher than when applying the BESS. The highest overshoot when without applying the BESS is  $0.35 \text{ Hz/s}$ . In addition, the result shows that the highest overshoot is not much difference when applying the BESS with only on a virtual inertia control, a virtual droop control and combined a virtual droop and a virtual inertia control. The highest overshoots are  $0.058 \text{ Hz/s}$ ,  $0.044 \text{ Hz/s}$ , and  $0.020 \text{ Hz/s}$ , respectively.

#### 5.1.2.3.3 Power and Energy Discharged from Battery

Figure 5.7d and Figure 5.7e represent the power and energy discharged from the battery, respectively. The result shows that the battery power instantaneous discharges the power after increasing load of  $2 \text{ MW}$  at  $t = 5 \text{ s}$ . The maximum power discharged from the battery has a large value in descending order when applying the BESS only with virtual droop control, combined a virtual droop and virtual inertia control, only with a virtual inertia control, respectively. The maximum of the powers discharged from the battery are  $1.73 \text{ MW}$ ,  $1.63 \text{ MW}$ , and  $1 \text{ MW}$ , respectively. After that, the battery charges the power back and continue discharging the power at  $1.41 \text{ MW}$  until to the end for both applying the BESS only with virtual droop control and combined a virtual and virtual inertia control. However, the power discharged from the battery goes to zero when applying the BESS only with a virtual inertia control.

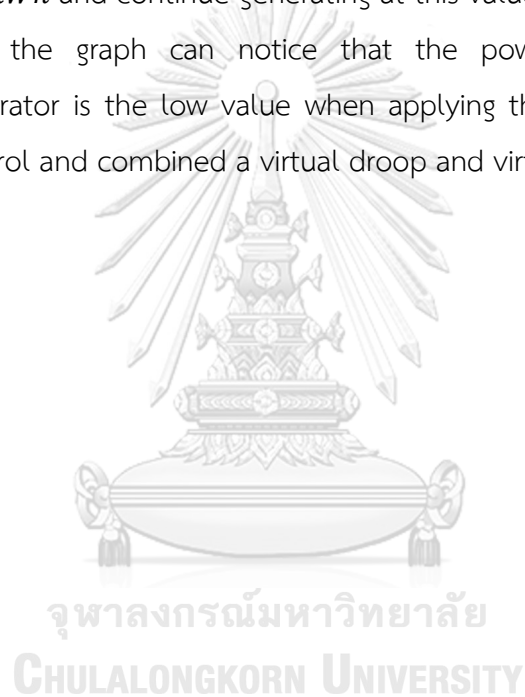
On the battery energy, the battery energy acts in the same result when applying the BESS only with virtual droop control and combined a virtual droop and virtual inertia control. The energy increases uniformly until to  $9.829 \text{ kWh}$  at  $t = 30 \text{ s}$  and continues going up in the end. In contrast, the battery energy discharges at  $0.267 \text{ kWh}$  and continue discharging at this value until to the end when applying the BESS only with a virtual inertia control.

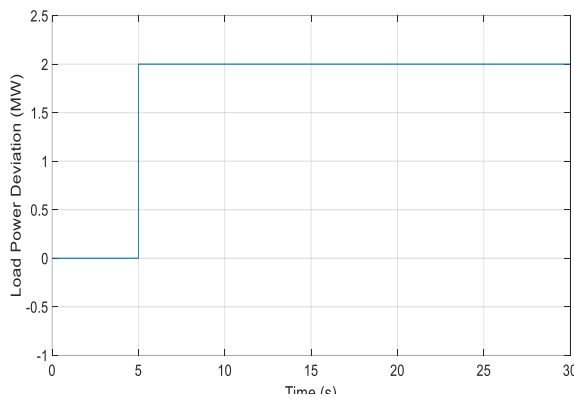
#### 5.1.2.3.4 Power Generation from the Synchronous Generator

Figure 5.7f presents the power generation from the synchronous generator. The initial power generation from the synchronous generator is  $3 \text{ MW}$ . The power

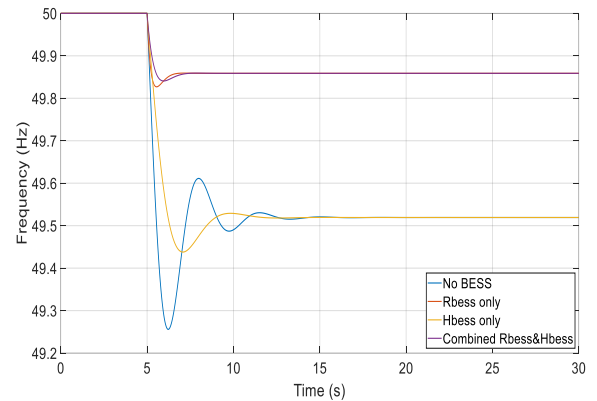
generation from the synchronous generator is high when without using the BESS and applying the BESS only with virtual inertia control. The highest powers generation from the synchronous generator are at 5.56 *MW* and 5.15 *MW*, respectively. The power generation from the synchronous generator decreases to 4.92 *kWh* and continue generating at this value until the end. In addition, the characteristic of power generation from the synchronous generator is commonly the same for applying BESS control only with virtual droop control and combined a virtual droop and virtual inertia control. The power generation from the synchronous generator generates at 3.57 *kWh* and continue generating at this value until to the end.

Moreover, the graph can notice that the power generation from the synchronous generator is the low value when applying the BESS control only with virtual droop control and combined a virtual droop and virtual inertia control.

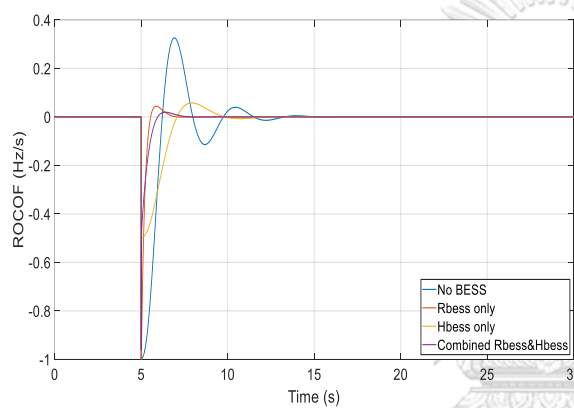




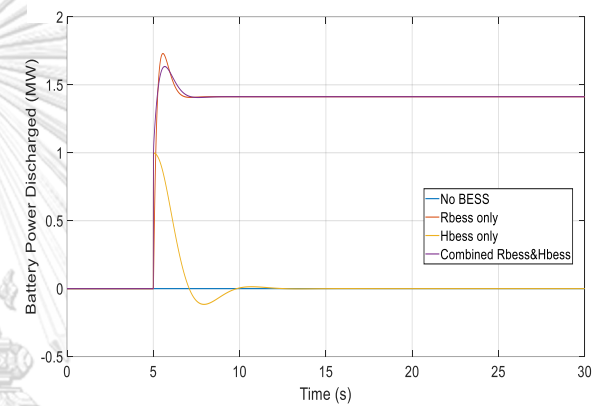
a) Instantaneous 2-MW load increase occurs at  $t = 5 \text{ s}$  in the Mueang Mae Hong Son province



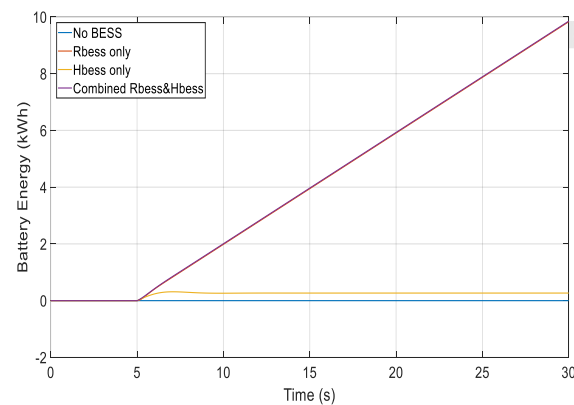
b) Frequency response with  $R_{BESS} = 2\%$ ,  $H_{BESS} = 10 \text{ s}$ , and combined  $R_{BESS}$  and  $H_{BESS}$  of the battery on only the primary response



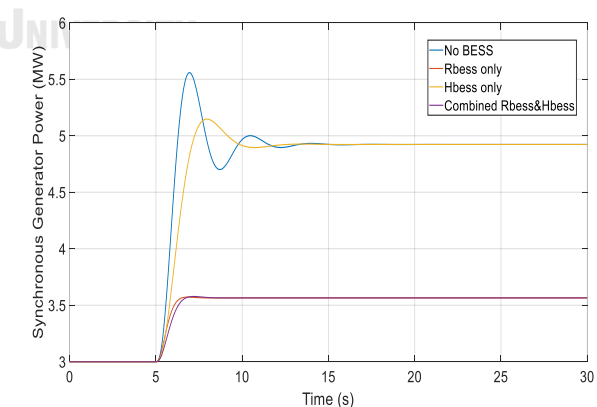
c)  $ROCOF$  with  $R_{BESS} = 2\%$ ,  $H_{BESS} = 10 \text{ s}$ , and combined  $R_{BESS}$  and  $H_{BESS}$  of the battery on only the primary response



d) Power discharged from the battery with  $R_{BESS} = 2\%$ ,  $H_{BESS} = 10 \text{ s}$ , and combined  $R_{BESS}$  and  $H_{BESS}$  of the battery on only the primary response



e) Energy discharged of the battery with  $R_{BESS} = 2\%$ ,  $H_{BESS} = 10 \text{ s}$ , and combined  $R_{BESS}$  and  $H_{BESS}$  of the battery on only the primary response



f) Power generation from the synchronous generator with  $R_{BESS} = 2\%$ ,  $H_{BESS} = 10 \text{ s}$ , and combined  $R_{BESS}$  and  $H_{BESS}$  of the battery on only the primary response

Figure 5.7 Effect of the microgrid with  $R_{BESS} = 2\%$ ,  $H_{BESS} = 10 \text{ s}$ , and combined  $R_{BESS}$  and  $H_{BESS}$  of the battery on only the primary response

## 5.2 Primary and Secondary Response

The simulation is an isolated mode microgrid with considering only the primary response. The BESS is installed in the microgrid to enhance the stability of the frequency response. The investigation compares the impacts of the virtual droop and the virtual inertia on the frequency deviation in the microgrid. Moreover, the investigation compares the impact of the secondary response integral gain on the frequency response in the microgrid. Furthermore, the simulation also investigates the connected mode microgrid. The simulation investigates the stability of the frequency response on both instantaneous load increases and a switch at tie-line disconnects.

### 5.2.1 Test System for the Microgrid on the Isolated Mode

Figure 5.1 represents the simplified single line diagram of the test system. Figure 5.8 presents the block diagram of the test system which has both the primary and secondary response. Table 5.4 shows each parameter value in a block diagram. The system inertia ( $H_{sys}$ ) is 5 s which can calculate from (2.9). The time constants  $T_g$  and  $T_t$  are 0.2 s and 0.5 s, respectively. The system droop constant ( $R_{sys}$ ) is 0.05 and the integral gain ( $K_i$ ) is 7. This thesis assumes that there is no frequency-dependent load, i.e.,  $D$  is zero.

In the simulation, the BESS can control to provide the primary response by using two control methods: the virtual droop control and the virtual inertia control. In addition, the simulation varies the value of the integral gain ( $K_i$ ) to investigate the effect of the stability of frequency on the isolated microgrid. For each simulation scenario, a 2-MW load increase occurs at  $t = 5$  s.

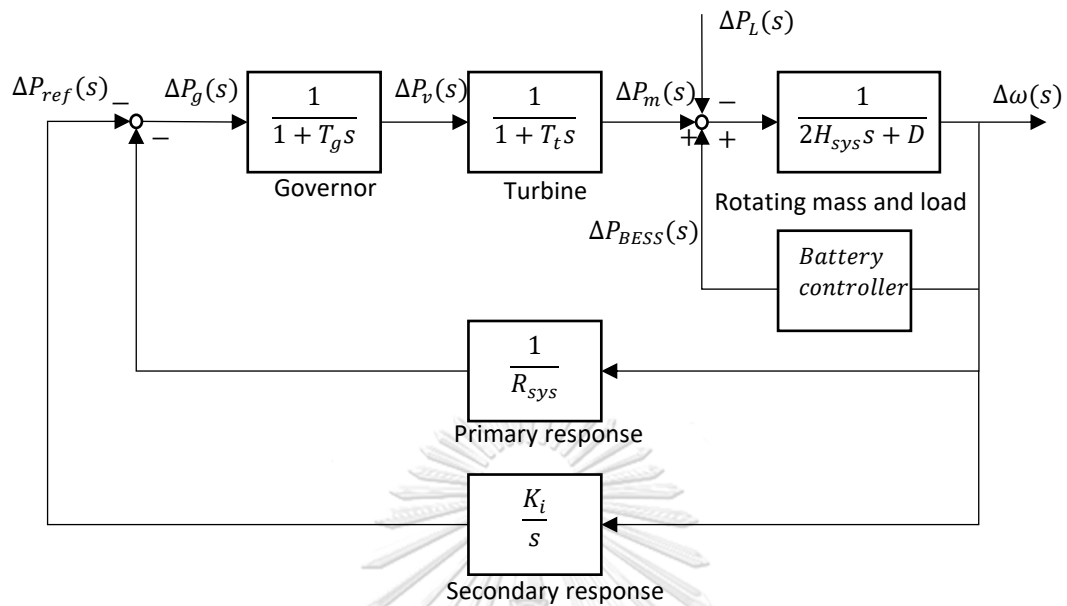


Figure 5.8 Block diagram of the test system

Parameter	Value
System inertia ( $H_{sys}$ )	5 s
Governor time constant ( $T_g$ )	0.2 s
Turbine time constant ( $T_t$ )	0.5 s
System droop constant ( $R_{sys}$ )	0.05
Integral gain ( $K_i$ )	7
Frequency-dependent load ( $D$ )	0

Table 5.4 Value of each parameter in a block diagram of the test system with primary and secondary response

### 5.2.2 Simulation Results for the Microgrid on the Isolated Mode

Three case studies investigate the effects of virtual droop control, virtual inertia control, and varying the integral gain ( $K_i$ ) approaches on the microgrid frequency response. The simulation analyses the performance of both control methods when the microgrid test system is operating in an isolated mode.

### 5.2.2.1 Effect of Various Virtual Droop Constant

A virtual droop can control by using (3.1). The dynamic model presents in figure 3.1 is added to the block diagram of the test system. Figure 5.9 shows a block diagram with a virtual droop control. Table 5.5 shows each parameter value in a block diagram.

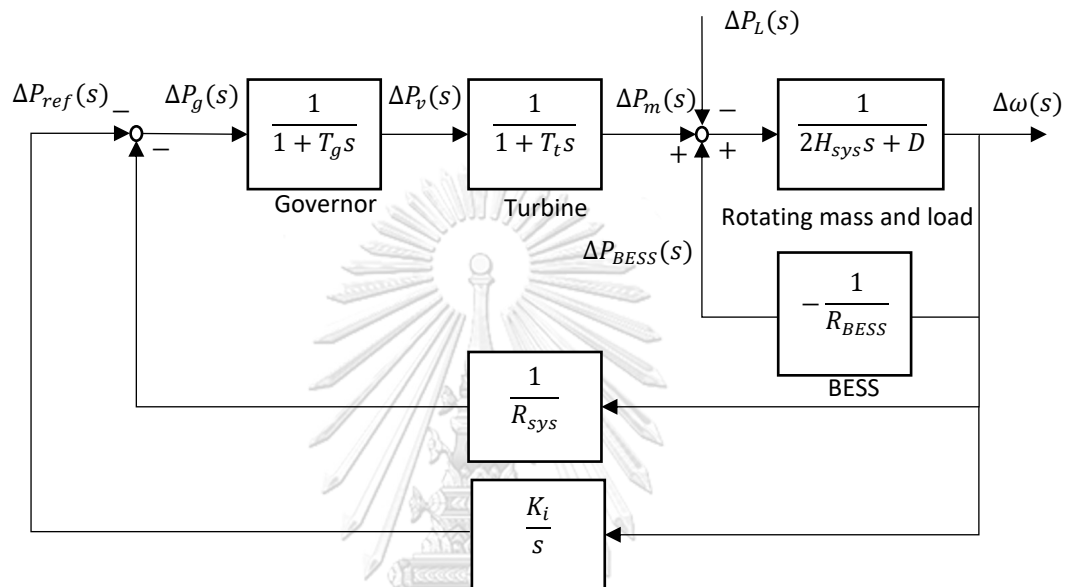


Figure 5.9 Block diagram of the test system with a virtual droop control

Parameter	Value
System inertia ( $H_{sys}$ )	5 s
Governor time constant ( $T_g$ )	0.2 s
Turbine time constant ( $T_t$ )	0.5 s
System droop constant ( $R_{sys}$ )	0.05
Integral gain ( $K_i$ )	7
Frequency-dependent load ( $D$ )	0
Virtual droop constant ( $R_{BESS}$ )	2% to 8%.

Table 5.5 Value of each parameter in a block diagram of the test system with a virtual droop control and secondary response

This case study varies the virtual droop constant from 2% to 8%. The definition of virtual droop constant in this article is the inverse of the gain. The

results are compared with the base case when the BESS does not install to provide frequency regulation. In this case, the energy storage uses for providing the primary response to stop the frequency deviation. Figure 5.10a shows that a 2-MW load increase occurs at  $t = 5$  s.

#### 5.2.2.1.1 Frequency Response

Figure 5.10b presents the frequency response in a microgrid. For the base case scenario, the frequency nadir is 49.29 Hz, and the frequency goes back to its nominal value because of the AGC from the synchronous generator. The period of the frequency response under 49.5 Hz is 1.664 s. When applying the virtual droop control, the frequency nadir is equal to 49.59 Hz at  $R_{BESS} = 8\%$ . When the virtual droop constant decreases, the frequency nadir is reduced to 49.83 Hz at  $R_{BESS} = 2\%$ . In other words, the results can suggest that the less the values of the virtual droop constant, the less the frequency deviation. However, the time using to go to steady-state acts oppositely. That is the more  $R_{BESS}$ , a shorter period to go to steady-state.

#### 5.2.2.1.2 Rate of Change of Frequency

Figure 5.10c presents the rate of change of the frequency (*ROCOF*). The graph indicates that the *ROCOF* for all ranges of the virtual droop constant, including the base case, is commonly equal to -1 Hz/s at  $t = 5$  s. After  $t = 5$  s, when the virtual droop constant has a small value, the *ROCOF* is lower than when the virtual droop constant has a large value. The highest *ROCOF* is -0.23575 Hz/s at  $R_{BESS} = 8\%$  and the lowest *ROCOF* is -0.055268 Hz/s at  $R_{BESS} = 2\%$ . For the base case, the highest *ROCOF* is equal to -1 Hz/s.

#### 5.2.2.1.3 Power and Energy Discharged from the Battery

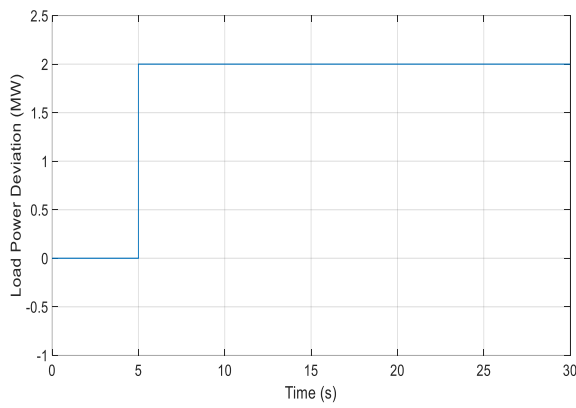
Figure 5.10d and Figure 5.10e show the power and energy discharged from the battery, respectively. Both the amounts of power and energy are large when the virtual droop constant is small. The highest power and energy discharged are 1.7233 MW and 3.964 kWh, respectively at  $R_{BESS} = 2\%$ . While the lowest power and energy discharged are 1.0252 MW and 0.9921 kWh, respectively at  $R_{BESS} = 8\%$ .

#### 5.2.2.1.4 Power Generated from the Synchronous Generator

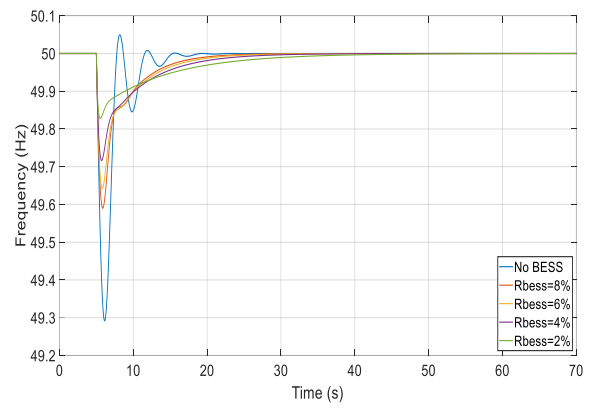
Figure 5.10f shows the power generated from the synchronous generator. The result shows that when the virtual droop constant has a small value, the power generation is lower than when the virtual droop constant has a large value. The synchronous generator provides a small overshoot of power when using the battery. Moreover, the graph suggests that when using the low values of the virtual droop constant, the power from the synchronous generator generates the power slightly smoother than the high virtual droop.



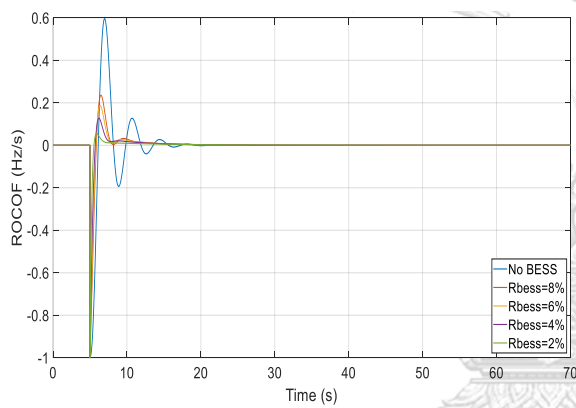




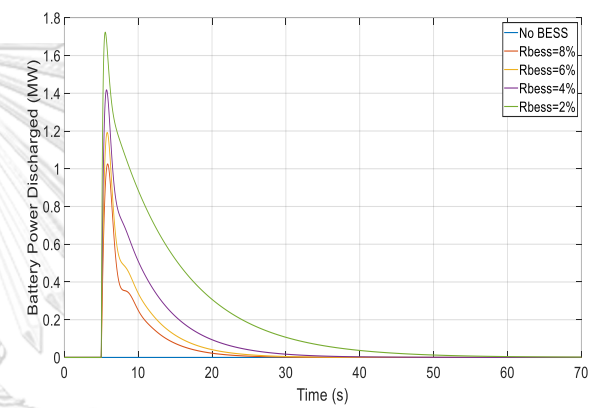
a) Instantaneous 2-MW load increase occurs at  $t = 5$  s in the Mueang Mae Hong Son province



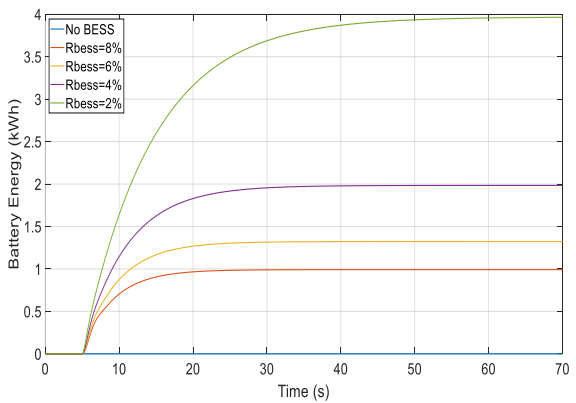
b) Frequency response with various virtual droop constant of the battery on both the primary and secondary response



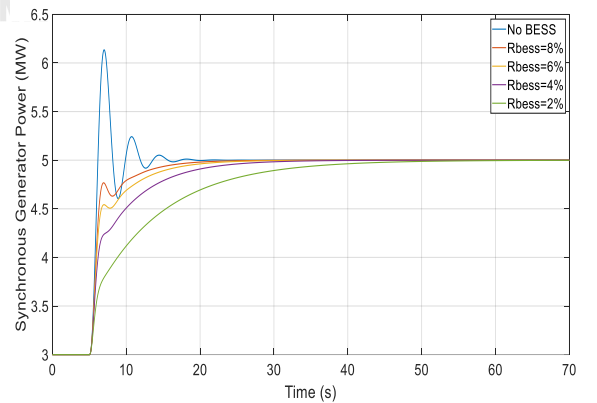
c) *ROCOF* with various virtual droop constant of the battery on both the primary and secondary response



d) Power discharged from the battery with various virtual droop constant of the battery on both the primary and secondary response



e) Energy discharged of the battery with various virtual droop constant of the battery on both the primary and secondary response



f) Power generation from the synchronous generator with various virtual droop constant of the battery on both the primary and secondary response

Figure 5.10 Effect of Various Virtual Droop Constant on Both the Primary and Secondary Response

### 5.2.2.2 Effect of Various Virtual Inertia Constant

The virtual inertia can control by using an equation 3.3. The dynamic model presents in figure 3.4 is added to the block diagram of the test system. Figure 5.11 shows a block diagram with a virtual inertia control. Table 5.6 shows each parameter value in a block diagram.

The virtual inertia control of the BESS acts the same as the inertia of the synchronous generators in the transient state. This case study investigates the effect of varying virtual inertia constant provided by the BESS between 2 s and 10 s and compares the results with the base case when the BESS is out of service. Figure 5.12a shows that a 2-MW load increase occurs at  $t = 5$  s.

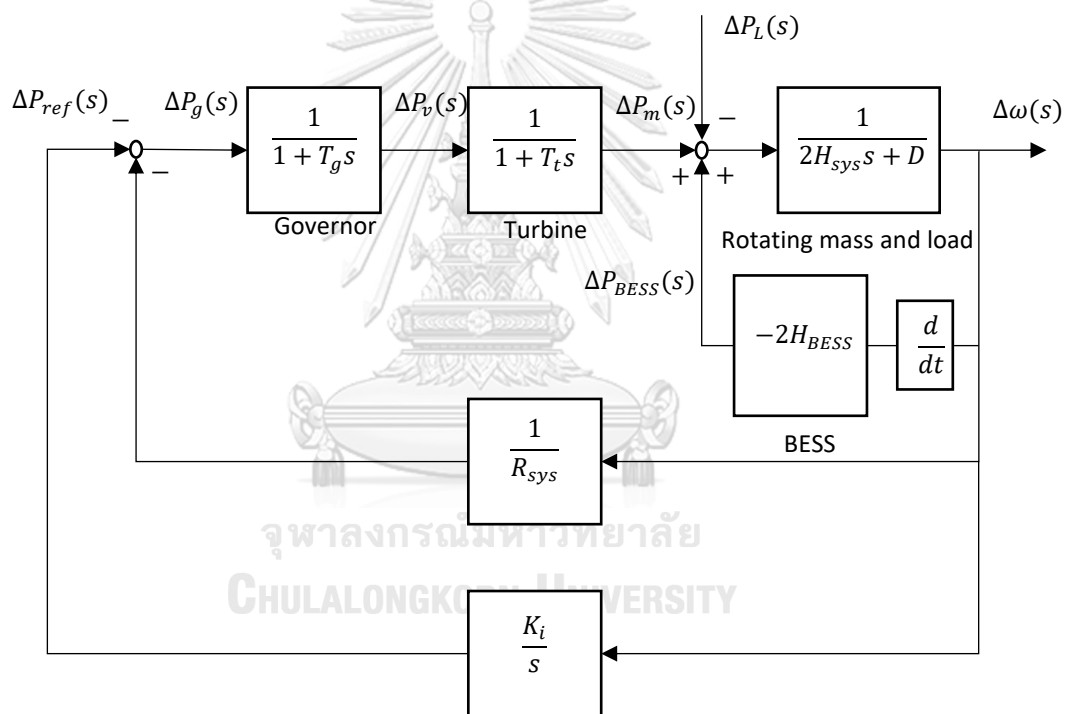


Figure 5.11 Block diagram of the test system with a virtual inertia control

Parameter	Value
System inertia ( $H_{sys}$ )	5 s
Governor time constant ( $T_g$ )	0.2 s
Turbine time constant ( $T_t$ )	0.5 s
System droop constant ( $R_{sys}$ )	0.05
Integral gain ( $K_i$ )	7
Frequency-dependent load ( $D$ )	0
Virtual inertia constant ( $H_{BESS}$ )	2 s to 10 s

Table 5.6 Value of each parameter in a block diagram of the test system with a virtual inertia control and secondary response

#### 5.2.2.2.1 Frequency Response

Figure 5.12b presents the microgrid frequency response. The graph shows that the frequency response deviates from the nominal value of 50 Hz when the load is instantaneously increased by 2 MW at  $t = 5$  s. For the base case scenario, the frequency nadir is 49.29 Hz. The period of the frequency response under 49.5 Hz is 1.664 s. The frequency response has a large deviation when the virtual inertia constant has a small value. The frequency nadir is 49.35 Hz at  $H_{BESS} = 2$  s and the frequency nadir is 49.49 Hz at  $H_{BESS} = 10$  s. The periods of the frequency response under 49.5 Hz are 1.181 s and 0.456 s, respectively. In contrast, the time using to go to a steady-state is inversely proportional to  $H_{BESS}$ . There suggest that the more value of  $H_{BESS}$ , the more extended period to go to a steady-state.

#### 5.2.2.2.2 Rate of Change of Frequency

Figure 5.12c shows the effects of the virtual inertia control on the *ROCOF*. For the base case, the highest *ROCOF* is equal to -1 Hz/s. The results suggest that when the virtual inertia constant has a small value, the *ROCOF* is higher than when the virtual inertia constant has a large value. The maximum *ROCOF* is -0.8296 Hz/s at  $H_{BESS} = 2$  s and the minimum *ROCOF* is -0.4992 Hz/s at  $H_{BESS} = 10$  s.

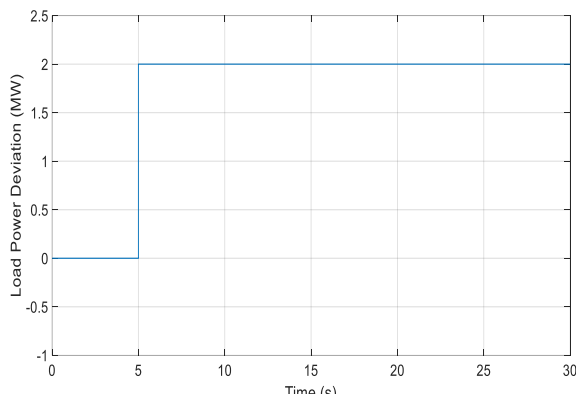
#### 5.2.2.2.3 Power and Energy Discharged from the Battery

Figure 5.12d and Figure 5.12e represent the power and energy discharged from the battery, respectively. The result shows that after increasing load of 2 MW at

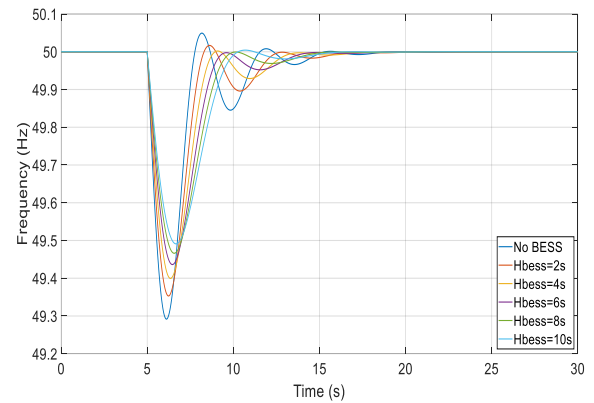
$t = 5 \text{ s}$ , the amount of power and energy which come from the battery discharge depends on the value of the virtual inertia constant. After that, the battery charges the power back until the frequency goes back to the nominal value. In the end, the energy discharged from the battery goes to zero. The maximum of the power and energy from the battery are  $0.9981 \text{ MW}$  and  $0.2828 \text{ kWh}$ , respectively at  $H_{BESS} = 10 \text{ s}$  and the minimum of the power and energy from the battery are  $0.3317 \text{ MW}$  and  $0.0719 \text{ kWh}$ , respectively at  $H_{BESS} = 2 \text{ s}$ .

#### 5.2.2.2.4 Power Generated from the Synchronous Generator

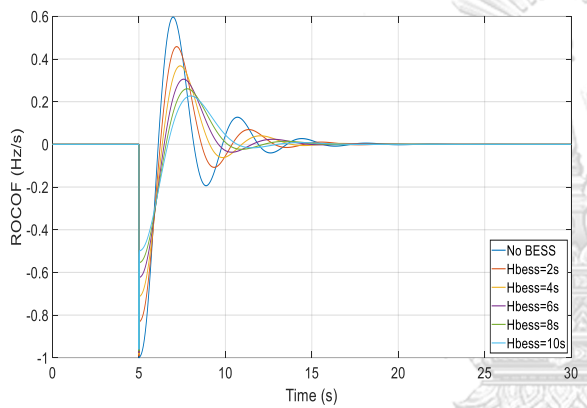
Figure 5.12f presents the power that can generate from the synchronous generator. The result has the opposite pattern of the power that can discharge from the battery. In other words, the less the value of the virtual inertia constant, the more power generation from the synchronous generator. Besides, for the base case, the synchronous generator provides the maximum overshoot of power at  $3.135 \text{ MW}$ . The graph indicates that the overshoot of power generation is  $3.043 \text{ MW}$  at  $H_{BESS} = 2 \text{ s}$  and the minimum overshoot of the power generation is  $2.859 \text{ MW}$  at  $H_{BESS} = 10 \text{ s}$ .



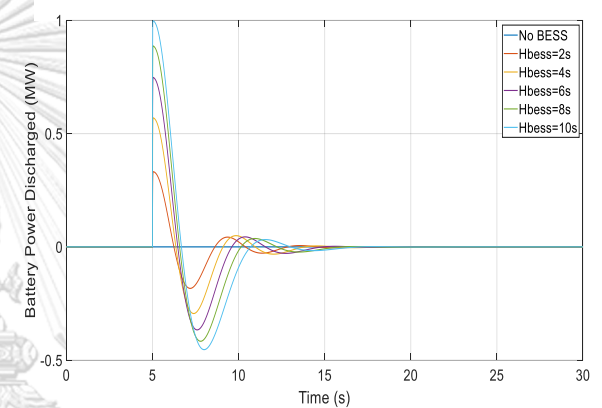
a) Instantaneous 2-MW load increase occurs at  $t = 5 \text{ s}$  in the Mueang Mae Hong Son province



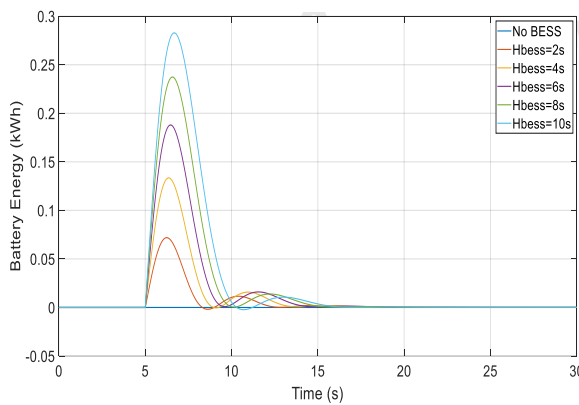
b) Frequency response with various virtual inertia constant of the battery on both the primary and secondary response



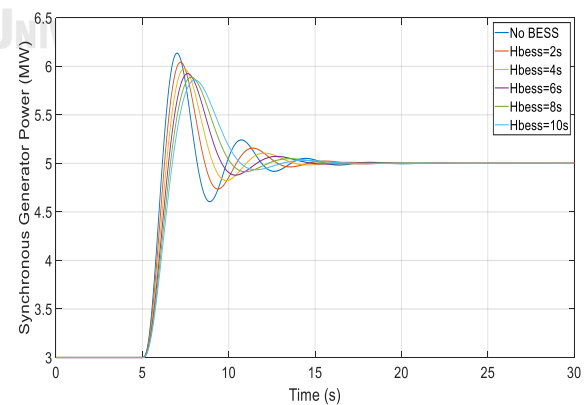
c) *ROCOF* with various virtual inertia constant of the battery on both the primary and secondary response



d) Power discharged from the battery with various virtual inertia constant of the battery on both the primary and secondary response



e) Energy discharged of the battery with various virtual inertia constant of the battery on both the primary and secondary response



f) Power generation from the synchronous generator with various virtual inertia constant of the battery on both the primary and secondary response

Figure 5.12 Effect of Various Virtual Inertia Constant on Both the Primary and Secondary Response

### 5.2.2.3 Effect of varying the integral gain on the secondary response

The investigation presents the stability of frequency response when varying the integral gain ( $K_i$ ). The microgrid also applies BESS control for increasing the stability of frequency response on both primary and secondary responses. The BESS control method is applying the combined a virtual droop and a virtual inertia control. The virtual droop constant ( $R_{BESS}$ ) and the virtual inertia constant ( $H_{BESS}$ ) of the BESS in the simulation are 2% and 10 s, respectively. The  $K_i$  value is the integral gain on the secondary response, which varies from 2 to 10. The secondary response refers to a supplementary control effort to return system frequency to the nominal value, e.g., 50 or 60 Hz, through an integral control action. Then, the time of the frequency deviation go back to the steady-state may affect when  $K_i$  value has changed.

Figure 5.13 shows a block diagram with combined the virtual droop constant ( $R_{BESS}$ ) and the virtual inertia constant ( $H_{BESS}$ ) of the BESS. Table 5.7 shows each parameter value in a block diagram. Figure 5.14a shows that a 2-MW load increase occurs at  $t = 5$  s.

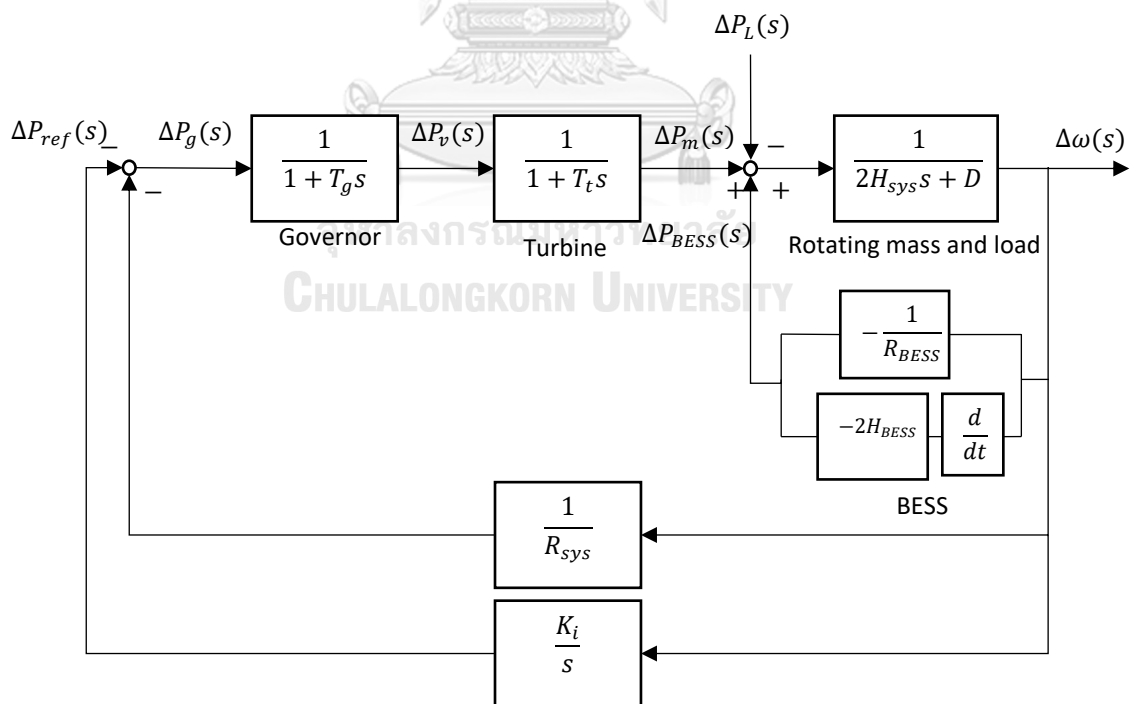


Figure 5.13 Block diagram of the test system with combined the two control methods

Parameter	Value
System inertia ( $H_{sys}$ )	5 s
Governor time constant ( $T_g$ )	0.2 s
Turbine time constant ( $T_t$ )	0.5 s
System droop constant ( $R_{sys}$ )	0.05
Frequency-dependent load ( $D$ )	0
Virtual droop constant ( $R_{BESS}$ )	2%
Virtual inertia constant ( $H_{BESS}$ )	10 s
Integral gain ( $K_i$ )	2 to 10

Table 5.7 Value of each parameter in a block diagram of the test system with combined the two control methods

#### 5.2.2.3.1 Frequency Response

Figure 5.14b presents the frequency response in a microgrid. The investigation shows that when the frequency rapidly decreases when the load instantaneous increases. The graph shows that the primary response does not change when varying the  $K_i$  value. The frequency nadir at  $t = 5$  s is approximately equal to 49.845 Hz for all ranges of  $K_i$  value from 2 to 10. However, the time going back to the steady-state is taking a longer period when the  $K_i$  value is low value. The graph shows that the frequency deviation can go back to the steady-state at the fastest rate when the  $K_i$  value. Moreover, the frequency deviation can go back to the steady-state under 60 s when the  $K_i$  value is less than or equal to 4.

#### 5.2.2.3.2 Rate of Change of Frequency

Figure 5.14c presents the rate of change of the frequency (*ROCOF*). The graph indicates that the *ROCOF* for all ranges of  $K_i$  value from 2 to 10 are commonly equal to -1 Hz/s at  $t = 5$  s. After that, the *ROCOF* is not much different when varying the  $K_i$  value. It can conclude that the *ROCOF* is not noticeable change when varies the  $K_i$  value.

#### 5.2.2.3.3 Power and Energy Discharged from the Battery

Figure 5.14d and Figure 5.14e show the power and energy discharged from the battery, respectively. The graph power discharged indicates that the power discharges from the BESS at  $t = 5$  s to the maximum power at 1.625 MW. Then, the

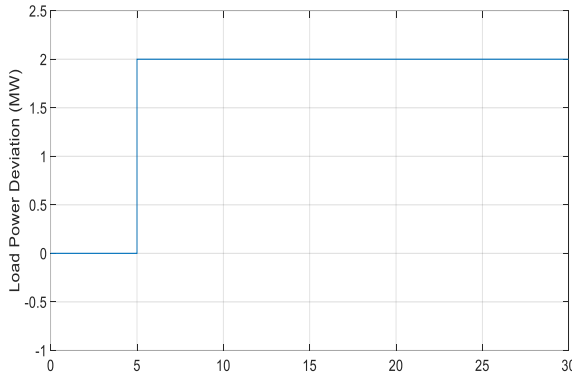
power discharged drops down and goes to constantly 1 *MW* in the end. In addition, the highest power is 1.625 *MW* for all ranges of  $K_i$  value from 2 to 10. However, the power discharged with the small value of  $K_i$  is taking a longer period to go down to 1 *MW* than the high value of  $K_i$ .

On the same direction, the battery energy graph shows that the BESS discharges high energy when the  $K_i$  value is small. When  $K_i$  value is 2, the BESS discharges 18 *kWh* at  $t = 60$  s and continue going up in the end.

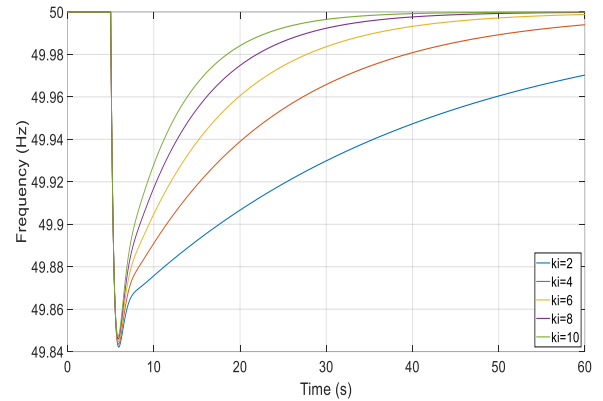
#### 5.2.2.3.4 Power Generated from the Synchronous Generator

Figure 5.14f shows the power generated from the synchronous generator. The initial power generation from the synchronous generator in the microgrid is 3 *MW*. The result shows that the power generated from the synchronous generator instantaneous increases to 3.6 *MW* at  $t = 5$  s. After that, the synchronous generator slowly increases until the power of the synchronous generator goes to 4 *MW* in the end. However, the power generated from the synchronous generator with the small value of  $K_i$  is taking a longer period to go down to 4 *MW* than the high value of  $K_i$ .

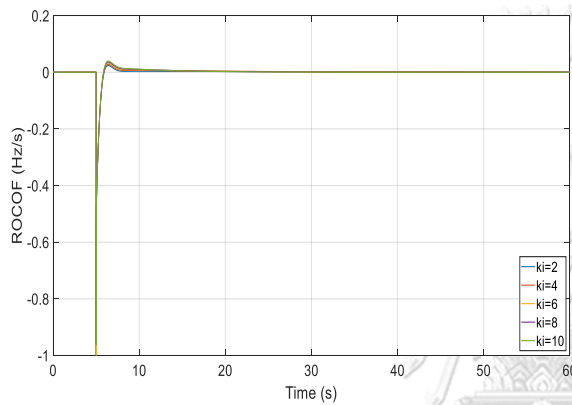




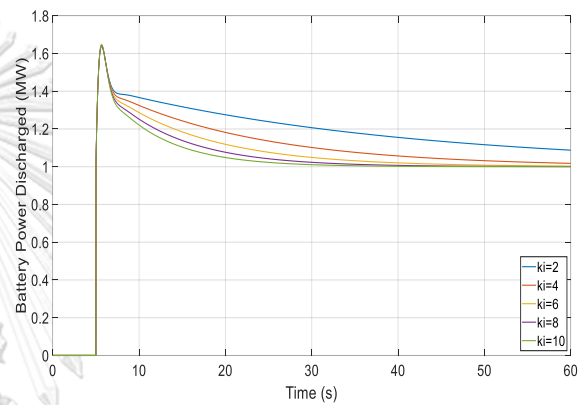
a) Instantaneous 2-MW load increase occurs at  $t = 5 \text{ s}$  in the Mueang Mae Hong Son province



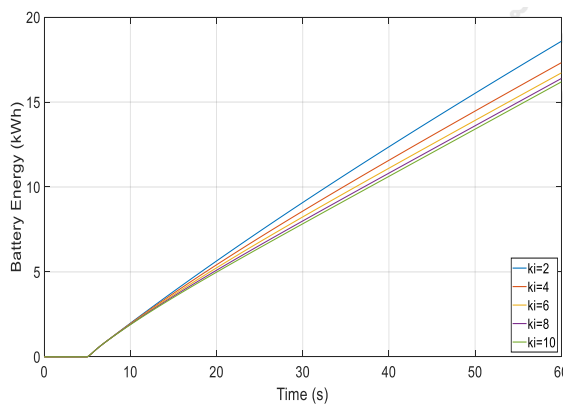
b) Frequency response with various integral gain of the microgrid and using the BESS with combined the virtual droop and virtual inertia.



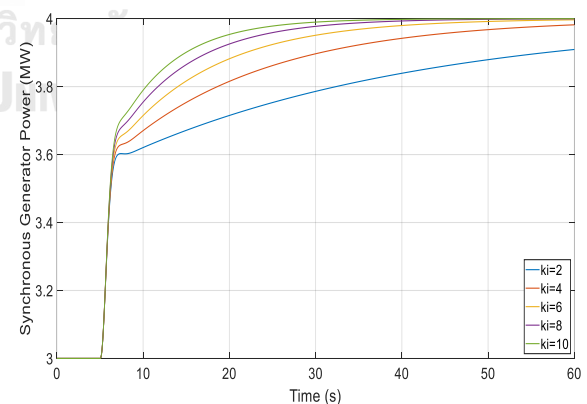
c) *ROCOF* with various integral gain of the microgrid and using the BESS with combined the virtual droop and virtual inertia.



d) Power discharged from the battery with various integral gain of the microgrid and using the BESS with combined the virtual droop and virtual inertia.



e) Energy discharged of the battery with various integral gain of the microgrid and using the BESS with combined the virtual droop and virtual inertia.



f) Power generation from the synchronous generator with various integral gain of the microgrid and using the BESS with combined the virtual droop and virtual inertia.

Figure 5.14 Effect of Various Integral Gain of the Microgrid and Using the BESS with Combined the Virtual Droop and Virtual Inertia

### 5.2.3 Test System for the Microgrid on the Connected Mode

The microgrid can operate in connected mode. The electric power can transfer from the main grid to the microgrid and vice versa by passing through a tie-line. The size of the microgrid is much smaller than the main grid. Therefore, the frequency reference point in the microgrid refers to the main grid. Moreover, the size of the main grid can suggest that the inertia value of the main grid should be much more than the microgrid. Therefore, the investigation sets the inertia value of the main grid that is five times larger than the inertia value of the microgrid.

The investigation presents the main grid and microgrid behaviour on the large disturbance either instantaneous load increases event or a switch at tie-line disconnects event. Figure 5.15 represents the simplified single line diagram of the test system. The microgrid system consists of a 3-*MW* synchronous generator on Mae Sa Nga small hydropower plant, a 3.5-*MW* solar cell generator installs on Pa Bong solar cell power plant, a 4-*MW* BESS system on Pa Bong hydropower plant, and a 3-*MW* load on Mueang Mae Hong Son district. The microgrid connects to the main grid by passing the power through a tie-line. The system operates at a steady-state frequency of 50 *Hz*. Figure 5.16 presents the simplified block diagram of the test system. Table 5.8 shows each parameter value in a block diagram.

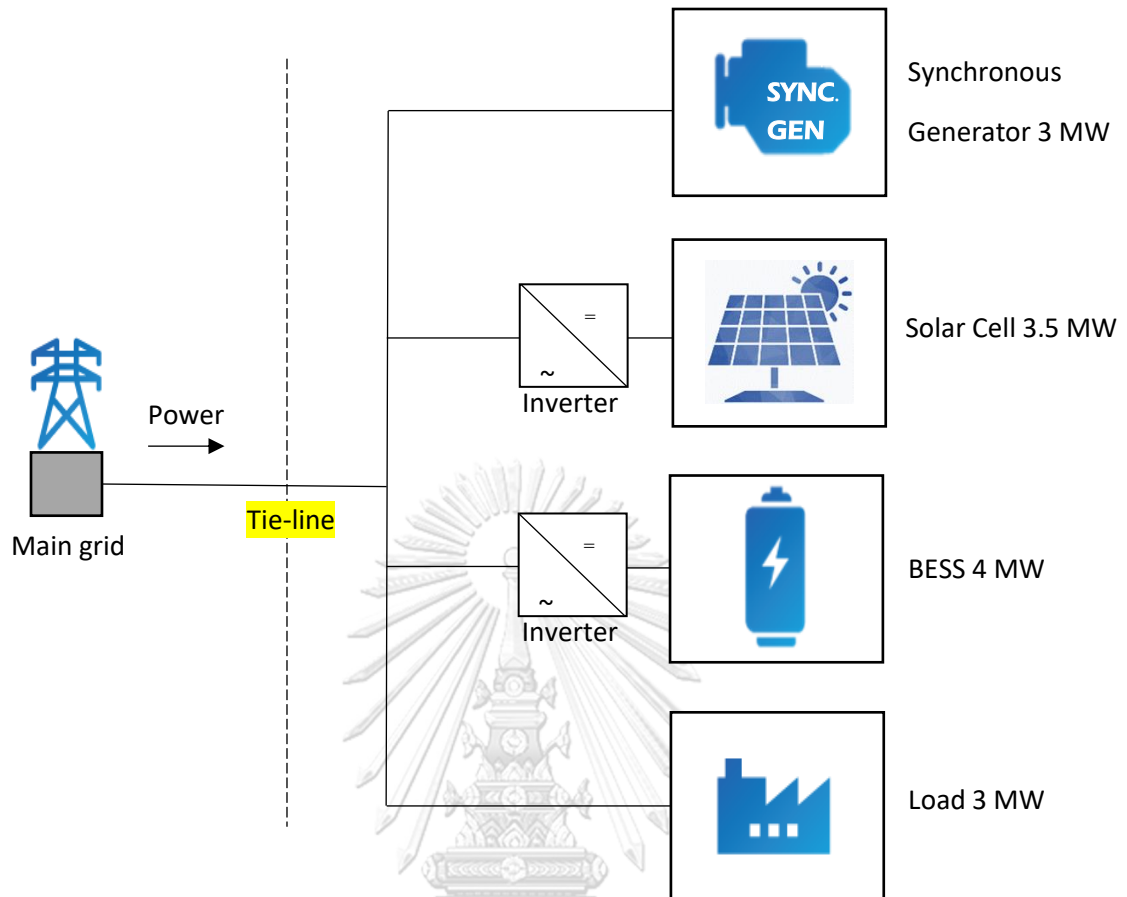


Figure 5.15 Simplified single line diagram of a system on the connected mode

The test systems can separate into two areas that are the main grid and the microgrid. The inertia of the main grid is five times of the microgrid which at 50 seconds and 10 seconds, respectively. The BESS on the microgrid can control to provide the primary response by using combined the virtual droop and the virtual inertia control. Figure 5.17a shows that a  $2\text{-MW}$  load increase occurs at  $t = 5\text{ s}$ .

Parameter	Value
Inertia of the main grid ( $H_{sys1}$ )	50 s
Governor time constant of the main grid ( $T_{g1}$ )	0.2 s
Turbine time constant of the main grid ( $T_{t1}$ )	0.5 s
System droop constant of the main grid ( $R_{sys1}$ )	0.05
Integral gain of the main grid ( $K_{i1}$ )	0.3
Frequency-dependent load of the main grid ( $D_1$ )	0
Frequency bias factor of the main grid ( $B_1$ )	20.6
Inertia of the microgrid ( $H_{sys2}$ )	5 s
Governor time constant of the microgrid ( $T_{g2}$ )	0.3 s
Turbine time constant of the microgrid ( $T_{t2}$ )	0.6 s
System droop constant of the microgrid ( $R_{sys2}$ )	0.0625
Integral gain of the microgrid ( $K_{i2}$ )	0.3
Frequency-dependent load of the microgrid ( $D_2$ )	0
Frequency bias factor of the main grid ( $B_2$ )	66.9
Virtual droop constant ( $R_{BESS}$ )	2%
Virtual inertia constant ( $H_{BESS}$ )	10 s
Integral gain of tie-line ( $P_s$ )	2

Table 5.8 Value of each parameter in a block diagram of the test system for two areas with the combined model between a virtual droop and a virtual inertia

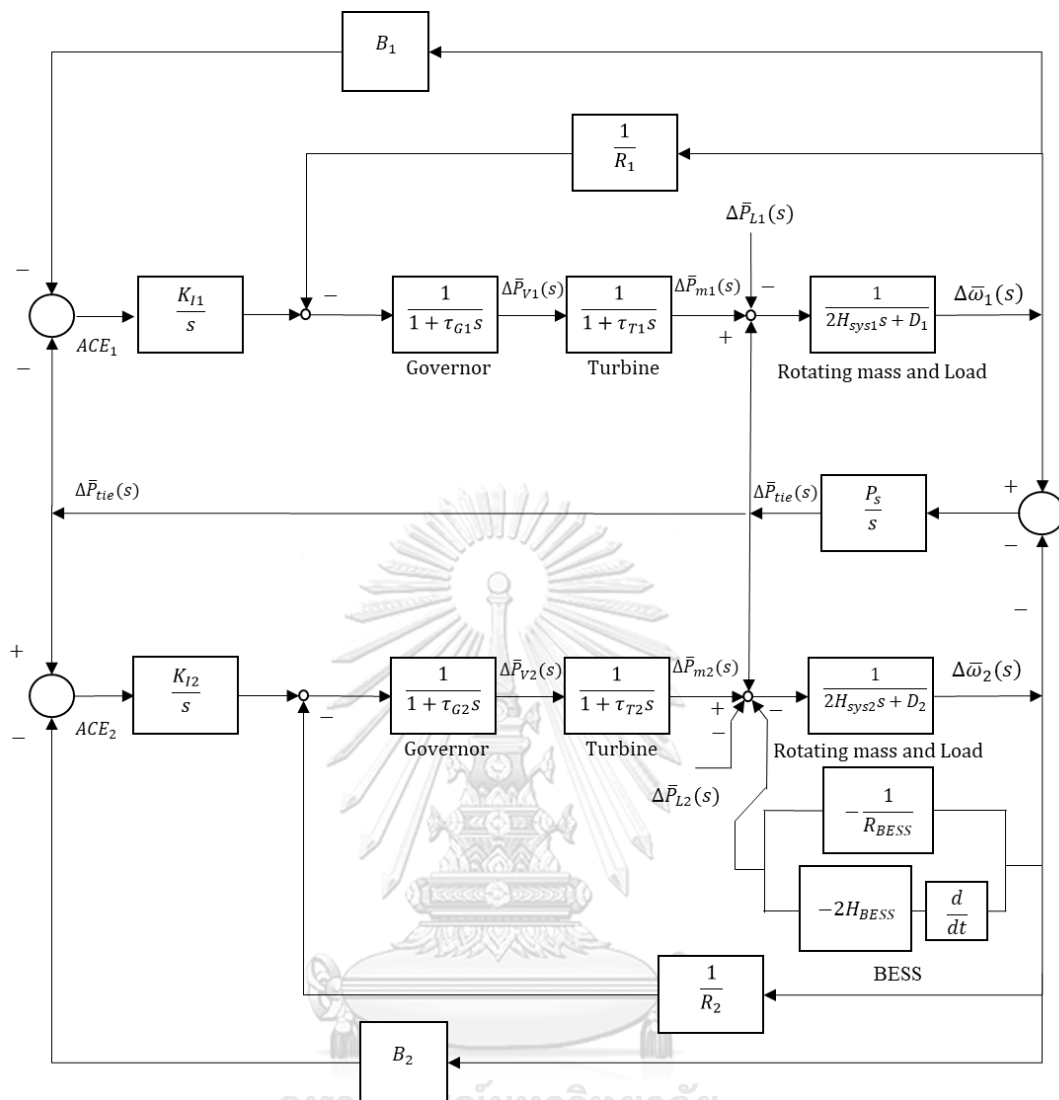


Figure 5.16 Block diagram for two areas with the combined model between a virtual droop and a virtual inertia

## 5.2.4 Simulation Results for the Microgrid on the Connected Mode

### 5.2.4.1 Effect of an Instantaneous Load Increases on the Microgrid

#### 5.2.4.1.1 Frequency Response

Figure 5.17b presents the frequency response in the main grid. The graph shows that the frequency deviation when without applying BESS is larger than when applying BESS either on only the primary response or both primary and secondary response. The frequency nadir when without applying BESS is 49.88 Hz. The frequency nadir when applying BESS either on only the primary response or both

primary and secondary response are not much difference, which are 49.96 *Hz* and 49.964 *Hz*, respectively.

Figure 5.17c presents the frequency response in the microgrid. The graph shows that the frequency deviation when without applying BESS is larger than the standard frequency deviation grid code which is no more than plus or minus 0.5 *Hz*. The graph also shows that the frequency deviation is in the standard frequency deviation grid code when applying BESS either on only the primary response or both primary and secondary response. The frequency nadir when without applying the battery is 49.2 *Hz*. The period of the frequency response under 49.5 *Hz* is 1.599 *s*. The frequency nadir of the frequency response when applying BESS either on only the primary response or both primary and secondary response are not much difference. The frequency nadir when applying BESS on only the primary response and on both primary and secondary response are 49.42 *Hz* and 49.83 *Hz*, respectively.

Moreover, the result can notice that the frequency response in the main grid is much lower than the frequency response in the microgrid. In addition, the result suggests that the frequency deviation on either the main grid or the microgrid are significantly decreasing when applying BESS in the microgrid.

#### 5.2.4.1.2 Rate of Change of Frequency

Figure 5.17d and figure 5.17e present the rate of change of frequency in the main grid and the microgrid, respectively. The graphs show that the *ROCOF* of the main grid when applying BESS either on only the primary response or both primary and secondary response is significantly decreasing than when without applying BESS. The maximum of the *ROCOF* for the main grid when without applying BESS, applying BESS on only the primary response, and applying BESS on both primary and secondary response are -0.046 *Hz/s*, -0.01 *Hz/s*, and -0.009 *Hz/s*, respectively.

However, the maximum of the *ROCOF* in the microgrid when without or with applying BESS either on only the primary response or both primary and secondary response are not much difference. The *ROCOF* of the microgrid are going to -1 *Hz/s* when the large disturbance happens at  $t = 5$  *s*. Although the BESS cannot decrease

the *ROCOF* in the microgrid, the result suggests that the *ROCOF* on the main grid can noticeably decrease when applying BESS in the microgrid.

#### 5.2.4.1.3 Power and Energy Discharged from Battery

Figure 5.17f and figure 5.17g present the power and energy discharged from the battery, respectively. The battery discharges the power to support the instantaneous decreasing of the frequency when the large disturbance happens on the microgrid at  $t = 5$  s. The battery recharges the power back to the battery after  $t = 5$  s. The graph also indicates that the power discharged from the battery goes to zero in the end when applying BESS on only the primary response. The power discharged from the battery goes to 1 MW in the end when applying BESS on both primary and secondary response. The highest battery discharged power when applying BESS on only primary response is 1.65 MW and the battery energy usage goes to constantly 1 kWh. The highest battery discharged power when applying BESS on both primary and secondary response are 1.7 MW and the battery energy usage goes to 15 kWh at  $t = 5$  s and continue going up.

#### 5.2.4.1.4 Power Generation from the Synchronous Generator

Figure 5.17h presents the deviated power generation from the synchronous generator on the main grid. The graph shows that the deviated power generation from the synchronous generator on the main grid when without a help from BESS on the microgrid is higher than when applying the battery on the microgrid. The power generation from the synchronous generator on the main grid when with or without applying BESS is increasing after the large disturbance happens at  $t = 5$  s. The power generation from the synchronous generator increases until to the maximum power generation at 0.39 MW at  $t = 14$  s. After that, the power generation decreases and goes to the zero in the end. The maximum of power generations from the synchronous generator on the main grid when with applying BESS either on only the primary response or both primary and secondary response are not much difference. The maximum of power generations from the synchronous generator on the main grid when with applying BESS either on only the primary response or both primary and secondary response are 0.136 MW and 0.132 MW, respectively.

Figure 5.17i presents the power generation from the synchronous generator on the microgrid. The initial power generation from the synchronous generator in the microgrid is 3 *MW*. The results show that the power generation from the synchronous generator on the microgrid when without applying BESS on the microgrid rapidly increases to 6.2 *MW* after the large disturbance happens at  $t = 5$  s. After that, the power generation decreases and goes to 5 *MW* in the end. The power generation from the synchronous generator on the microgrid when applying BESS increases slower than without applying BESS. The power generation from the synchronous generator on the microgrid when applying BESS on only primary response increases and then constantly produces at 5 *MW* in the end as the same at when without applying BESS.

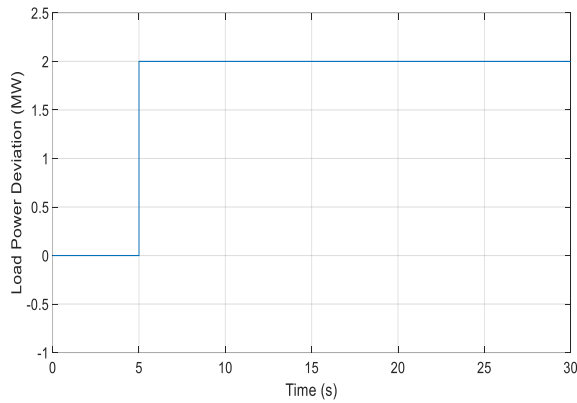
However, the power generation from the synchronous generator on the microgrid is noticeable less decrease when applying the battery on both primary and secondary response. The power from the synchronous generator increases and then constantly produces at 4 *MW*.

#### 5.2.4.1.5 Power at Tie-Line

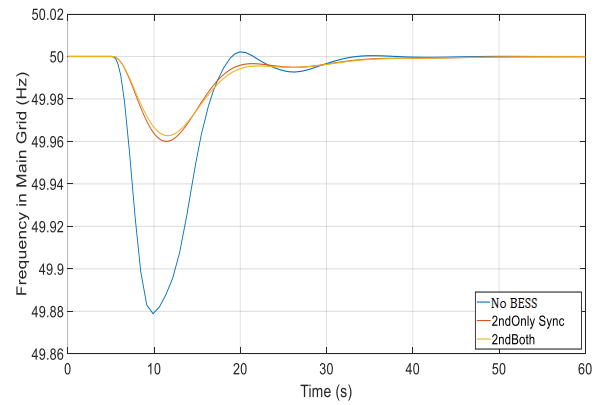
Figure 5.17j presents the power at tie-line that is between the main grid and the microgrid. The positive power at tie-line represents the power that transmits from the main grid to the microgrid. The power at tie-line when without applying BESS on the microgrid is much higher than when applying the battery on the microgrid. The power transfers from the main grid to the microgrid after the large disturbance happens at  $t = 5$  s. The maximum of the power transferred from the main grid to the microgrid when without a help from BESS is 0.54 *MW*. The maximum of the power transferred from the main grid to the microgrid when applying the battery on either only primary response or on both primary and secondary response are not different. The maximum of the power transferred from the main grid to the microgrid when applying the battery on only primary response and on both primary and secondary response are 0.135 *MW* and 0.124 *MW*, respectively.

In addition, the main grid and the microgrid provide frequency regulation until the frequency goes back to the nominal value. The power at tie-line slowly decreases and goes to zero in the end.

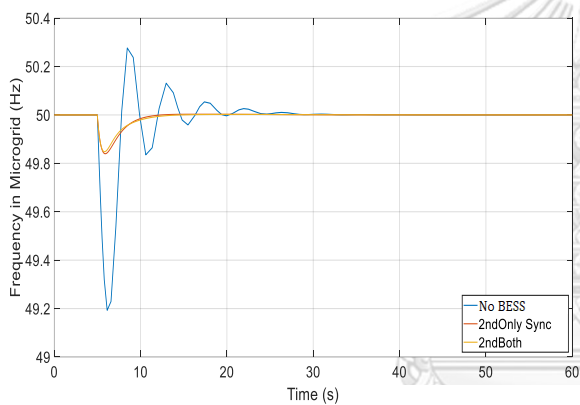




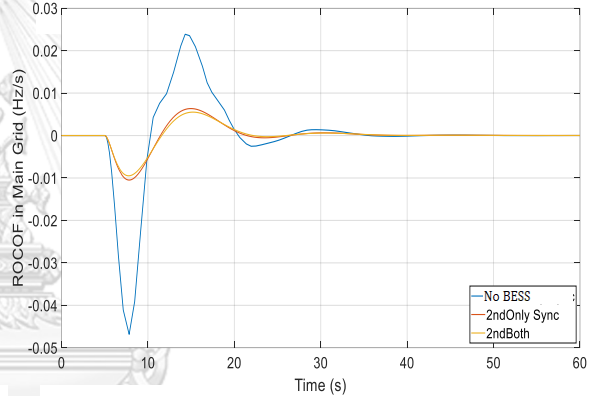
a) Instantaneous 2-MW load increase occurs at  $t = 5$  s in the Mueang Mae Hong Son province



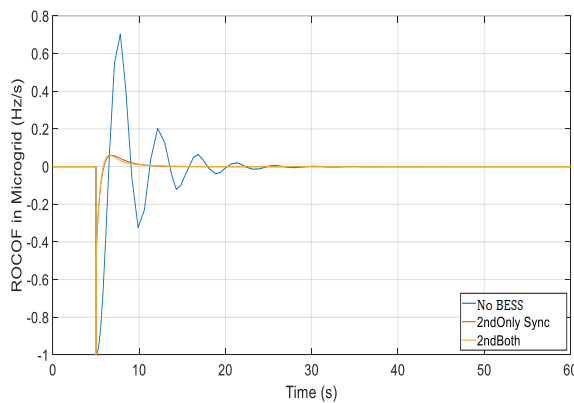
b) Frequency response in the main grid with various BESS; no BESS, BESS on only primary response, and BESS on both primary and secondary response



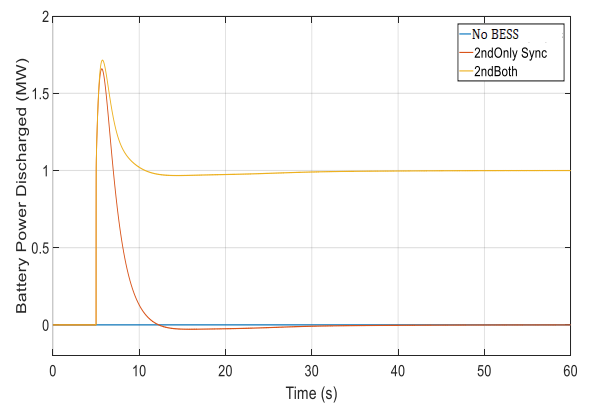
c) Frequency response in the microgrid with various BESS; no BESS, BESS on only primary response, and BESS on both primary and secondary response



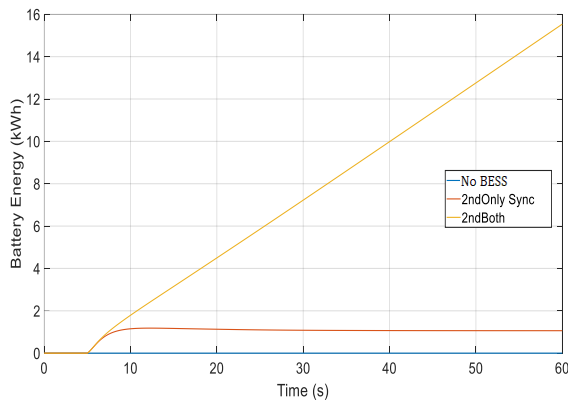
d) ROCOF in the main grid with various BESS; no BESS, BESS on only primary response, and BESS on both primary and secondary response



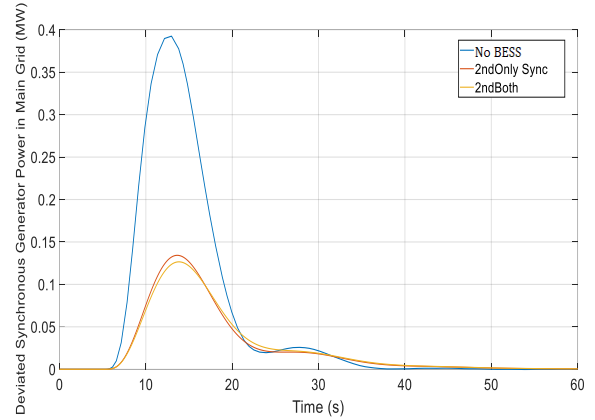
e) ROCOF in the microgrid with various BESS; no BESS, BESS on only primary response, and BESS on both primary and secondary response



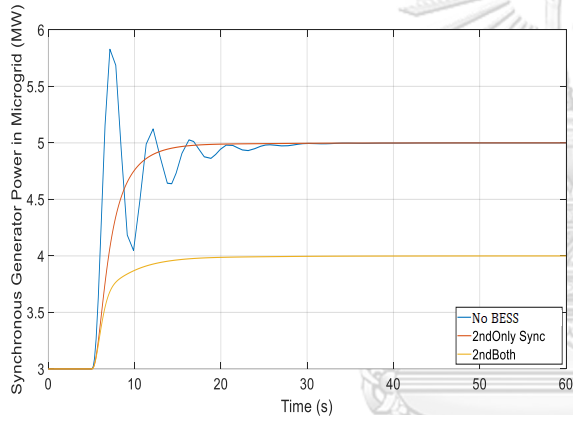
f) Power discharged from the battery with various BESS; no BESS, BESS on only primary response, and BESS on both primary and secondary response



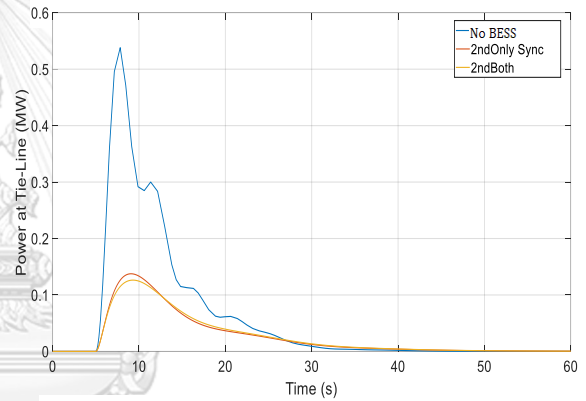
g) Energy output from the battery with various BESS; no BESS, BESS on only primary response, and BESS on both primary and secondary response



h) deviated power generation from the synchronous generator in the main grid with various BESS; no BESS, BESS on only primary response, and BESS on both primary and secondary response



i) Power generation from the synchronous generator in the microgrid with various BESS; no BESS, BESS on only primary response, and BESS on both primary and secondary response



j) Power at tie-line with various BESS; no BESS, BESS on only primary response, and BESS on both primary and secondary response

Figure 5.17 Effect of the Microgrid with or without Applying the BESS when the Large Disturbance Happens on the Microgrid

#### 5.2.4.2 Effect of Power at Tie-Line Instantaneous Disconnects

The initial power transferred from the main grid to the microgrid is  $2\text{ MW}$  at  $t = 0\text{ s}$ . The power at tie-line is cut off at  $t = 5\text{ s}$ . Figure 5.18a shows that the load in the microgrid instantaneous increases  $2\text{ MW}$  after  $t = 5\text{ s}$ .

##### 5.2.4.2.1 Frequency Response

Figure 5.18b presents the frequency response in the main grid. The graph shows that the frequency deviation when with or without applying BESS is commonly the same. The frequency of the main grid increases after the tie-line instantaneous disconnects from each other at  $t = 5\text{ s}$ . The highest frequency response is  $50.035\text{ Hz}$ .

Figure 5.18c presents the frequency response in the microgrid when the tie-line instantaneous disconnects at  $t = 5\text{ s}$ . The graph shows that the frequency deviation when without applying BESS is larger than the standard frequency deviation grid code which is no more than plus or minus  $0.5\text{ Hz}$ . The frequency nadir when without applying the battery is  $49.12\text{ Hz}$ . The graph can noticeable that the frequency deviation much decreases and lives in the standard frequency deviation grid code when applying BESS either on only the primary response or both primary and secondary response. The frequency nadir of the frequency response when applying BESS either on only the primary response or both primary and secondary response are not much difference. The frequency nadir when applying BESS on only the primary response and on both primary and secondary response are  $49.12\text{ Hz}$  and  $49.13\text{ Hz}$ , respectively.

Moreover, the result can noticeable that the frequency response in the microgrid is much lower than the frequency response in the main grid when applying the BESS in the microgrid. In addition, the result suggests that the frequency deviation on either the main grid or the microgrid are significantly decreasing when applying BESS in the microgrid.

##### 5.2.4.2.2 Rate of Change of Frequency

Figure 5.18d and figure 5.18e present the rate of change of frequency in the main grid and the microgrid, respectively. The graphs show that the *ROCOF* of the main grid when with or without applying BESS in the microgrid is not much different. The maximum of the *ROCOF* for the main grid happens when the tie-line

instantaneous disconnects from each other at  $t = 5$  s. The maximum of the *ROCOF* for the main grid is  $0.25$  Hz/s.

In the same direction, the maximum of the *ROCOF* in the microgrid when without or with applying BESS is not much difference. The *ROCOF* of the microgrid are going to  $-1$  Hz/s when the tie-line instantaneous disconnects from each other at  $t = 5$  s. Although the BESS cannot decrease the *ROCOF* in the microgrid, the result can noticeable that the *ROCOF* on the microgrid when applying BESS in the microgrid is less vary than without BESS.

#### 5.2.4.2.3 Power and Energy Discharged from Battery

Figure 5.18f and Figure 5.18g present the power and energy discharged from the battery, respectively. The battery discharges the power to support the instantaneous decreasing of the frequency in the microgrid when the tie-line instantaneous disconnects from each other at  $t = 5$  s. The battery recharges the power back to the battery after  $t = 5$  s. The graph also indicates that the power discharged from the battery goes to zero in the end when applying BESS on only the primary response. The power discharged from the battery to the microgrid constantly at  $1$  MW in the end when applying BESS on both primary and secondary response. The highest battery discharged power when applying BESS on only primary response is  $1.65$  MW and the battery energy usage goes to constantly  $1.36$  kWh. The highest battery discharged power when applying BESS on both primary and secondary response are  $1.7$  MW and the battery energy usage goes to  $15.8$  kWh at  $t = 60$  s and continue going up.

#### 5.2.4.2.4 Power Generation from the Synchronous Generator

Figure 5.18h presents the deviated power generation from the synchronous generator on the main grid. The graph shows that the deviated power generation from the synchronous generator on the main grid when with or without applying BESS on the microgrid is commonly the same. After the tie-line instantaneous disconnects from each other at  $t = 5$  s, the main grid must regulate and maintain the frequency deviation by itself without helping from BESS in the microgrid. The power generation from the synchronous generator deviates down until to the maximum

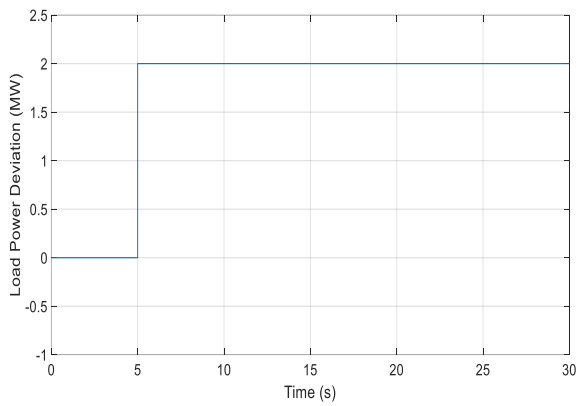
power generation at  $-2.7 \text{ MW}$  at  $t = 12 \text{ s}$ . After that the deviation of power generation increases and goes to  $-2 \text{ MW}$  in the end.

Figure 5.18i presents the power generation from the synchronous generator on the microgrid. The initial power generation from the synchronous generator in the microgrid is  $3 \text{ MW}$ . The results show that the power generation from the synchronous generator on the microgrid when without applying BESS on the microgrid rapidly increases to  $6.2 \text{ MW}$  after the tie-line instantaneous disconnects from each other at  $t = 5 \text{ s}$ . After that, the power generation decreases and goes to  $5 \text{ MW}$  in the end.

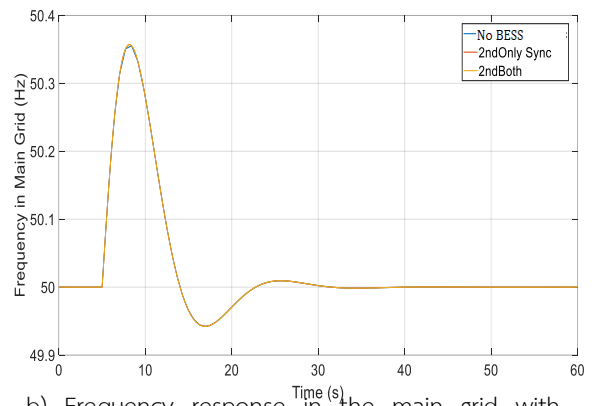
In the opposite direction, the power generation from the synchronous generator on the microgrid when applying BESS increases slower than without applying BESS. The power generation from the synchronous generator on the microgrid when applying BESS on only primary response increases and then constantly produces at  $5 \text{ MW}$  in the end as the same at when without applying BESS. However, the power generation from the synchronous generator on the microgrid is noticeable less decrease when applying the battery on both primary and secondary response. The power from the synchronous generator increases and then constantly produces at  $4 \text{ MW}$ .

#### 5.2.4.2.5 Power at Tie-Line

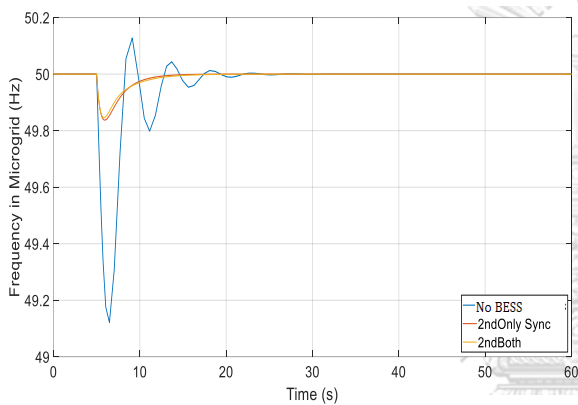
Figure 5.18j presents the power at tie-line that is between the main grid and the microgrid. The positive power at tie-line represents the power that transmits from the main grid to the microgrid. The initial power at tie-line is  $2 \text{ MW}$  which the power transfers from the main grid to the microgrid. The power goes to zero after the tie-line instantaneous disconnects from each other at  $t = 5 \text{ s}$ .



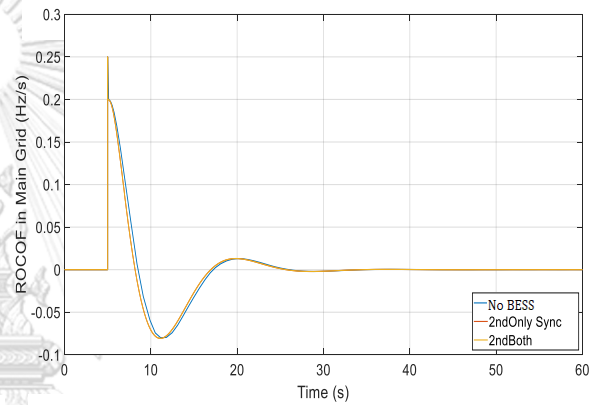
a) Instantaneous 2-MW load increase occurs at  $t = 5\text{ s}$  in the Mueang Mae Hong Son province



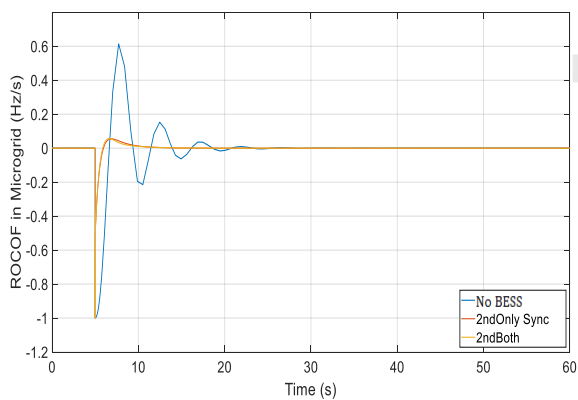
b) Frequency response in the main grid with various BESS; no BESS, BESS on only primary response, and BESS on both primary and secondary response



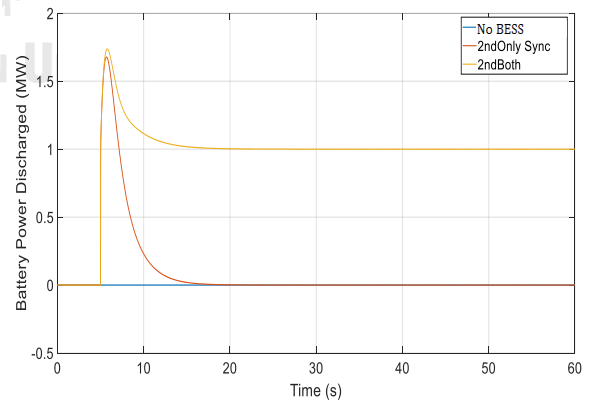
c) Frequency response in the microgrid with various BESS; no BESS, BESS on only primary response, and BESS on both primary and secondary response



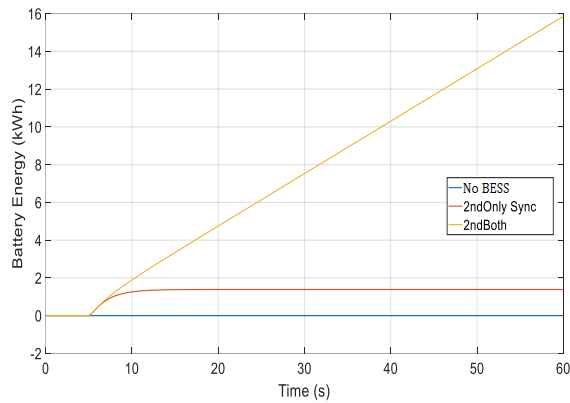
d) *ROCOF* in the main grid with various BESS; no BESS, BESS on only primary response, and BESS on both primary and secondary response



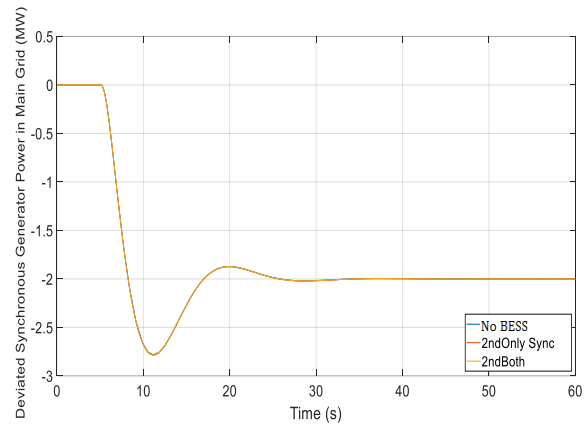
e) *ROCOF* in the microgrid with various BESS; no BESS, BESS on only primary response, and BESS on both primary and secondary response



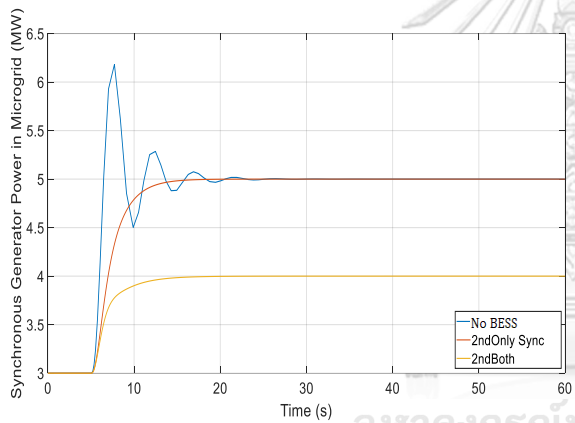
f) Power discharged from the battery with various BESS; no BESS, BESS on only primary response, and BESS on both primary and secondary response



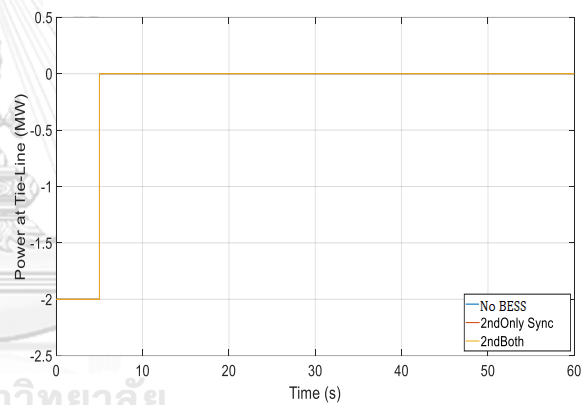
g) Energy output from the battery with various BESS; no BESS, BESS on only primary response, and BESS on both primary and secondary response



h) deviated power generation from the synchronous generator in the main grid with various BESS; no BESS, BESS on only primary response, and BESS on both primary and secondary response



i) Power generation from the synchronous generator in the microgrid with various BESS; no BESS, BESS on only primary response, and BESS on both primary and secondary response



j) Power at tie-line with various BESS; no BESS, BESS on only primary response, and BESS on both primary and secondary response

Figure 5.18 Effect of Disconnecting Switch at Tie-Line with or without Applying the BESS on the Microgrid

## Chapter 6

### Investigation the Possibility of BESSs Design for Increasing the Stability of Frequency Response when Using the Power from the Solar Cell

This chapter shows an investigation of BESS control for increasing the stability of frequency response when the microgrid has an installation of solar cells. The power generation from solar cells depends on an intensity of light from the sun during the day, which is not constant. Therefore, the power generation from solar cells is not consistent as same as the power from a synchronous generator. Sometimes, solar cells generate electricity at the maximum capacity, and then the power generation suddenly drops down to zero due to some clouds pass by the sun. This situation leads to the high variation of frequency response on the microgrid due to the rapid change of the power generation from solar cells.

Moreover, the beginning of the day has an issue of frequency response. Solar cells start generating electric power at the beginning of the day. The frequency of the microgrid is over frequency response due to an instantaneous increasing power from solar cells. The objective of the chapter is to investigate the performance of BESS on the stability of the microgrid in the islanding mode and connected mode. This chapter compares the impacts of BESS, which uses only the virtual droop control, only a virtual inertia control, and combined a virtual droop and a virtual inertia control on the frequency deviation in the microgrid. This chapter divides an investigation of the frequency response into two modes, islanding mode and connected mode. For each mode of operation, there are two parts of the study, first, on the highest variation of power output from the solar cells during the day, second, solar cells start generating electric power at the beginning of the day.

#### 6.1 Islanding mode

Islanding mode uses the Mueang Mae Hong Son province to be a test system. Figure 3.2 presents a single line diagram of Mueang Mae Hong Son province. The test system consists of 3 MW-synchronous generators from Mae Sa Nga small hydropower plant, 3.5 MW-solar cells from Pa Bong solar-PV power plant, 4 MW-BESS from Pa Bong battery system, and 3 MW-total loads in Mueang Mae Hong Son province.



### 6.1.1 The Highest Variation of Power Output from the Solar Cells During the Day

The highest variation of power output from the solar cells mostly happen in the middle of the day from 12:00 to 13:00. Solar cells generate the maximum capacity of power in that period. Therefore, the power generation rapidly drop-down when some clouds pass by the sun. Then, the large gap of power output from solar cells occurs in that period. Moreover, the high variation of power output also occurs on the day, which has a high density of the cloud. Figure 6.1a shows the high variation of power output from the solar cells in the Mueang Mae Hong Son province between 12:52:30 and 12:53:30.

The investigation presents the microgrid behaviour on the highest variation of power output from the solar cells during the day with or without BESS in the microgrid. When applying the BESS to the microgrid, this investigation also compares between a help from BESS on only primary response and on both primary and secondary response.

#### 6.1.1.1 Test System

Figure 5.1 represents the simplified single line diagram of the test system. Figure 5.13 shows a block diagram with combined the virtual droop constant ( $R_{BESS}$ ) and the virtual inertia constant ( $H_{BESS}$ ) of the BESS. Table 5.7 shows each parameter value in a block diagram. Figure 6.1a shows the power output from the solar cells in the Mueang Mae Hong Son province between 12:52:30 and 12:53:30.

#### 6.1.1.2 Simulation results

##### 6.1.1.2.1 Frequency Response

Figure 6.1b presents the frequency response in the microgrid. For no BESS on the microgrid, the frequency nadir is 49.9 Hz. The standard deviation of the frequency response is 0.048. When applying BESS on the only primary response, the frequency nadir is 49.94 Hz. The standard deviation of the frequency response is 0.03. As same as, when applying BESS on the both primary and secondary response, the frequency nadir is 49.945 Hz. The periods of the frequency response over 50.05 Hz are 9.89 s, 5.39 s, and 5.1 s, respectively. The periods of the frequency response under 49.96 Hz are 10.24 s, 4.28 s, and 2.97 s, respectively. The standard deviation of the frequency response is 0.029. The results suggest that when applying BESS to

help the frequency response, the frequency deviation is significantly reduced. Moreover, the variation of frequency response decreases when using BESS to help the frequency response. In addition, the results show that when applying BESS either on only primary response or on both primary and secondary response, the frequency response of two methods is hardly difference.

#### 6.1.1.2.2 Rate of Change of Frequency

Figure 6.1c presents the rate of change of frequency (*ROCOF*). The graph shows that the *ROCOF* is not only high the rate but also high the variation of the *ROCOF* when without a help from BESS, the highest *ROCOF* is  $-0.09 \text{ Hz/s}$  and the standard deviation is equal to 0.02, respectively. The *ROCOF* is close to zero and vary less when applying a help from BESS. The *ROCOF* of two methods, either on only primary response or on both primary and secondary response, are the same. The highest *ROCOF* are  $-0.015 \text{ Hz/s}$  and the standard deviation is equal to 0.005, respectively.

#### 6.1.1.2.3 Power and Energy Discharged from Battery

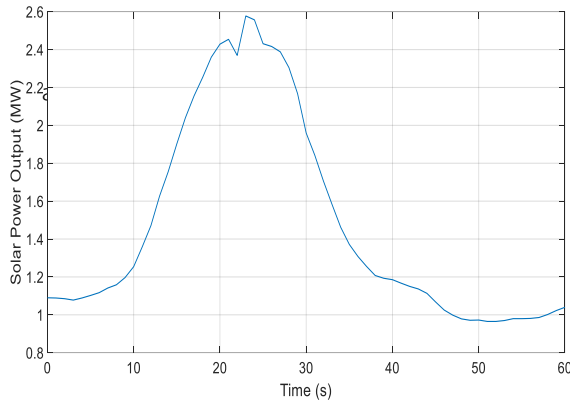
Figure 6.1d and figure 6.1e present the power and energy discharged from the battery, respectively. The power from solar cells is charged to the battery when solar cells generate instantaneous increasing power to the microgrid. The battery discharges the power to the microgrid when the power output from solar cells rapidly decrease. The graph shows that the power is charged to battery for the first 24 seconds, on between 12:52:30 to 12:52:54, and then is discharged from the battery for after 24 seconds, on between 12:52:54 to 12:53:30. The highest battery discharged power/energy is  $0.6 \text{ MW}/2.1 \text{ kWh}$  when applying BESS on only primary response and is  $0.9 \text{ MW}/3.8 \text{ kWh}$  when applying BESS on both primary and secondary response, respectively.

#### 6.1.1.2.4 Power Generation from the Synchronous Generator

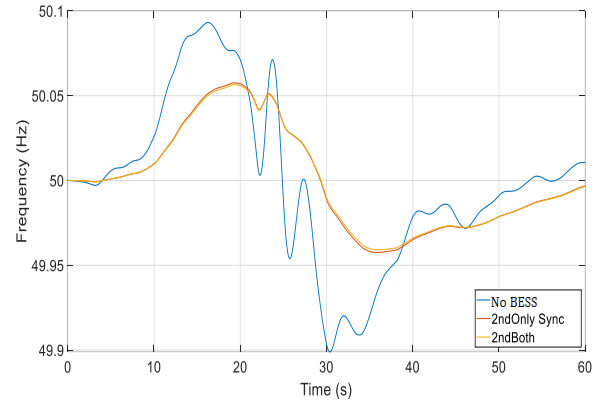
Figure 6.1f presents the power generation from the synchronous generator. The initial power generation from the synchronous generator is  $3 \text{ MW}$  at 12:52:30. The results show that the power generation from the synchronous generator is rapidly decreasing to  $1.4 \text{ MW}$  when without a help from BESS on the microgrid. The variation of power generation from the synchronous generator is also high, the

standard deviation is 0.55. Furthermore, the power generation from the synchronous generator decrease when applying BESS either on only primary response or on both primary and secondary response, the lowest power generations from the synchronous generator go to 1.9 *MW* and 2.4 *MW*, respectively. The variation of power generation from the synchronous generator vary less. The standard deviation decreases to 0.385 and 0.215, respectively.

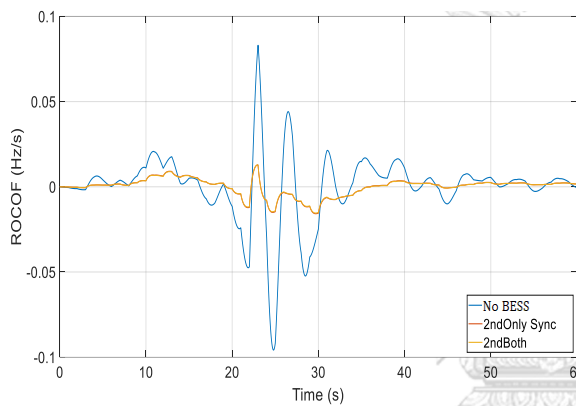




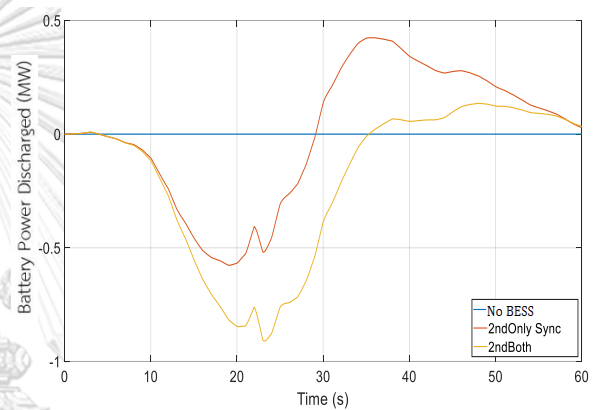
a) Power output from the solar cells in the Mueang Mae Hong Son province between 12:52:30 and 12:53:30



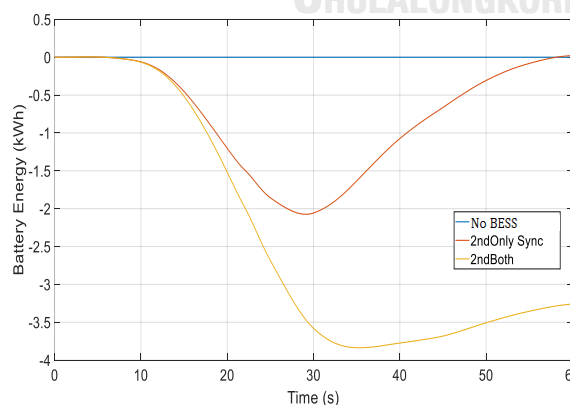
b) Frequency response with various BESS; no BESS, BESS on only primary response, and BESS on both primary and secondary response



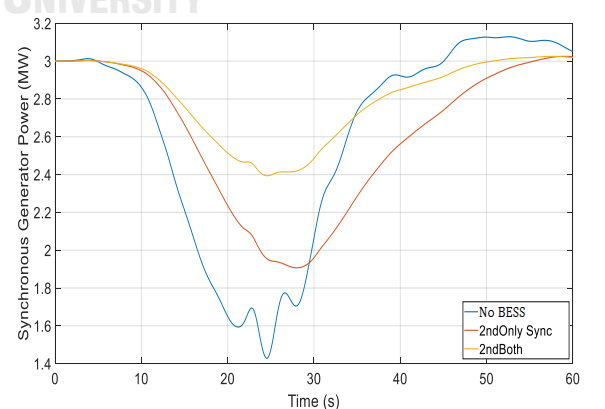
c) *ROCOF* with various BESS; no BESS, BESS on only primary response, and BESS on both primary and secondary response



d) Power discharged from the battery with various BESS; no BESS, BESS on only primary response, and BESS on both primary and secondary response



e) Energy output from the battery with various BESS; no BESS, BESS on only primary response, and BESS on both primary and secondary response



f) Power generation from the synchronous generator with various BESS; no BESS, BESS on only primary response, and BESS on both primary and secondary response

Figure 6.1 The Highest Variation of Power Output from the Solar Cells During the Day on an Isolated Microgrid

## 6.2 Grid Connected

### 6.2.1 The Highest Variation of Power Output from the Solar Cells During the Day

The microgrid can operate in connected mode. The electric power can transfer from the main grid to the microgrid and vice versa by passing through a tie-line. The size of the microgrid is much smaller than the main grid. Therefore, the frequency reference point in the microgrid refers to the main grid. Figure 6a shows the power output from the solar cells in the Mueang Mae Hong Son province between 12:52:30 and 12:53:30. The highest variation of power output from the solar cells happens on that period.

The investigation presents the main grid and microgrid behaviour on the highest variation of power output from the solar cells during the day with or without BESS in the microgrid. When applying the BESS to the microgrid, this investigation also compares between a help from BESS on only primary response and on both primary and secondary response.

#### 6.2.1.1 Test System

The test systems can separate into two areas that are the main grid and the microgrid. The inertia of the main grid is five times of the microgrid which at 50 seconds and 10 seconds, respectively. Figure 3.7 presents a combined model of BESS control between a virtual droop control and a virtual inertia control. Figure 5.15 represents the simplified single line diagram of the test system. The microgrid system consists of a 3-*MW* synchronous generator on Mae Sa Nga small hydropower plant, a 3.5- *MW* solar cell generator installs on Pa Bong solar cell power plant, a 4-*MW* BESS system on Pa Bong hydropower plant, and a 3-*MW* load on Mueang Mae Hong Son district. The microgrid connects to the main grid by passing the power through a tie-line. The system operates at a steady-state frequency of 50 *Hz*. Figure 5.16 presents the simplified block diagram of the test system. Table 5.8 shows each parameter value in a block diagram.

The power output from solar cells is an input value of the diagram. Figure 6.4a shows that the power output from the solar cells in the Mueang Mae Hong Son province between 12:52:30 and 12:53:30. The input value is injected at  $\Delta\bar{P}_{L2}$  as per unit.

### 6.2.1.2 Simulation Results

#### 6.2.1.2.1 Frequency Response

Figure 6.4b presents the frequency response in the main grid. The graph shows that the frequency deviation when without applying BESS is larger than when applying BESS either on only the primary response or both primary and secondary response. The frequency nadir when without applying BESS is 49.9489 *Hz*. The frequency nadir when applying BESS either on only the primary response or both primary and secondary response are not much difference, which are 49.9817 *Hz* and 49.9824 *Hz*, respectively. The periods of the frequency response over 50.01 *Hz* are 16.2 *s*, 11.07 *s*, and 11.01 *s*, respectively. The periods of the frequency response under 49.99 *Hz* are 23.47 *s*, 8.56 *s*, and 8.27 *s*, respectively.

Figure 6.4c presents the frequency response in the microgrid. The graph shows that the frequency deviation when without applying BESS is larger than when applying BESS either on only the primary response or both primary and secondary response. The frequency variation when without applying BESS is also higher than when applying BESS. The frequency nadir and standard deviation of the frequency response when without applying BESS are 49.8611 *Hz* and 0.0439, respectively. The maximum frequency deviation and standard deviation of the frequency response when applying BESS either on only the primary response or both primary and secondary response are also not much difference. The frequency nadir and standard deviation of the frequency response for applying BESS on only the primary response are 49.9708 *Hz* and 0.0149, respectively. The frequency nadir and the standard deviation of the frequency response applying on both primary and secondary response are 49.972 *Hz* and 0.0143, respectively. The frequency response is over 50.01 *Hz* for 15.522 *s*, 10.94 *s*, and 10.89 *s*, respectively. The frequency response is under 49.99 *Hz* for 14.41 *s*, 11.27 *s*, and 11.19 *s*, respectively.

Moreover, the result shows that the frequency response in the main grid is lower than the frequency response in the microgrid. In addition, the result suggests that the frequency deviation on either the main grid or the microgrid are significantly decreasing when applying BESS in the microgrid.

#### 6.2.1.2.2 Rate of Change of Frequency

Figure 6.4d and figure 6e present the rate of change of frequency in the main grid and in the microgrid, respectively. The graphs show that the *ROCOF* on either the main grid or the microgrid act in the same direction. The *ROCOF* when applying BESS either on only the primary response or both primary and secondary response is significantly decreasing and vary less than when without applying BESS. The *ROCOF* for the main grid and the microgrid when without applying BESS are  $-0.01027 \text{ Hz/s}$  and  $-0.09843 \text{ Hz/s}$ , respectively. The standard deviation of the *ROCOF* when without applying BESS for the main grid and the microgrid are 0.00425 and 0.0251, respectively.

The maximum of the *ROCOF* and standard deviation of the *ROCOF* when applying BESS either on only the primary response or both primary and secondary response are not much difference. The *ROCOF* for the main grid and the microgrid when applying BESS on only the primary response are  $-0.00238 \text{ Hz/s}$  and  $-0.01511 \text{ Hz/s}$ , respectively. The standard deviation of the *ROCOF* when applying BESS on only the primary response are 0.00145 and 0.00402, respectively. The *ROCOF* for the main grid and the microgrid when applying BESS on both primary and secondary response are  $-0.00225 \text{ Hz/s}$  and  $-0.01467 \text{ Hz/s}$ , respectively. The standard deviation of the *ROCOF* when applying BESS on both primary and secondary response are 0.00225 and 0.00384, respectively.

Moreover, the result shows that the *ROCOF* in the microgrid is higher than the *ROCOF* in the main grid. In addition, the result suggests that the *ROCOF* on either the main grid or the microgrid are noticeable decrease when applying BESS in the microgrid.

#### 6.2.1.2.3 Power and Energy Discharged from Battery

Figure 6.4f and figure 6.5g present the power and energy discharged from the battery, respectively. The battery charges the power from solar cells when solar cells generate instantaneous increasing power to the microgrid. The battery discharges the power to the microgrid when the power output from solar cells rapidly decrease. The graph shows that the battery charges the power from solar cells for the first 24

seconds, on between 12:52:30 to 12:52:54, and then discharges the power from battery after 12:52:54. The highest battery charged and discharged power/energy when applying BESS on only primary response are 0.29 *MW*/0.82 *kWh* and 0.32 *MW*/0.82 *kWh*, respectively. The highest battery charged and discharged power/energy when applying BESS on both primary and secondary response are 0.78 *MW*/3.43 *kWh* and 0.064 *MW*/3.43 *kWh*, respectively.

#### 6.2.1.2.4 Power Generation from the Synchronous Generator

Figure 6.4h presents the deviated power generation from the synchronous generator on the main grid. The graph shows that the deviated power generation from the synchronous generator on the main grid when without a help from BESS on the microgrid is higher than when applying the battery on the microgrid. The power generation from the synchronous generator is decreasing on the first 24 seconds, on between 12:52:30 to 12:52:54, and then power generation is increasing after 12:52:54. The maximum of decreasing and increasing power generations from the synchronous generator on the main grid when without a help from BESS are 0.187 *MW* and 0.171 *MW*, respectively. The maximum of decreasing and increasing power generations from the synchronous generator on the main grid when applying the battery on either only primary response or on both primary and secondary response are not difference. The maximum of decreasing and increasing power generations from the synchronous generator on the main grid when applying the battery are 0.067 *MW* and 0.055 *MW*, respectively.

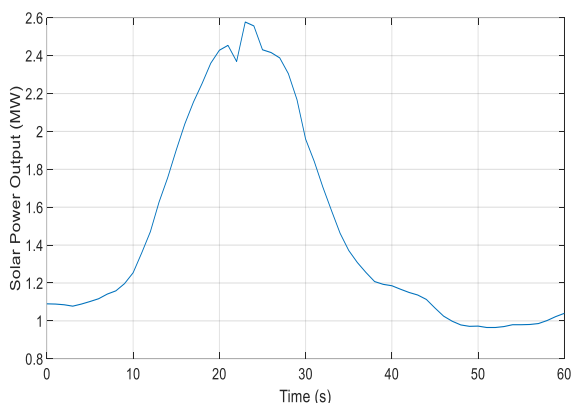
Figure 6.4i presents the power generation from the synchronous generator on the microgrid. The initial power generation from the synchronous generator in the microgrid is 3 *MW* at 12:52:30. The results show that the power generation from the synchronous generator on the microgrid rapidly decreases to 1.56 *MW* when without a help from BESS on the microgrid. In the same direction, the power generation from the synchronous generator on the microgrid is not much difference when applying the battery on only the primary response. The power from the synchronous generator is rapidly decreasing to 1.62 *MW*. However, the power generation from the synchronous generator on the microgrid is noticeable less decrease when applying



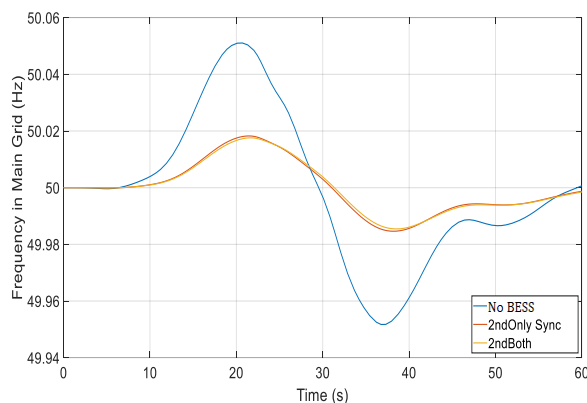
the battery on both primary and secondary response. The power from the synchronous generator decreases to 2.32 *MW*.

#### 6.2.1.2.5 Power at Tie-Line

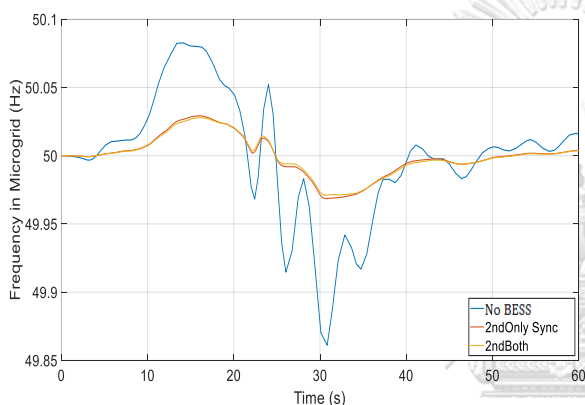
Figure 6.4j presents the power at tie-line that is between the main grid and the microgrid. The positive and negative powers at tie-line represent the power that transmits from the main grid to the microgrid and vice versa, respectively. The power at tie-line when without a help from BESS on the microgrid is higher than when applying the battery on the microgrid. The power transfers from the main grid to the microgrid on the first 24 seconds, on between 12:52:30 to 12:52:54, and then the power retransfers from the microgrid back to the main grid after 12:52:54. The maximum of the power transferred between the main grid and the microgrid when without a help from BESS are 0.180 *MW* and 0.162 *MW* for the main grid to the microgrid and the microgrid to the main grid, respectively. The maximum of the power transferred between the main grid and the microgrid when applying the battery on either only primary response or on both primary and secondary response are not difference. The maximum of the power transferred between the main grid and the microgrid when applying the battery are 0.065 *MW* and 0.049 *MW* for the main grid to the microgrid and the microgrid to the main grid, respectively.



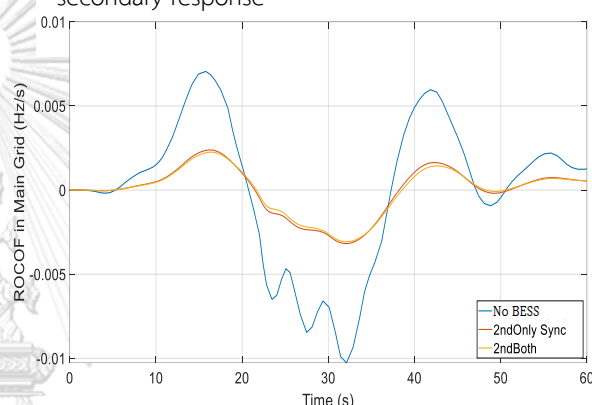
a) Power output from the solar cells in the Mueang Mae Hong Son province between 12:52:30 and 12:53:30



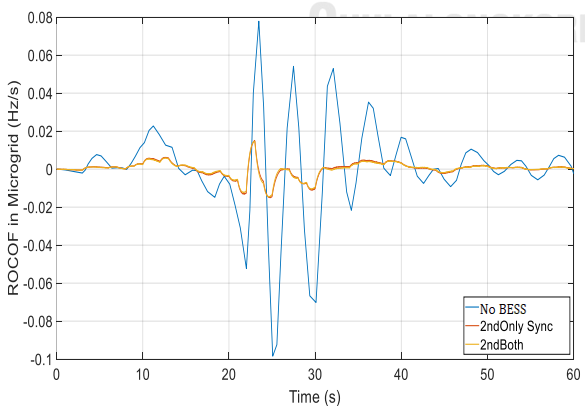
b) Frequency response in the main grid with various BESS; no BESS, BESS on only primary response, and BESS on both primary and secondary response



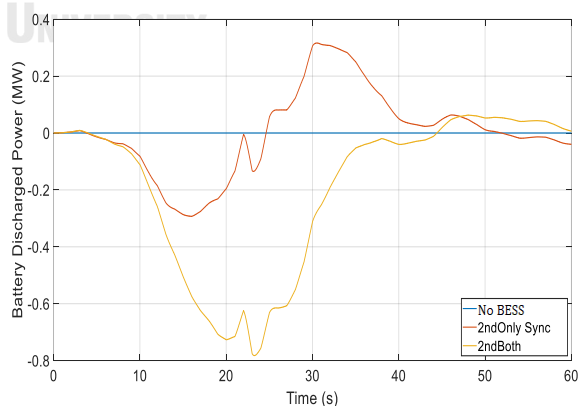
c) Frequency response in the microgrid with various BESS; no BESS, BESS on only primary response, and BESS on both primary and secondary response



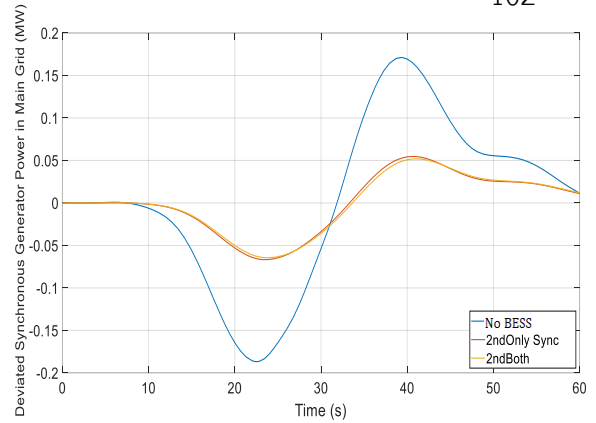
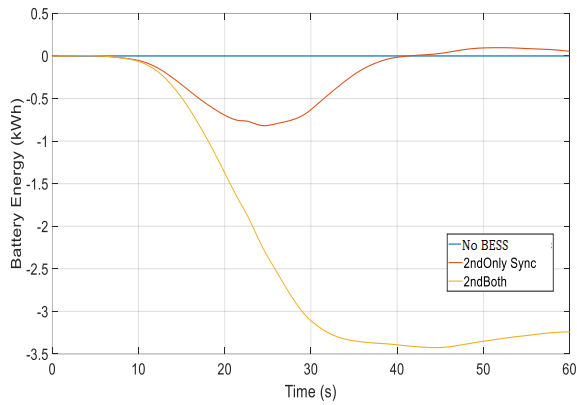
d) *ROCOF* in the main grid with various BESS; no BESS, BESS on only primary response, and BESS on both primary and secondary response



e) *ROCOF* in the microgrid with various BESS; no BESS, BESS on only primary response, and BESS on both primary and secondary response

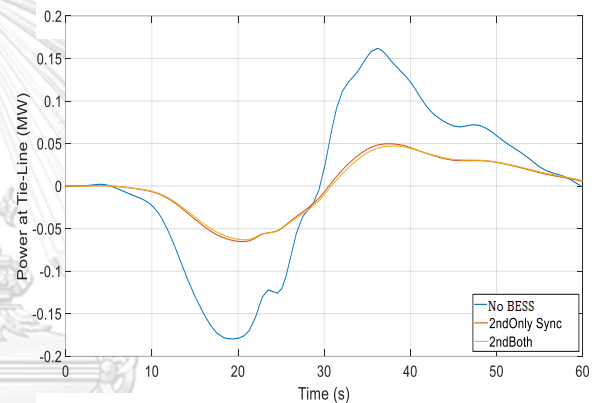
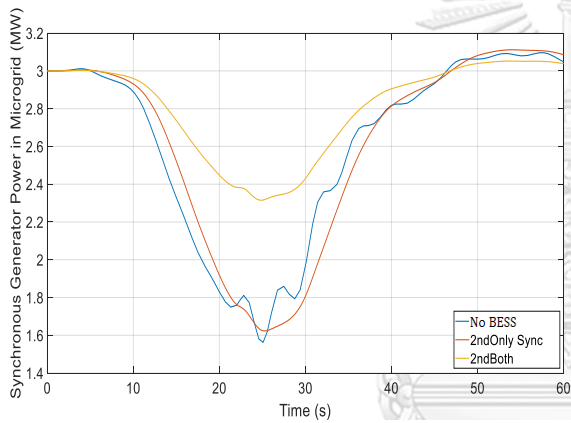


f) Power discharged from the battery with various BESS; no BESS, BESS on only primary response, and BESS on both primary and secondary response



g) Energy output from the battery with various BESS; no BESS, BESS on only primary response, and BESS on both primary and secondary response

h) deviated power generation from the synchronous generator in the main grid with various BESS; no BESS, BESS on only primary response, and BESS on both primary and secondary response



i) Power generation from the synchronous generator in the microgrid with various BESS; no BESS, BESS on only primary response, and BESS on both primary and secondary response

j) Power at tie-line with various BESS; no BESS, BESS on only primary response, and BESS on both primary and secondary response

Figure 6.2 The Highest Variation of Power Output from the Solar Cells During the Day on a Connected Mode Microgrid

## Chapter 7

### Conclusion and Future Work

#### 7.1 Conclusion

The purpose of the thesis is to investigate microgrid control strategies of BESS for providing frequency support for the Mae Hong Son microgrid in a control strategy for grid-connected and isolated modes. The expected contribution of this thesis is to investigate Mae Hong Son microgrid to increase the frequency stability performance in both grid-connected and islanding modes with the help from BESS when a disturbance happens.

This thesis can be divided into three parts: an investigation a possibility of BESSs design when the large disturbance happens, frequency response with various integral gain ( $K_i$ ), and an investigation a possibility of BESSs design when using power from the solar cell.

An investigation a possibility of BESSs design when the large disturbance happens can categorise into two methods: virtual droop and virtual inertia. Both virtual droop and virtual inertia approaches can reduce the frequency nadir on applying only the primary response and applying both the primary and secondary response. However, the *ROCOF* of the virtual droop when BESS using is the same for each virtual droop constant, while the *ROCOF* when BESS using the virtual inertia has a different value. The larger amount of virtual inertia constant gives the smaller *ROCOF*. Moreover, a virtual droop investigation suggests that the higher  $R_{BESS}$  takes the shorter period time to go to steady-state and a virtual inertia investigation suggests that the smaller value of  $H_{BESS}$  takes a shorter period to go to a steady-state. Furthermore, BESS with using virtual droop is discharging the power until the frequency of the microgrid goes back to a steady-state condition; therefore, it consumes much energy from BESS. On the opposite, BESS with using virtual inertia is not only discharging the power but also charging the power back to BESS. This method makes the energy in the BESS goes back to the initial value when the frequency reaches the steady-state condition. From the reason above, the Mae Hong Son microgrid should use the combined virtual droop and virtual inertia with  $R_{BESS} =$

2% and  $H_{BESS} = 10$  s, respectively. Not only the BESS control method can increase the frequency stability, but the period of over/under frequency response also performs under the time setting delay of protection device.

Frequency response with various integral gain ( $K_i$ ) can conclude that the value of  $K_i$  dose not affect to the primary response. However, the frequency response with the smaller value of  $K_i$  takes a longer period to go to a steady-state. Furthermore, the synchronous generator generates a higher power when the value of  $K_i$  is a large value.

An investigation a possibility of BESSs design when using power from the solar cell is the varying ratio of the BESS on the primary and secondary response. The BESS can significantly reduce the deviation of frequency on both grid-connected and isolated modes. The variation of frequency deviation on the short period of the highest variation of power output noticeable reduces when applying the BESS on either only primary response or both primary and secondary. Furthermore, the results of the frequency nadir are not much different when applying the BESS on either only primary response or both primary and secondary response for 60 seconds, high variation of the solar cells. However, the synchronous generator power in the microgrid significantly reduces the power generation when applying the BESS on both primary and secondary response.

Meanwhile, the synchronous generator power in the microgrid does not reduce the power generation when applying the BESS on only the primary response. Moreover, the power at tie-line significantly decreases when applying the BESS on either only the primary response or both primary and secondary response. However, the results of the reduction of the power at tie-line when applying the two BESS control methods are not much different. From the reason above, the Mae Hong Son microgrid should apply the BESS on only the primary response. Not only decreasing the frequency variation and the period of over/under frequency response, but the power/energy charge/discharge from the BESS is also less than apply on both primary and secondary response.

## 7.2 Future Work

The next step is to design the optimum ratio of combining virtual droop and virtual inertia to a single BESS control system to maximise the stability of the microgrid on both grid-connected and isolated modes.

Moreover, this thesis does not consider the voltage stability of a microgrid and considering only the photovoltaic power plant to be the renewable energy in the system. The next step is to investigate the control strategy of BESS to increase the stability of the microgrid on both frequency and voltage stability. In addition, the next step is to consider the other renewable energy resources or considering the microgrid with various renewable energy generation.



## REFERENCES

1. A. Ulbig, T. S. Borsche, and G. Andersson, *Impact of Low Rotational Inertia on Power System Stability and Operation*, in the *19th IFAC World Congress, B. Edward, Ed.* 2014: Cape Town, South Africa. p. 7290-7297.
2. K. Kpoto, A. M. Sharma, and A. Sharma, *Effect of the energy storage system(ESS) in low inertia power system with high renewable energy sources*, in *2019 Fifth International Conference on Electrical Energy Systems (ICEES)*. 2019: Chennai, India. p. 1-6.
3. P. Zhongmei, H. Tonghui, and W. Yuqing, *Voltage sags/swells subsequent to islanding transition of PV-battery microgrids*, in *2016 IEEE 11th Conference on Industrial Electronics and Application (ICIEA)*. 2016: Hefei, China. p. 1-6.
4. A. Husain, V. Bui, and H. Kim, *Demand response for enhancing the survivability of microgrids during islanded operation*, in *2018 IEEE Region 10 Conference*. 2018: Jeju, Korea (South). p. 2159-3442.
5. Y. Ma, et al., *Frequency control of islanded microgrid based on wind-PV-diesel-battery hybrid energy sources*, in *2014 17th International Conference on Electrical Machines and Systems (ICEMS)*. 2014: Hangzhou, China. p. 290-294.
6. P. F. Frack, et al., *Control strategy for frequency control in autonomous microgrids*. *IEEE journal of emerging and selected topics in power electronics*, 2015. **3**(4): p. 1046-1055.
7. F. M. Uriarte, et al., *Microgrid ramp rates and the inertial stability margin*. *IEEE Transactions on Power Systems*, 2015. **30**(6): p. 3209-3216.
8. L. Toma, et al., *On the virtual inertia provision by BESS in low inertia power systems*, in *2018 IEEE International Energy Conference (ENERGYCON)*. 2018: Limassol, Cyprus. p. 1-6.
9. G. Delille, B. Francois, and G. Malarange, *Dynamic frequency control support by energy storage to reduce the impact of wind and solar generation on isolated power system's inertia*. *IEEE Transaction on Sustainable Energy*, 2012. **3**(4): p. 931-939.

10. R. Yan and T.K. Saha, *Cascading contingencies in low inertia power systems: Frequency response challenges and a potential solution*, in *2017 IEEE Power & Energy Society General Meeting*. 2017: Chicago, Illinois, USA. p. 1-5.
11. B. I. Crăciun, et al., *Frequency support functions in large PV power plants with active power reserves*. IEEE Journal of Emerging and Selected Topics in Power Electronics, 2014. **2**(4): p. 849-858.
12. S. M. Ashabani and Y.A. Mohamed, *A flexible control strategy for grid-connected and islanded microgrids with enhanced stability using nonlinear microgrid stabiliser*. IEEE Transactions on Smart Grid, 2012. **3**(3): p. 1291-1301.
13. IEEE, *IEEE guide for AC Generator Protection*, in *IEEE C37*,. 2006.
14. D. E. Olivares, et al., *Trends in microgrid control*. IEEE Trans. Smart Grid, 2014. **5**(4): p. 1905–1919.
15. A. Bidram and A. Davoudi, *Hierarchical structure of microgrids control system*. IEEE Trans. Smart Grid, 2012. **3**(4): p. 1963–1976.
16. T. Vandoorn, et al., *Review of primary control strategies for islanded microgrids with power electronic interfaces*. Renew. Sust. Energy Rev., 2013. **19**: p. 613 – 628.
17. A. M. Bouzid, et al., *A survey on control of electric power distributed generation systems for microgrid applications*. Renew. Sust. Energy Rev., 2015. **44**: p. 751 – 766.
18. A. Mehrizi-Sani and R. Iravani, *Potential-function based control of a microgrid in islanded and grid-connected modes*. IEEE Trans. Power Syst., 2010. **25**(4): p. 1883–1891.
19. J. A. P. Lopes, C. L. Moreira, and A.G. Madureira, *Defining control strategies for microgrids islanded operation*. IEEE Trans. Power Syst., 2006. **21**(2): p. 916–924.
20. E. Unamuno and J.A. Barrena, *Hybrid ac/dc microgrids—part II: Review and classification of control strategies*. Renew. Sust. Energy Rev., 2015. **52**: p. 1123 – 11342015.
21. J. Rocabert, et al., *Control of power converters in ac microgrids*. IEEE Trans. Power Electron., 2012. **27**(11): p. 4734–4749.
22. M. P. Kazmierkowski and L. Malesani, *Current control techniques for three-phase*



- voltage-source pwm converters: a survey*. IEEE Trans. Ind. Electron., 1998. **45**(5): p. 691–703.
23. G. Shahgholian, J. Faiz, and P. Shafaghi, *Nonlinear control techniques in uninterruptible power supply inverter: A review*, in *2009 Second International Conference on Computer and Electrical Engineering*. 2009: Dubai, United Arab Emirates. p. 51–55.
  24. A. Timbus, et al., *Evaluation of current controllers for distributed power generation systems*. IEEE Trans. Power Electron., 2009. **24**(3): p. 654–664.
  25. J. M. Guerrero, J. C. Vázquez, and R. Teodorescu, *Control of droop-controlled dc and ac microgrids—a approach towards standardisation*, in *2009 Ind. Electron., IECON '09. 35th Annual Conf. of IEEE*. 2009.
  26. Q. Shafiee, J. M. Guerrero, and J.C. Vasquez, *Distributed secondary control for islanded microgrids—a novel approach*. IEEE Trans. Power Electron., 2014. **29**(2): p. 1018–1031.
  27. E. Planas, et al., *General aspects, hierarchical controls and droop methods in microgrids: A review*. Renew. Sust. Energ. Rev., 2013. **17**: p. 147 – 159.
  28. M. Yazdani and A. Mehrizi-Sani, *Distributed control techniques in microgrids*. IEEE Trans. Smart Grid, 2014. **5**(6): p. 2901–2909.
  29. Y. Pei, et al., *Auto-master-slave control technique of parallel inverters in distributed ac power systems and ups*, in *Power Electronics Specialists Conference, 2004. PESC 04. 2004 IEEE 35th Annual*. 2004. p. 2050–2053.
  30. R. Ramos, et al., *Master-slave sliding mode control design in parallel-connected inverters*. AUTOMATIKA, 2001. **42**(1-2): p. 37–44.
  31. A. Kaur, J. Kaushal, and P. Basak, *A review on microgrid central controller*. Renew. Sust. Energy Rev., 2016. **55**: p. 338 – 345.
  32. F. Chen, et al., *Multiagent based reactive power sharing and control model for islanded microgrids*. IEEE Transactions on Sustainable Energy, 2016. **7**(3): p. 1232 - 1244.
  33. A. Bidram, et al., *Distributed cooperative secondary control of microgrids using feedback linearisation*. IEEE Trans. Power Syst., 2013. **28**(3): p. 3462–3470.
  34. T. Morstyn, B. Hredzak, and V.G. Agelidis, *Distributed cooperative control of*

- microgrid storage*. IEEE Trans. Power Syst., 2015. **30**(5): p. 2780–2789.
35. M. Mao, et al., *Multi agent-based hybrid energy management system for microgrids*. IEEE Trans. Sust. Energy, 2014. **5**(3): p. 938–946.
  36. Q. Li, et al., *Agent-based decentralised control method for islanded microgrids*. IEEE Trans. Smart Grid, 2016. **7**(2): p. 637–649.
  37. M. Moradzadeh, R. Boel, and L. Vandeveldel, *Voltage coordination in multi-area power systems via distributed model predictive control*. IEEE Trans. Power Syst., 2013. **28**(1): p. 513–521.
  38. J.W. Simpson-Porco, et al., *Secondary frequency and voltage control of islanded microgrids via distributed averaging*. IEEE Trans. Ind. Electron., 2015. **62**(11): p. 7025–7038.
  39. M. A. Mahmud, et al., *Robust nonlinear distributed controller design for active and reactive power sharing in islanded microgrids*. IEEE Trans. Energy Convers., 2014. **29**(4): p. 893–903.
  40. P. K. Ray, S. R. Mohanty, and N. Kishor, *Small-Signal Analysis of Autonomous Hybrid Distributed Generation Systems in the Presence of Ultracapacitor and Tie-Line Operation*. Journal of Electrical Engineering, 2010. **61**(4): p. 205-214.
  41. S. M. Alhejaj and F.M. Gonzalez-Longatt, *Investigation on grid-scale BESS providing inertial response support*, in *2016 IEEE Int. Conf. Power Syst. Technol. POWERCON*. 2016. p. 1–6.
  42. S. Lee, et al., *Frequency control of energy storage system based on hierarchical cluster structure*, in *2015 IEEE Eindhoven PowerTech*. 2015: Netherlands. p. 1-5.
  43. J. W. Shim, et al., *On Droop Control of Energy-Constrained Battery Energy Storage Systems for Grid Frequency Regulation*. IEEE Access, 2019. **7**: p. 166353-166364.
  44. D. J. Lee and L. Wang, *Small-Signal Stability Analysis of an Autonomous Hybrid Renewable Energy Power Generation/Energy Storage System Part I: Time-Domain Simulations*. IEEE Transactions on Energy Conversion, 2008. **23**(1): p. 311-320.



จุฬาลงกรณ์มหาวิทยาลัย  
**CHULALONGKORN UNIVERSITY**



จุฬาลงกรณ์มหาวิทยาลัย  
**CHULALONGKORN UNIVERSITY**

## VITA

**NAME** Arnon Teawnarong

**DATE OF BIRTH** 29 July 1992

**PLACE OF BIRTH** Bangkok, Thailand

**INSTITUTIONS ATTENDED** B. Eng. (Electrical Eng.) at Chulalongkorn University  
M. Eng. (Electrical Eng.) at Chulalongkorn University

**HOME ADDRESS** Power System Research Lab (PSRL) 12th floor, Building 4,  
Department of Electrical Engineering, Faculty of  
Engineering, Chulalongkorn University

**PUBLICATION** A. Teawnarong and P. Chirapongsananurak, "Providing  
Frequency Response in Isolated Microgrids Using Battery  
Energy Storage Systems," 2020 8th International Electrical  
Engineering Congress (iEECON), Chiang Mai, Thailand, 2020,  
pp. 1-4, doi: 10.1109/iEECON48109.2020.233042.